Active Site Studies of DmpFG, a Bifunctional Aldolase/Dehydrogenase from *Pseudomonas* sp. Strain CF600

Yu Lei

A Thesis

In

The Department

of

Chemistry and Biochemistry

Presented in Partial Fulfillment of the Requirements

for the Degree of Doctor of Philosophy at

Concordia University

Montreal, Quebec, Canada

September 2008

Your file Votre référence
ISBN: 978-0-494-45669-9
Our file Notre référence
ISBN: 978-0-494-45669-9

ABSTRACT

Active Site Studies of DmpFG, a Bifunctional Aldolase/Dehydrogenase from *Pseudomonas* sp. Strain CF600

Yu Lei, Ph.D.
Concordia University, 2008

DmpFG, a bifunctional aldolase/dehydrogenase (acylating), comprises the last two enzymes of the (dimethyl)phenol degradation pathway in *Pseudomonas* sp. strain CF600. DmpG, a class II divalent cation dependent aldolase belonging to the HMGL-like family, cleaves 4-hydroxy-2-ketovalerate to pyruvate and acetaldehyde while DmpF, an NAD^+/CoA dependent aldehyde dehydrogenase (acylating), oxidizes the acetaldehyde to acetyl-CoA.

Studies of the DmpF active site focused on delineation of the coenzyme A binding site, and involvement of a conserved cysteine residue, Cys132, in catalysis and substrate-mediated inactivation. By coupling hydrogen–deuterium exchange experiments with peptic digest/mass spectrometric analysis, coenzyme A was shown to share the same binding site as NAD^+. Cys132 was identified as an essential cysteine, and was shown to form an acetyl-Cys132 intermediate which was trapped and identified by mass spectrometry. Coenzyme A–mediated inactivation resulted from disulfide bond formation between thiol groups of Cys132 and coenzyme A. Loss of activity in the presence of acetaldehyde was incurred by the oxidation of Cys132 to cysteine sulfinic acid, as observed by mass spectrometry.

Studies of DmpG focused on the roles of metal ions and putative active site residues. Purified preparations contained a mixture of Fe, Mn, Zn and Cu, in order of decreasing content, with one mol total metal per mol protein. However, this tightly-bound metal

could only support residual adolase activity, with full activity requiring high concentrations of Mn^{2+} or Co^{2+} in the assay, suggesting two classes of metal binding sites. Site-directed mutagenesis was carried out on the three ligands to the tightly bound metal ion, Asp18, His200 and His202, as well as another three residues, potentially involved in catalysis, Arg17, His21 and Tyr291. D18N, H200A and H202A variants were depleted of bound metals, concomitant with complete loss of the residual aldolase activity. In the presence of Mn^{2+} or Co^{2+}, aldolase activities of D18N and H200A variants remained very low in comparison with WT, but H202A aldolase activity was comparable to WT. Substitutions of Arg17 or His21 significantly impaired aldolase activity, while Tyr291 variants had activity similar to WT. Properties of these variants are discussed in relation to the family of HMGL-like enzymes.

ACKNOWLEDGEMENTS

First and foremost, I thank my supervisor Dr. Justin Powlowski for his unending support, his constructive guidance, encouragement and advice he has provided throughout my time as his student.

My sincere gratitude goes out to Dr. Joanne Turnbull who often serves as the trigger of wisdom in my research work.

Appreciation goes to Dr. M. J. Kornblatt for useful suggestions and discussion.

Special thanks Dr. Ann M. English for unconditional contributions to my research and constant support.

I also wish to thank to Dr. P. D. Pawelek for his patience and helpful conversation.

A big thanks to my lab mates, Dr. Lena Sahlman, Amy Wong and Andrew Tait, whose bright spirits and willingness to help each other out made working in the lab a pleasure.

Thanks to Bonny Choy for the unselfish help in the life and research.

Thanks to Alain Tessier for all his excellent MS work and to Dr. B. Gibbs for help with starting peptide sequencing using MS techniques.

Finally I want to thank my family: my wife Zhongzhen Du, my son Chi Lei, my own parents and my parents in law for their love and encouragement.

Table of Contents

List of Figures

List of Tables

List of Abbreviations

4H2KV, 4-hydroxy-2-ketovalerate

α-IPMS, α-isopropylmalate synthase

ALDH, aldehyde dehydrogenase

AUC, analytical ultracentrifugation

BCA, bicinchoninic acid

CoA, coenzyme A

Da, dalton

DEAE, diethyl aminoethyl

DHAP, dihydroxyacetone phosphate

DMF, dimethylformamide

DTPA, diethylenetriaminepentaacetic acid

DTT, dithiothreitol

EDTA, ethylenedinitrilotetraacetic acid

ESI, electrospray ionization

FBPA, fructose-1, 6-biphosphate aldolase

FCT, formyl-CoA transferase

Far-UV CD, far ultraviolet circular dichroism

GAPDH, glyceraldehyde-3-phosphate dehydrogenase (phosphorylating)

HEPES, N-(2-hydroxyethyl)-piperazine-N'-2-ethanesulfonic acid

H–D exchange, hydrogen–deuterium exchange

HMGL-like, hydroxymethylglutaryl-CoA lyase like

HPLC, high-performance liquid chromatography

IC_{50}, the half maximal inhibitory concentration

ICP-MS, inductively coupled plasma mass spectrometry

KDa, kilodalton

LDH, lactate dehydrogenase

MALDI, matrix-assisted laser desorption ionization

MS/MS, tandem mass spectroscopy

PD, 50 mM Na^+ K^+ phosphate buffer with 1 mM dithiothreitol

PDB, Protein Databank

SCS, succinyl-CoA synthetase

SDS–PAGE, sodium dodecylsulfate polyacrylamide gel electrophoresis

TC, transcarboxylase

TCA, trichloroacetic acid

TCEP, Tris[2-carboxyethyl]phosphine hydrochloride

TFA, trifluoroacetic acid

TIM, triose-phosphate isomerase

TNM, tetranitromethane

TOF, time of flight

WT, wild type

Contributions of Authors

I wrote Chapter 1, the general introduction to DmpFG, the bifunctional aldolase/dehydrogenase.

Chapter 2 was published in *Biochemistry* (2008) 47, 6870-6882 with Dr. Peter D. Pawelek and Dr. Justin Powlowski. I carried out all the experiments reported in the paper except for automated docking of CoASH to DmpF, and I prepared the original version of the manuscript as well.

Chapter 3 is a manuscript submitted for publication with the authors of Zeinab Aziz and Justin Powlowski. I wrote the first version of the manuscript. I performed all the experiments except for the plasmid preparations of variants D209A (ZA) and C132S (JP) of DmpF.

Chapter 4 is a manuscript prepared for publication with the authors Andrew Tait and Justin Powlowski. I wrote the first version of the manuscript. Andrew Tait prepared the plasmids for variants H200A, H202A and H203A and carried out preliminary characterization of the corresponding enzymes. I performed further experiments on and extended investigation on these variant proteins, and carried out all other experiments reported in the manuscript.

Chapter 1 Introduction

1.1 General Introduction

Pseudomonas sp. strain CF600 is able to efficiently decompose phenol, cresols and dimethylphenols via the *dmp*-operon encoded *meta*-cleavage pathway (Figure 1.1) (1). The last two enzymes in this pathway are DmpF (32.7 kDa) and DmpG (37.3 kDa), which form an active heterotetramer (F2G2) (Figure 1.2) (2). They constitute an aldolase (DmpG) and an aldehyde dehydrogenase (DmpF) which together convert 4-hydroxy-2-ketovalerate to pyruvate and acetyl-CoA (Figure 1.3) (*1, 2*). Previous work indicates (*2, 3*) that DmpF and DmpG, are tightly associated, co-purifying and requiring co-expression to obtain fully active enzymes. More recently, structural data, summarized below, has revealed the intimate details of the association between the subunit components. Accordingly, DmpFG is referred to as a bifunctional aldolase/dehydrogenase.

1.1.1 Overall structure of DmpFG

The crystal structure of this novel bifunctional enzyme was solved in the presence and absence of the cofactor, NAD^+ (4). The structure consists of 8 polypeptide chains in the asymmetric unit, 4 DmpG and 4 DmpF, arranged as two heterotetramers. The 345-residue DmpG, which catalyzes the cleavage of 4-hydroxy-2-ketovalerate to pyruvate and acetaldehyde, is composed of two domains. At the N-terminus of the structure is a classic $(\alpha/\beta)_8$ TIM barrel domain (residues 1–250) where a metal ion, tentatively assigned as Mn^{2+} (4), is positioned in the active site at the bottom end of the barrel (Figure 1.4). At the C-terminus there is an entirely helical structure, called the communication domain (residues 251–345), which mediates the interaction with DmpF. DmpF, which converts acetaldehyde to acetyl-CoA, is arranged into two domains: the NAD^+-binding domain (covering residues 1–130 and 286–312) where a typical Rossmann fold provides

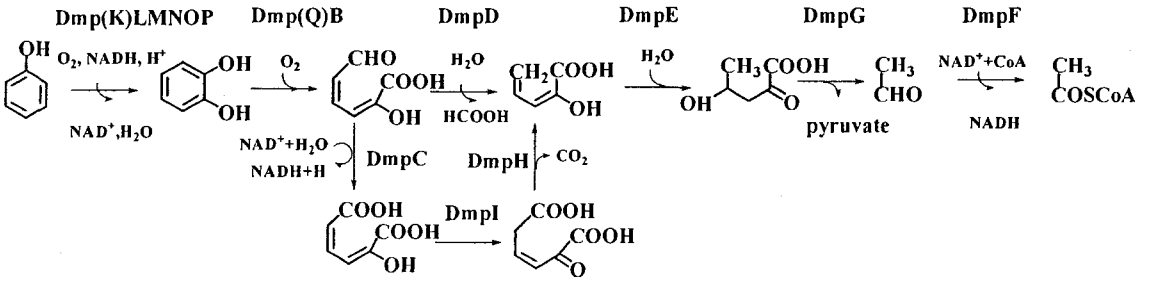

Figure 1.1 *Meta*-cleavage pathway for phenol degradation in *Pseudomonas* sp. strain CF600.

Adapted from reference (1).

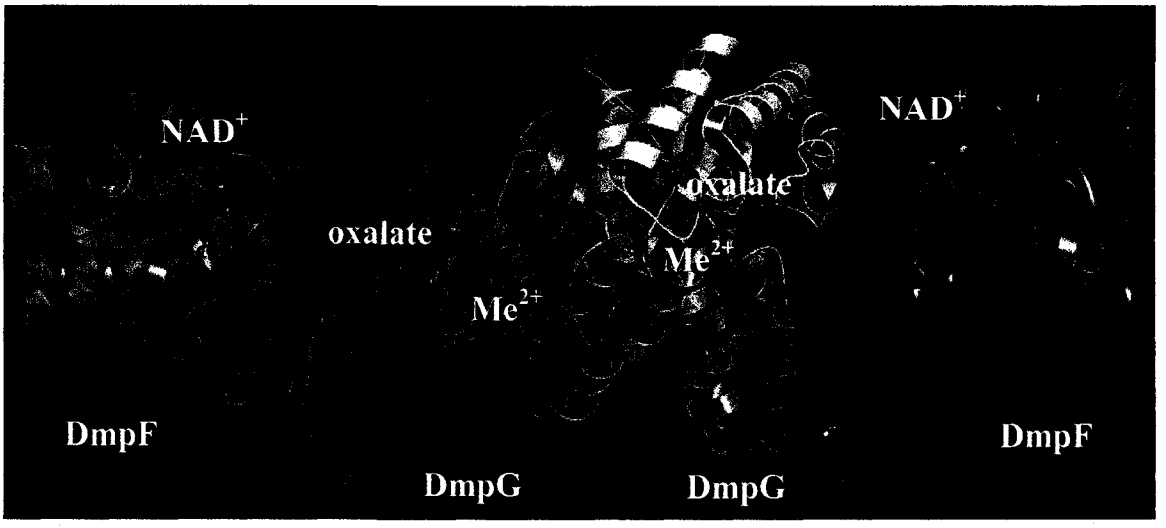

Figure 1.2 The structure of biologically active DmpFG - a heterotetramer.

DmpF complexed with cofactor NAD^+; the TIM barrel domain of DmpG contains a divalent cation and the product analogue, oxalate (Figure prepared from PDB entry 1NVM using PyMol).

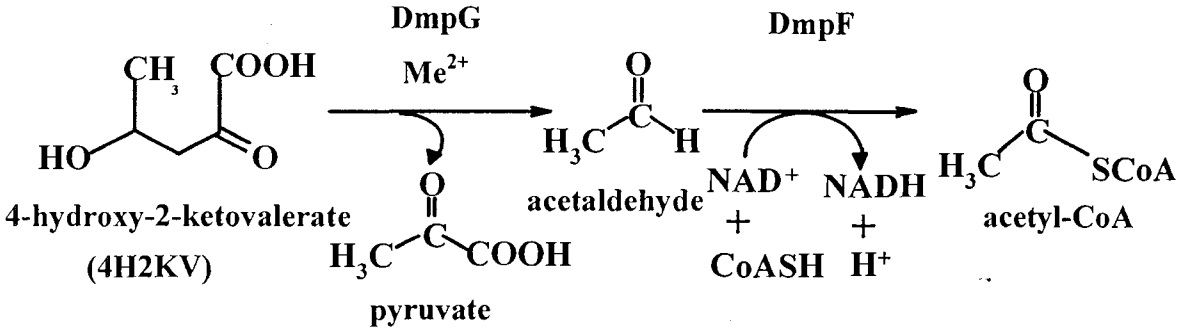

Figure 1.3 DmpFG –catalyzed reaction.

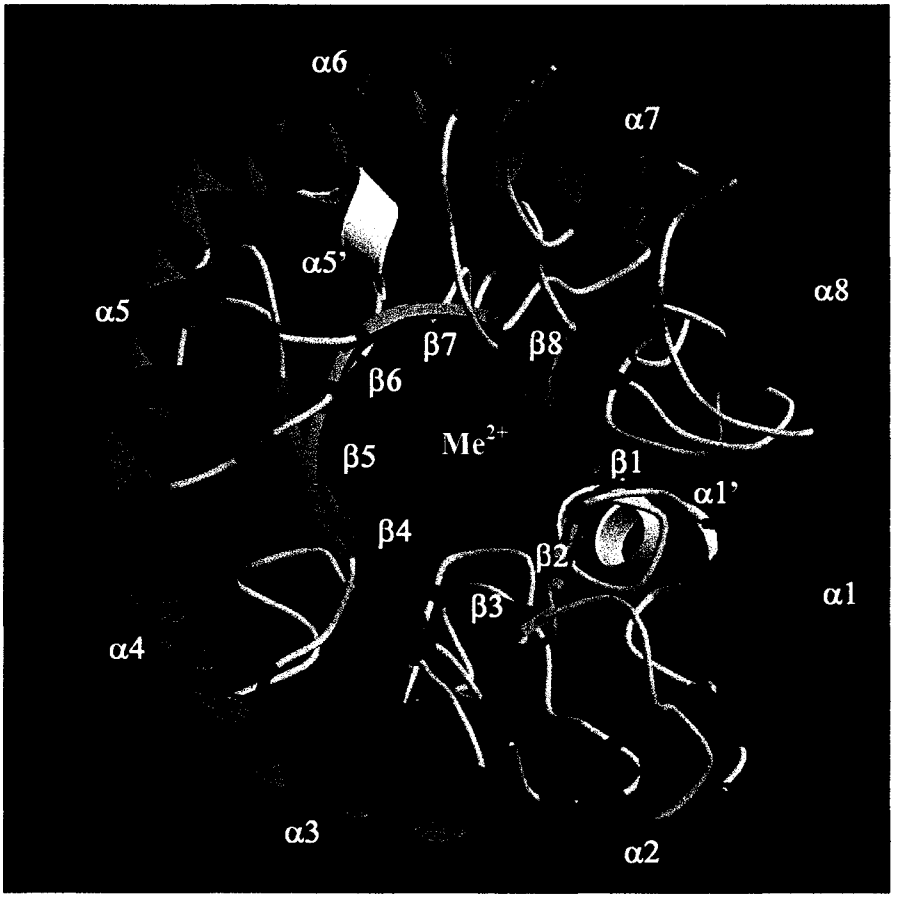

Figure 1.4 The $(\alpha/\beta)_8$ TIM barrel of DmpG.

The DmpG active site locates at a classic TIM barrel domain which consists of eight parallel β strands arranged to make up a barrel structure and surrounded by eight α helices. Two additional helices, α'1 and α'5, are inserted into the barrel motif between β1 and α1 and β5 and α5. Inside the barrel a metal ion, tentatively assigned as Mn^{2+}, is positioned at the active site at the bottom end of the barrel (Figure prepared using PyMol on the basis of PDB entry 1NVM).

accommodation for NAD^+ (Figure 1.5), and the dimerization domain (residues 131-285) which mediates interaction with DmpG (4).

1.1.2 Structure and function of DmpG and related HMGL-like family enzymes

DmpG is a member of the HMGL-like family (where HMGL signifies HMG-CoA lyase, another member of the family), which in turn is one of the members of the xylose isomerase-like TIM barrel superfamily (5). The HMGL-like family comprises a variety of enzymes that catalyze diverse C-C cleavage/condensation reactions, such as 3-hydroxy-3-methylglutaryl-CoA (HMG-CoA) lyase (EC 4.1.3.4) (*6, 7*), α-isopropylmalate synthase (α-IPMS) (EC 2.3.3.13) (8), 4-hydroxy-2-ketovalerate aldolase (DmpG) (EC 4.1.3.39) (4) and transcarboxylase (TC) 5S subunit (EC 2.1.3.1) (9). Active sites of HMGL-like proteins locate within a canonical $(\alpha/\beta)_8$ barrel which consists of 8 parallel β-strands arranged as a barrel and surrounded by 8 α-helices, each of which brings the chain back to one side of the structure for the next strand in the barrel.

The $(\alpha/\beta)_8$ barrel of members of the HMGL-like family is highly conserved, with similar active site organization in the barrel interior. The active sites of different family members include divalent metal ions such as Mn^{2+}, Mg^{2+}, Co^{2+} or Zn^{2+}, and they share several invariant residues involved in metal coordination and/or enzyme catalysis. Although there is still uncertainty about the details of catalysis by enzymes in the HMGL-like family, a mechanism which involves general base/acid catalysis and an enolate intermediate has been proposed (6).

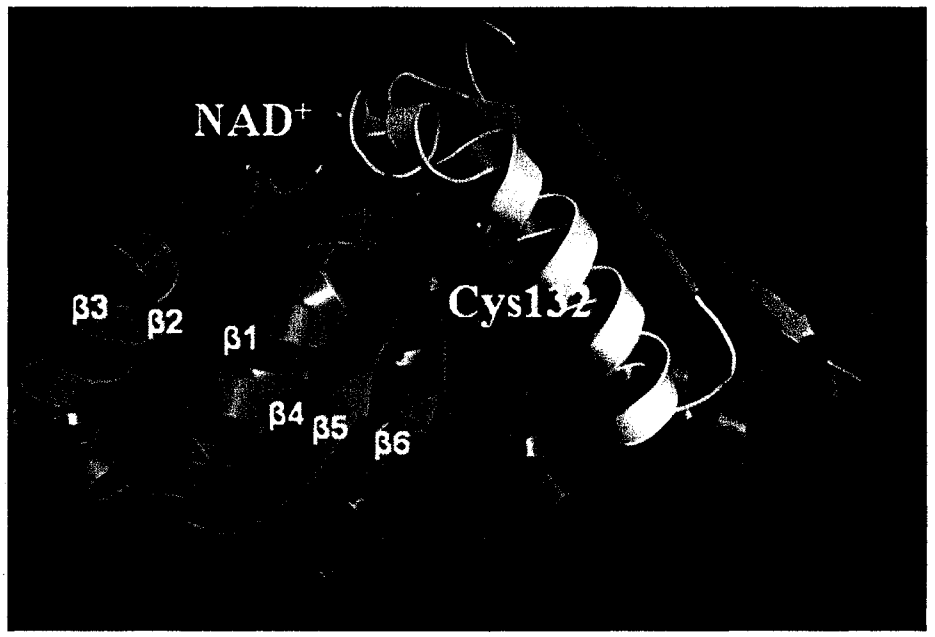

Figure 1.5 Rossmann fold of DmpF bound with NAD^+.

The typical Rossmann fold consists of six parallel β-strands. The nicotinamide ring of the bound NAD^+ is close (~ 4Å) to the proposed active site residue Cys132 (Figure prepared from PDB entry 1NVM using PyMol).

1.1.2.1 DmpG

The metal ion in DmpG is coordinated by six ligands in octahedral geometry (4), including three residues, Asp18, His200 and His202, that are conserved in the HMGL-like family (6-9), as well as two carboxylate oxygens of the product analogue and one H_2O (Figure 1.6). However, little is known about the roles that the metal ions play in either the structure or the catalytic action of DmpFG.

Although the mechanism of 4-hydroxy-2-ketovalerate cleavage has not previously been investigated, one has been proposed on the basis of the crystal structure of DmpFG (4), and is summarized in Figure 1.7. His21 and Tyr291 of DmpG (Figure 1.6) were proposed to act as general base and acid, respectively, in the reaction. It was also proposed that catalysis is correlated with the movement of these two residue side chains to gate the entrance of the substrate intermediate channel in the DmpG active site. The histidine residue (His21) is positioned where it may act as a base for abstraction of the hydroxyl proton of the substrate, 4-hydroxy-2-ketovalerate. Upon carbon-carbon bond cleavage, acetaldehyde and enol-pyruvate are produced, leaving His21 protonated. His21 does not lie near enough to the enol-pyruvate to facilitate protonation and pyruvate formation, but has been proposed to be involved in a proton shuttle using the Tyr291 side chain. The Tyr291 sidechain moves so that its hydroxyl group approaches NE2 of the protonated histidine side chain and deprotonates it. This movement of Tyr291, which is possible in the space present at the active site of DmpG, effectively opens access for acetaldehyde to the tunnel between the DmpF and DmpG active sites. When the side chain of Tyr291 moves back to its original position, it closes off the tunnel and in so doing protonates the enolate to complete formation of the second product of the DmpG reaction, pyruvate.

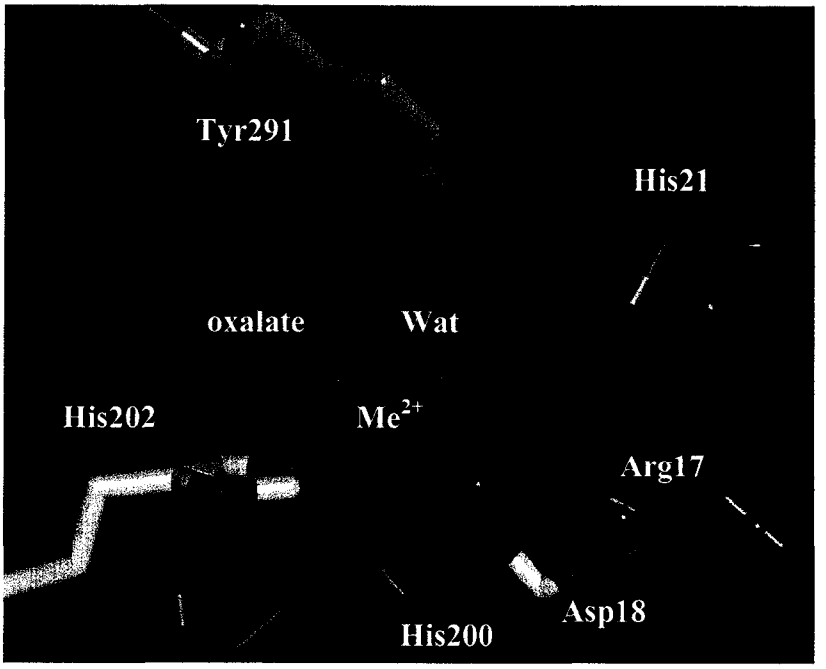

Figure 1.6 The active site of DmpG in complex with a product analogue, oxalate. The divalent cation is coordinated in octahedral geometry: the six ligands include Asp18, His200, His202, one ordered H_2O molecule and two carboxylate and carbonyl oxygens of the product analogue oxalate, respectively (Figure prepared using PyMol based on PDB entry 1NVM).

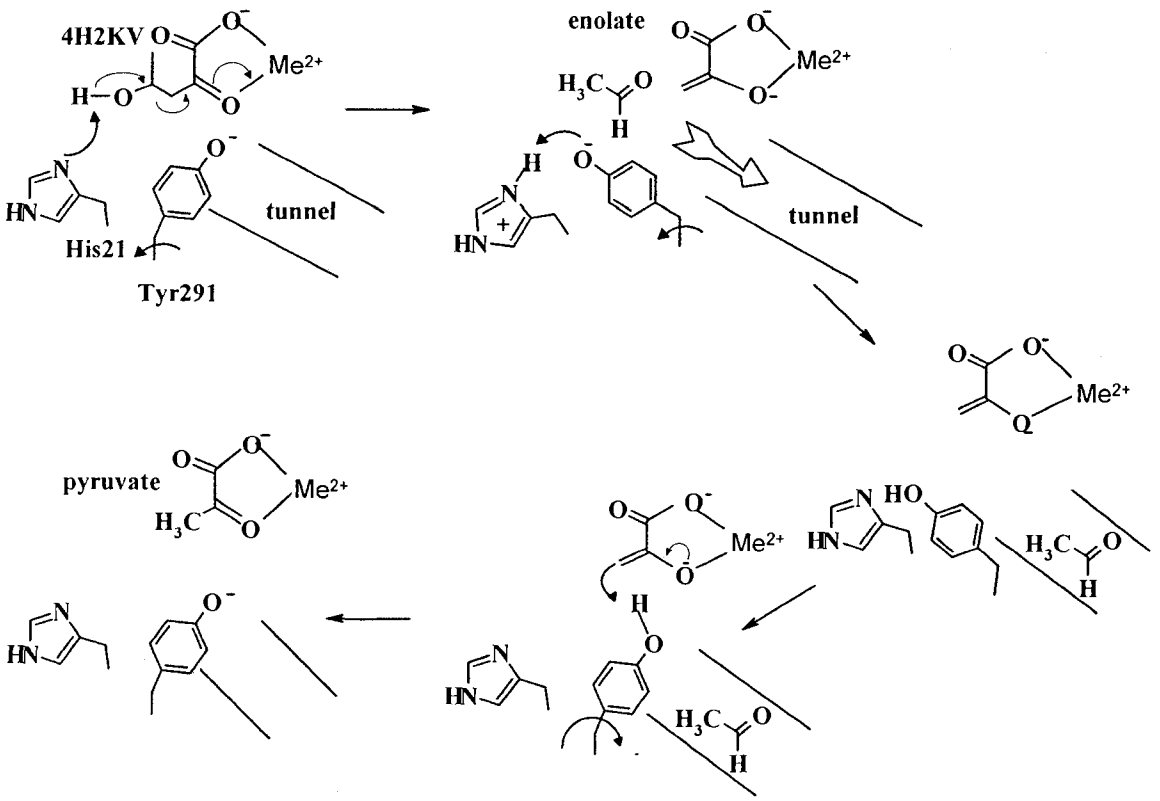

Figure 1.7 The proposed roles of His21 and Tyr291 in DmpG catalysis and substrate intermediate channeling in DmpFG reaction.

Adapted from reference (4).

Arg-17, another conserved residue in HMGL-like proteins, is a candidate for stabilizing the oxyanion in the formation of a pyruvate enolate intermediate. Arg-17 is also likely to serve as a proton donor which functions as a general acid (10). These proposals are based on the structural analysis of product analogue-DmpG (Figure 1.6) and product-TC 5S complex (PDB entries 1RQH and 1RQE) (9), as well as the investigation of the corresponding Arg in human HMG-CoA lyase (*6, 10*).

1.1.2.2 3-Hydroxy-3-methylglutaryl-CoA lyase

HMG-CoA lyase, which catalyzes the cleavage of 3-hydroxy-3-methylglutaryl-CoA into acetyl-CoA and acetoacetate, is a divalent cation-dependent enzyme involved in ketone body formation and leucine catabolism (11-13). An EBI SSM (14) search for the three dimensional structural alignment of DmpG with all PDB entries shows that HMG-CoA lyases are the structures most similar to DmpG. With 18.0 % sequence identity, DmpG shares the highest homology with HMG-CoA lyase from *Brucella melitensis* (PDB entry 1YDN) in their TIM barrel domains with a 0.44 Q quality score, 1.92 Å RMSD, a Z score of 9.7 and a P score of 8.7, for 244 Cα alignments.

Since mutations of HMG-CoA lyase are associated with hereditary HMG-CoA lyase deficiency diseases, human HMG-CoA lyase has been quite extensively investigated, as have some bacterial forms. General acid/base catalysis is believed to be required (*7, 15*), with a general base removing the proton from the 3-hydroxy group of HMG-CoA prior to cleavage of the C2-C3 bond to form acetoacetate and the enol form of acetyl-CoA. Acetyl-CoA is released after being protonated on C2 by a general acid (Figure 1.8).

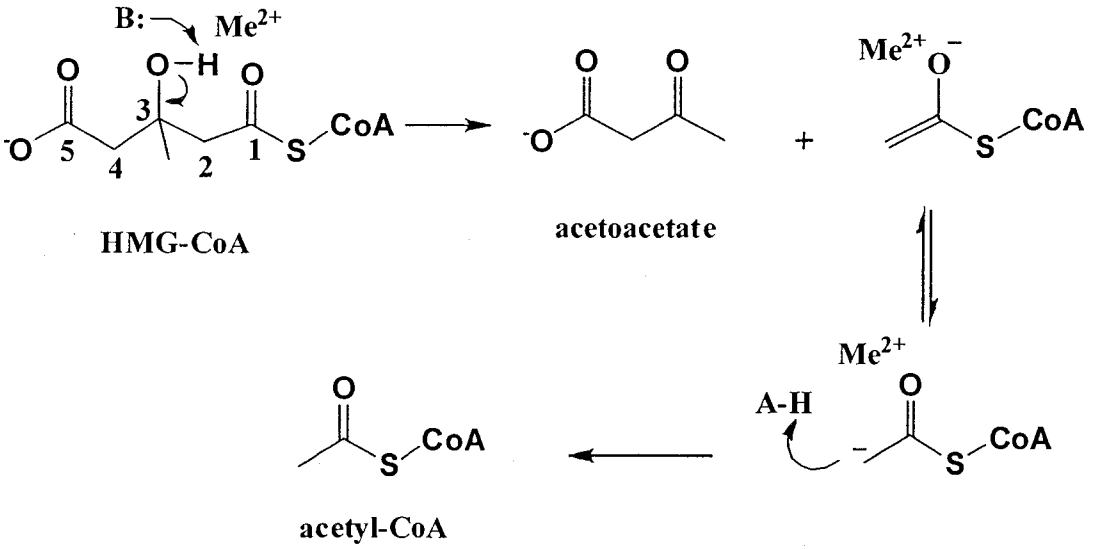

Figure 1.8 Schematic of the proposed mechanism for the reaction catalyzed by HMG-CoA lyase.

Adapted from reference (10).

As indicated in Figure 1.8, HMG-CoA lyase activity requires the presence of a divalent cation, such as Mg^{2+}, Mn^{2+} or Ca^{2+}. The metal ion has been proposed to coordinate the oxygen atoms of the thioester and hydroxyl groups of HMG-CoA, facilitating enolization of the substrate and stabilization of a carbanion intermediate (16). Several active site residues which are conserved in HMG-CoA lyases, including some metal ion ligands, were identified on the basis of characterization of natural or site-directed variants, enzyme kinetics, and NMR studies (*10, 15, 17-19*). The structural similarity of HMG-CoA lyase to DmpG, suggests that comparison to the better-characterized HMG-CoA lyase may provide useful insights into catalysis by DmpG.

Two histidine and one aspartate residue have recently been shown to ligate a metal ion in the crystal structure of HMG-CoA lyase (*6, 7*). Substitution of His233 of human HMG-CoA lyase, the first histidine of the HXH metal-binding motif, with Arg, Ala, or Asp diminished activity by 10^4-fold in comparison with WT lyase. The K_m values of the variants for both substrate, HMG-CoA, and divalent cation were comparable to the values measured for WT, supporting assignment to His233 of a catalytic role (18). Variants of His235, the second histidine in the HXH metal binding motif, exhibited 15-fold reduced catalytic activity and a K_m for substrate increased 4-fold compared with WT. The interaction of enzyme with divalent cation was completely destroyed, indicating that His235 is essential for ligating the metal ion (17). HMG-CoA lyase deficiency can result from mutations at Asp42, which is the conserved aspartate residue involved in metal binding by HMGL-like family proteins. Substitutions that eliminated a carboxyl group at Asp42 perturbed metal ion binding and substantially lowered catalytic efficiency, but did

not impair substrate binding. Such observations support assignment of Asp42 to roles in catalysis and metal ion binding (19).

Active site cysteine and arginine residues have been implicated in catalysis by HMG-CoA lyase. The significant diminution in catalytic efficiency of Cys266 variants, which display no apparent structural perturbations, is consistent with an active site assignment, possibly as a general base catalyst (15). Inspection of the structures of human and bacterial enzymes indicated that this conserved Cys is located on a flexible loop whose position may change upon substrate binding to bring the Cys into close enough proximity to participate in general base catalysis (*6, 7*). There is no comparable Cys residue in DmpG. Arg-41, which corresponds to Arg-17 of DmpG and is also highly conserved in the HMGL-like family, is the best-studied active site residue in HMG-CoA lyase. The variant R41Q is associated with human HMG-CoA lyase deficiency. The R41Q and R41M variants exhibited 10^5-fold and 10^6-fold decreases in activity, respectively, and based on Mn^{2+} binding and affinity labeling stoichiometry, no structural perturbation was observed. Together, these results are consistent with a role for Arg-41 in catalysis. Acetyldithio-CoA, an analogue of the reaction product, acetyl-CoA, was used to further probe the function of Arg-41: proton exchange NMR data suggest it is involved in deprotonation or enolization of acetyldithio-CoA, implicating this residue in the HMG-CoA cleavage reaction chemistry that leads to acetyl-CoA product formation (10).

1.1.2.3 α-Isopropylmalate synthase

α-Isopropylmalate synthase (α-IPMS), which catalyzes acetyl group transfer from acetyl-CoA to α-ketoisovalerate to produce α-isopropylmalate (α-IPM) and CoA, is the first enzyme in the leucine biosynthetic pathway. The crystal structure of α-IPMS from

Mycobacterium tuberculosis, in complex with Zn^{2+} and its substrate, α-ketoisovalerate, was solved recently (PDB entry 1SR9) (8). The enzyme is dimeric and each monomer encompasses an $(\alpha/\beta)_8$ TIM barrel domain, a helical linker domain, and a regulatory domain of novel fold. When the three-dimensional structure of DmpG was aligned with that of *M. tuberculosis* α-IPMS using the EBI SSM program, 16 % sequence identity and 2.09 Å RMSD were observed over a Cα alignment of 240 residues, together with a Q quality score of 0.2 and a Z score of 9.4. The TIM barrel domains of DmpG (sequence 10–249) and α-IPMS (sequence 73–332) matched extremely closely. Furthermore, three residues, Asp-81, His-285 and His-287 of α-IPMS, which are involved in octahedral coordination to Zn^{2+}, are aligned with the metal ligands Asp-18, His-200 and His- 202 of DmpG, respectively. Similar to DmpG, the Zn^{2+} ion of α-IPM synthase is observed in the crystal structure to interact with two carbonyl oxygens of the substrate, α-ketoisovalerate.

1.1.2.4 Transcarboxylase 5S subunit

Transcarboxylase (TC) (EC 2.2.3.1) is a multienzyme complex made up of three different subunits, 12S, 5S and 1.3S, which together transfer a carboxyl group from methylmalonyl-CoA to pyruvate via two carboxylation half-reactions to form oxaloacetate and propionyl-CoA. The 5S subunit of TC catalyzes oxalacetate production by shuttling the carboxyl group from the 1.3S-carboxylated-biotin to pyruvate in the second half reaction. Six 5S structures from *Propionibacterium shermanii* have been published (9), and show significant structural similarity with DmpG at the active site. The catalytically active Co^{2+} locates at the C-terminal of the $(\alpha/\beta)_8$ TIM barrel octahedrally coordinated with Asp-23, His-215, His-217, one H_2O molecule and two carboxylate oxygen atoms of oxaloacetate, the substrate for the back-reaction (PDB

entry 1RQE). These are the metal ligands that are conserved in the other HMGL-like family members.

1.1.2.5 Metal ion involvement in HMGL-like family enzymes and class II aldolases

As discussed above, all HMGL-like family members include a conserved Asp-His-His triad that is observed to coordinate a metal ion in the x-ray structure. In some cases, the metal ion is observed in crystals obtained from solutions without added metal ion (*4, 9*), while for others crystals were obtained from solutions supplemented with metal salts (6-8).

Other types of evidence are consistent with a requirement for more than a single metal in catalysis. HMG-CoA lyase from *Pseudomonas mevalonii* was isolated with tightly-bound Cu^{2+} and while addition of Mn^{2+} (micromolar) or Mg^{2+} (millimolar) to the assay buffer was essential to activate the enzyme, Cu^{2+} or Zn^{2+} addition had no effect on enzyme activity (20). However, for either human or bacterial HMG-CoA lyases crystallized from solutions containing either Mg^{2+} or Ca^{2+}, respectively, only one metal atom was visualized in the active site ligated to the Asp-His-His motif (*6, 7*). A divalent cation was observed in the crystal structure of α-IPM synthase from *Mycobacterium tuberculosis* (8), and has been linked by kinetics studies to catalysis, but a monovalent cation must also be present for optimal activity (*21, 22*). In transcarboxylase 5S from *Propionibacterium shermanii*, one mol of the protein contained two mol of a mixture of Co, Zn and Cu atoms, but only Co^{2+} and Zn^{2+}, rather than Cu^{2+}, could stimulate the enzyme activity (23). In the x-ray structure of the enzyme, only a single bound metal ion was observed at the conserved active site Asp-His-His metal-binding motif typical of the HMGL-like family (9). Although these types of evidence suggest involvement of more

than a single metal ion at the active sites of these enzymes, binding characteristics and roles in catalysis of the second metal ion have not been delineated.

The relatively well-characterized class II fructose-1, 6-bisphosphate aldolases (FBPA) from lower organisms are unrelated to DmpG, although like DmpG they are divalent cation-dependent aldolases which catalyze C-C bond cleavage or condensation within $(\alpha/\beta)_8$ barrel catalytic domains. A divalent cation is an absolute requirement for class II FBPA activity and stability (*24, 25*), and monovalent cation (e.g. K^+) is also required to activate these enzymes [e.g. (24)]. Various divalent cations, such as Zn^{2+}, Co^{2+}, Fe^{2+}, Mn^{2+} and Ni^{2+}, could restore the activity of yeast apo-aldolase to different degrees: Zn^{2+} was found in the native enzyme in the highest amount and was the optimal activator (24). Structural studies of FBPA have revealed binding sites for more than a single divalent cation, although the divalent cation involved in catalysis is ligated to three His residues in all available FBPA structures (25-29). During catalysis, the Zn^{2+} in *E. coli* FBPA is thought to function as a Lewis acid to polarize the carbonyl bond of the substrate, dihydroxyacetone phosphate (25). The other metal ion binding sites identified in several FBPA structures, either for divalent or monovalent cations, are not all identical to one another and may include both specific and non-specific metal binding sites (25-29). The monovalent cation binding site in *E. coli* FBPA is clearly defined and has, on the basis of its position in a complex of enzyme with substrate analogue, been proposed to be involved in tethering substrate at the active site (25).

Characterization of DmpG will add to our understanding of the roles of the metal ion in catalytic activity and structural stability, as well as the mechanism of the enzymes in the HMGL-like family.

1.1.3 Structure and function of DmpF and related enzymes

DmpF is an NAD^+- and CoA-dependent acetaldehyde dehydrogenase which catalyzes oxidation to acetyl-CoA of the intermediate acetaldehyde generated by DmpG. Acetaldehyde is likely to be highly toxic to the cell (30-32). It has been proposed that this intermediate is channeled via a 29 Å long connecting hydrophobic tunnel from the active site of DmpG to that of DmpF where it is converted to the non-toxic and metabolically useful final product, acetyl-CoA (4).

The proposed DmpF active site is positioned between the NAD^+ binding domain and the dimerization domain. The nicotinamide ring of NAD^+, which must accept a hydride from acetaldehyde, is close to a cysteine residue, Cys132, which was proposed to be an essential catalytic residue (Figure 1.9) (*3, 4*). Cysteine residues become more reactive when they are deprotonated, and in the aldehyde dehydrogenase literature there is considerable discussion about the structural basis for active site thiol activation (33-41). In the apo (ligand-free) structure of DmpF, a water molecule is positioned within H-bonding distance of Cys132 and also within H-bonding distance of an aspartate residue, Asp209. Interestingly, the water molecule is not present in the holo (NAD^+-bound) structure and the cysteine side chain adopts two conformations, one similar to that in the apo enzyme and one where the thiol group is pointing towards the cofactor, suggesting that it may function in water mediated proton abstraction from Cys132 (4). Thus, it was proposed that in the absence of the cofactor, Cys132 is first activated by Asp209 via a water molecule: this facilitates binding of NAD^+, the presence of which also accelerates the DmpG reaction.

Aldehyde dehydrogenases comprise a superfamily in which members may be classified into two families on the basis of cofactor dependence: the $NAD(P)^+$-dependent, CoA-independent enzymes and the $NAD(P)^+$- and CoA-dependent family. Two subfamilies are included in the former group of enzymes. One subfamily consists of phosphorylating $NAD(P)^+$-dependent aldehyde dehydrogenases, which reversibly oxidize the aldehyde substrate to a phosphoester with the participation of inorganic phosphate (42-44). The other subfamily includes the non-phosphorylating $NAD(P)^+$-dependent aldehyde dehydrogenases, which irreversibly oxidize the aldehyde substrate to the corresponding acid (*33, 45*). Both CoA-dependent and phosphorylating $NAD(P)^+$-dependent aldehyde dehydrogenases follow ping-pong reaction mechanisms during catalysis, where NAD(P)H is released prior to the binding of the last substrate (inorganic phosphate or coenzyme A). By contrast, non-phosphorylating $NAD(P)^+$-dependent aldehyde dehydrogenases follow an ordered sequential kinetic mechanism with NAD(P)H dissociating last (*34, 46*).

In spite of the different kinetic mechanisms, both phosphorylating (*42, 43*) and non-phosphorylating $NAD(P)^+$-dependent aldehyde dehydrogenases (*33, 45*) share a similar two-step chemical reaction which involves the acylation and deacylation of a conserved cysteine residue in the active site of the enzyme (Figure 1.10). In the first step, the activated cysteine thiolate group nucleophilically attacks the carbonyl carbon of substrate aldehyde to form a thiohemiacetal enzyme complex. This is followed by hydride transfer to $NAD(P)^+$, resulting in a covalent acylenzyme intermediate. Finally, the acyl group is displaced by an inorganic phosphate, or hydroxyl group from water, via a nucleophilic reaction to form a phosphoester or an organic acid product, respectively.

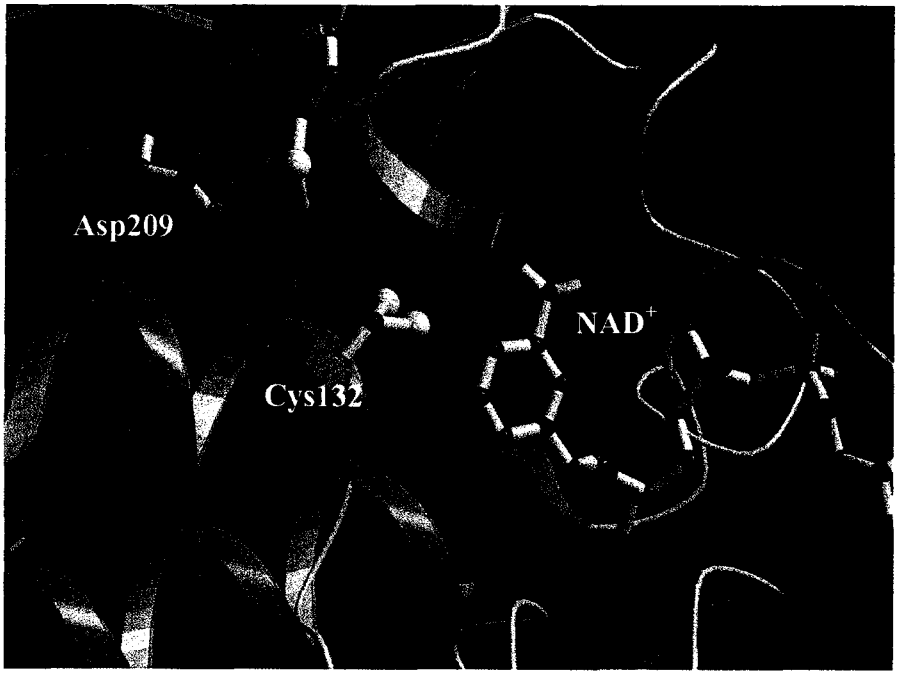

Figure 1.9 The proposed active site of DmpF in complex with the cofactor, NAD^+.

The Asp209 residue of DmpF is located where it may act as a general base for activation of the essential Cys132 via an H_2O molecule (not shown) during the DmpF reaction (Figure prepared using PyMol on the basis of PDB entry 1NVM).

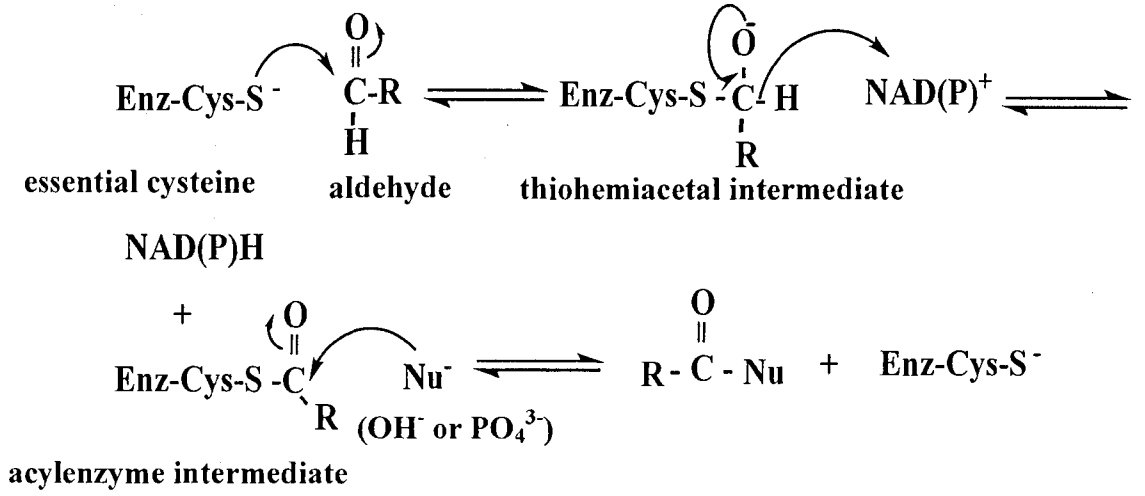

Figure 1.10 Proposed catalytic mechanism of $NAD(P)^+$-dependent, CoA-independent aldehyde dehydrogenase.

See text for a description.

The architectures of a thiohemiacetal complex and an acylenzyme intermediate were characterized in two recently-solved crystal structures of aspartate-β-semialdehyde dehydrogenase, which is a representative of the phosphorylating $NAD(P)^+$-dependent aldehyde dehydrogenases (*35, 47*). The structure of the thioacylenzyme intermediate of the E268A-glyceraldehyde 3-phosphate dehydrogenase from *Streptococcus mutans* provides similar insights into the catalytic mechanism of the non-phosphorylating $NAD(P)^+$-dependent aldehyde dehydrogenases (36). The acylation and deacylation mechanisms for phosphorylating and non-phosphorylating $NAD(P)^+$-dependent aldehyde dehydrogenase appear to be different. The phosphorylating $NAD(P)^+$-dependent enzymes have been proposed to involve a catalytic triad in activation of the essential active site cysteine (*35, 37, 38*). There is still discussion about the detailed catalytic mechanism for the non-phosphorylating $NAD(P)^+$-dependent ALDHs (*33, 34, 36, 39-41*). The idea that the activation of the essential cysteine is induced by the protein environment has been proposed (*39, 41*).

The $NAD(P)^+$-and CoA-dependent aldehyde dehydrogenase subfamily, which includes DmpF, is one of the classes that has not been well characterized in the aldehyde dehydrogenase extended family. Most of the studies in the literature have focused on the kinetics of a few of these enzymes (48-54). As is the case for the phosphorylating $NAD(P)^+$-dependent aldehyde dehydrogenases, the $NAD(P)^+$- and CoA-dependent enzymes have also been postulated to catalyze reactions involving covalent acyl-S-enzyme intermediates (*48, 49, 52, 54*). However, the existence of such acylenzyme intermediates has not been reported in the literature. Interestingly, CoA-mediated inhibition has been observed and shown to involve the formation of a dead-end E−CoA

inhibition complex (52).

Details of the structure and function of the $NAD(P)^+$- and CoA-dependent aldehyde dehydrogenase enzymes are still far from being understood. Characterization of DmpF will not only provide insight into the cofactors' binding sites, catalytic mechanism, and the substrate-mediated inhibition of this enzyme and of its relatives, but also help to address substrate intermediate acetaldehyde channeling and regulation of DmpF in complex with DmpG.

1.1.4 Substrate Intermediate Channeling of DmpFG

Channeling of intermediates in enzyme reactions involves movement of reaction intermediates between distant active sites within a multi-step enzymatic transformation (*55, 56*). Specifically, the intermediate is passed to the next active site without prior dissociation into the bulk solvent by free diffusion. Intermediate substrate channeling has many advantages over the free diffusion of reaction intermediates within the bulk cellular environment. First, it prevents the loss of intermediates by diffusion and speeds up the rate of the overall enzymatic reaction since the path taken by the intermediate is more direct. Second, it avoids unfavorable equilibria and kinetics that may occur within the cellular environment. In particular, competing enzymatic or non-enzymatic transformations within the cell can be avoided by maintaining the intermediate in a sequestered milieu. Third, an intermediate that is toxic or unstable that is channeled provides a mechanism whereby the cell and the intermediate can be protected. Fourth, since the highly dense nature of the cell cytoplasm results in very scarce solvation capacity, sequestering the intermediate from the cellular environment can conserve this

solvation capacity. Finally, channeling decreases the unfavorable energetics associated with desolvation of the intermediate.

Various data are consistent with the existence of a channelling mechanism for transferring acetaldehyde between DmpG and DmpF active sites. For example, the two proteins are physically associated with one another to form the biological active heterotetramer (F2G2) (*1, 2*). Furthermore, the aldolase reaction is significantly enhanced in the presence of a cofactor, NAD^+, which is likely bound to the dehydrogenase active site (2). More directly, the crystal structure of DmpFG indicates the presence of a 29Å hydrophobic channel extending from the DmpG active site towards the active site of DmpF upon the binding of cofactor NAD^+ (4). Thus, the structure of this complex would support transport or channeling of the toxic acetaldehyde intermediate from the active site of DmpG, where it is generated, to DmpF, where it is converted to acetyl-CoA. In the absence of the NAD^+ cofactor this tunnel does not extend all the way to the active site of DmpF, suggesting that binding of NAD^+ at the active site of DmpF is essential to control the movement of the intermediate between distant active sites by inducing domain movement of DmpF. This may facilitate the DmpF active site's ability to accept the intermediate and has been proposed to be crucial for efficient channeling (4).

1.2 Thesis Objectives

DmpFG, a bifunctional enzyme, has both a divalent cation-dependent class II aldolase (DmpG) activity and an NAD^+/CoA-dependent acetaldehyde dehydrogenase (DmpF) activity (2). This enzyme is involved in the bacterial degradation of phenol and methyl-substituted phenols, and its many homologues are found in bacterial catabolic pathways for degradation of other aromatics, such as naphthalene, salicylate, toluene and biphenyl

(57). Relatively little has been reported on the characteristics of DmpFG, or related enzymes in aromatic catabolism, so learning more about how they function will fill a gap in our knowledge of the enzymology of these pathways. In addition, studies of these enzymes will lead to improved understanding of how microbes accomplish the task of degrading relatively inert and often toxic aromatic compounds.

DmpG belongs to the newly-identified HMGL-like family, members of which share similar active site structures inside an $(\alpha/\beta)_8$ TIM barrel fold: these enzymes catalyze diverse C-C bond cleavage reactions and are believed to employ a common catalytic reaction mechanism (58). However, we are still far from a complete understanding their catalytic mechanisms, with unresolved questions such as existence of enolate intermediates during the reaction, and the identities of residues involved in catalysis (6). Crystal structures of DmpFG and a complex of DmpFG with substrate analogue have suggested residues that could be targeted for site-directed mutagenesis (4) to help address such questions, contributing to the broader picture of the whole HMGL-like family.

A second topic, about which little is currently known, is the function of the bound metal ion in DmpG and other HMGL-like family members. Different divalent metal ions show varying ability to activate these enzymes and active site variants, while others, including some that activate other aldolases, have no effect on activity, or even inhibit. Although a metal ion is observed in the crystal structure of DmpG and other HMGL-like family members, it is not currently known how much it contributes to catalysis, enzyme stability, or even whether it is the only metal ion that binds at the active site. Based on what is already known about DmpFG and a survey of the literature of HMGL-like family

proteins (*6-9, 59, 60*), as well as class II fructose-1, 6-bisphosphate aldolases (FBPA) (*24, 25, 61, 62*), the bound metal ion in DmpG may function to stabilize the DmpFG complex, participate in substrate binding and/or contribute to DmpG catalysis. Site-directed mutagenesis, enzyme kinetics and ICP-MS techniques are combined here to investigate these possible functions.

Glyceraldehyde-3-phosphate dehydrogenase (phosphorylating, GAPDH), is the best-characterized structurally similar aldehyde dehydrogenase to DmpF (*37, 38, 42, 43, 63, 64*) . Thus, it provides an instructive model for probing DmpF catalytic mechanism, despite the fact that GAPDH is not CoA dependent. In general, the NAD^+/CoA-dependent aldehyde dehydrogenases have not previously been subjected to structural and structure-function studies, with literature about them mostly limited to few detailed steady-state kinetics studies (*49, 51, 52*). In this thesis, the binding site of the coenzyme A cofactor is investigated by coupling hydrogen–deuterium exchange with mass spectrometric analysis after proteolysis. Aspects of the catalytic mechanism of DmpF are studied, such as kinetics, site-directed mutagenesis of Cys132, formation of acetyl-Cys132 intermediate enzyme complex, and reaction of Cys132 with substrate-derived inhibitors. The characterization of DmpF adds to our knowledge of a relatively poorly-understood subfamily of the aldehyde dehydrogenase superfamily.

Several lines of evidence suggest that the tight association of DmpG and DmpF is to allow acetaldehyde channeling from the aldolase active site to the dehydrogenase active site without free diffusion via the bulk solution (*3, 4*). However, the functional significance of the tunnel architecture and its regulation remain unexamined. Channeling has been unequivocally demonstrated in relatively few enzymes (65-69), so future studies

of channeling in DmpFG will increase our knowledge in this area. The work done here on catalytic properties of the two active sites is a useful and necessary prelude to channeling studies in the future.

Chapter 2 A Shared Binding Site for NAD^+ and Coenzyme A in an Acetaldehyde Dehydrogenase Involved in Bacterial Degradation of Aromatic Compounds

2.1 Abstract

The *meta*-cleavage pathway for catechol is a central pathway for the bacterial dissimilation of a wide variety of aromatic compounds, including phenols, methylphenols, naphthalenes, and biphenyls. The last enzyme of the pathway is a bifunctional aldolase/dehydrogenase that converts 4-hydroxy-2-ketovalerate to pyruvate and acetyl-CoA via acetaldehyde. The structure of the NAD^+/CoASH-dependent aldehyde dehydrogenase subunit is similar to that of glyceraldehyde-3-phosphate dehydrogenase, with a Rossmann fold-based NAD^+ binding site observed in the NAD^+–enzyme complex [Manjasetty, B. A., et al. (2003) *Proc. Natl. Acad. Sci. U.S.A*, *100*, 6992-6997]. However, the location of the CoASH binding site was not determined. In this study, hydrogen–deuterium exchange experiments, coupled with peptic digest and mass spectrometry, were used to examine cofactor binding. The pattern of hydrogen–deuterium exchange in the presence of CoASH was almost identical to that observed with NAD^+, consistent with the two cofactors sharing a binding site. This is further supported by the observations that either CoASH or NAD^+ is able to elute the enzyme from an NAD^+ affinity column and that preincubation of enzyme with NAD^+ protects against inactivation by CoASH. Consistent with these data, models of the CoASH complex generated using AUTODOCK showed that the docked conformation of CoASH can fully occupy the cavity containing the enzyme active site, superimposing with the NAD^+ cofactor observed in the X-ray crystal structure. Although CoASH binding Rossmann folds have been described previously, this is the first reported example of a Rossmann fold that can alternately bind CoASH or NAD^+ cofactors required for enzymatic catalysis.

2.2 Introduction

Aldehyde dehydrogenases make up a diverse group of enzymes that are present in a wide variety of organisms including mammals, plants, bacteria, and fungi. These enzymes may be categorized on the basis of cofactor dependence: (i) $NAD(P)^+$-independent aldehyde dehydrogenases such as EC 1.2.99.3 and EC 1.2.7.5, which are found in some bacteria (*70, 71*); (ii) $NAD(P)^+$-dependent aldehyde dehydrogenases such as EC 1.2.1.3 and related enzymes, which have been isolated from both prokaryotes and eukaryotes (72-74); and (iii) $CoASH/NAD(P)^+$-dependent aldehyde dehydrogenases such as EC 1.2.1.10 and EC 1.2.1.27 , which are mainly associated with a few species of bacteria (*48-54, 75-77*). While $NAD(P)^+$-dependent members of the aldehyde dehydrogenase (ALDH) extended family have been well characterized (72-74), $CoASH/NAD(P)^+$-dependent aldehyde dehydrogenases have received much less attention.

The literature on $CoASH/NAD(P)^+$-dependent aldehyde dehydrogenases focuses mainly on the steady-state kinetics and some other properties of a few individual members (*48-54, 77*). For example, a relatively well-characterized coenzyme A-linked aldehyde dehydrogenase from *Clostridium kluyveri* (52) catalyzes the transformation of acetaldehyde to acetyl-CoA accompanied by NAD^+ reduction with a pH optimum of 9.1. On the basis of initial velocity and product inhibition experiments, a ping-pong mechanism was proposed. Thus, NAD^+ and acetaldehyde bind first, NADH is released prior to CoASH binding, and then the final product, acetyl-CoA, is released. Formation of an acetyl–enzyme intermediate during the reaction was postulated. Interestingly,

inhibition by CoASH was also reported, and the formation of a dead-end E–CoASH inhibition complex was demonstrated (52).

DmpF (EC 1.2.1.10) is the only CoASH/NAD(P)$^+$-dependent aldehyde dehydrogenase for which a high-resolution structure has been published. DmpF and DmpG form an active heterotetramer (F_2G_2) which catalyzes the last two reactions in the *meta*-cleavage pathway of phenol degradation in *Pseudomonas* sp. strain CF600 (2). DmpG (EC 4.1.3.39) is a type II aldolase that converts 4-hydroxy-2-ketovalerate to acetaldehyde and pyruvate, while DmpF catalyzes the transformation of acetaldehyde to acetyl-CoA using NAD$^+$ and CoASH. The X-ray structure of DmpFG (4) shows eight polypeptide chains in the asymmetric unit: four DmpGs (A, C, E, and G) and four DmpFs (B, D, F, and H) that form two heterotetramers each with a molecular mass of 280 kDa. DmpF comprises two domains, including the NAD$^+$ binding domain (residues 1–130 and 286–312), and the dimerization domain (residues 131–285) which mediates the interaction with DmpG.

The NAD$^+$-binding domain of DmpF is similar to that of glyceraldehyde-3-phosphate dehydrogenase (phosphorylating) (4). Sequence analysis using the Pfam database (78) shows that the NAD$^+$ -binding domain belongs to the NADP_Rossmann clan and most closely resembles the family Semialdhyde_dh with an *E* value of 1.4×10^{-24}: the structure of aspartate semialdehyde dehydrogenase, also a phosphorylating enzyme, has an NAD$^+$ binding fold similar to that of glyceraldehyde-3-phosphate dehydrogenase (79). By contrast, another CoASH/NAD(P)$^+$-dependent enzyme, methylmalonate semialdehyde dehydrogenase (EC 1.2.1.27), is instead structurally related to the large superfamily of nonphosphorylating aldehyde

dehydrogenases and is the only member which is CoASH-dependent (*74, 77, 80*). As discussed below, DmpF, like glyceraldehyde-3-phosphate dehydrogenase (phosphorylating), binds NAD^+ via a canonical Rossmann fold. By contrast, nonphosphorylating aldehyde dehydrogenases exhibit noncanonical Rossmann folds for NAD^+ binding (*33, 80-82*). Thus, CoASH-dependent aldehyde dehydrogenases belonging to the two families may bind CoASH differently. However, no structure has yet been published for a member of either class in complex with CoASH.

Two glycine-rich motifs that are characteristic of nucleotide binding domains are found in DmpF: $G_{11}XGXXG_{16}$ is located between the loop following the first β strand and the adjacent α helix of the Rossmann fold, and $G_{165}XGXXA_{170}$ in the loop adjacent to α8, in the α9 helix and in its following loop, which are located in the dimerization domain (Figure 2.1). The NAD^+-binding Rossmann fold consists of one each of $(\beta\alpha)_3$ and $(\alpha\beta)_3$ units in which the $(\beta\alpha)_3$ unit (residues 5–65) is mainly involved in AMP moiety binding and the $(\alpha\beta)_3$ unit (residues 67–128) is mainly responsible for NMN moiety binding (Figure 2.2): these units are connected via the α3 and α4 helices. Like glyceraldehyde-3-phosphate dehydrogenase (phosphorylating) and aspartate semialdehyde dehydrogenase, the dimerization domain of DmpF is also involved in NAD^+ binding, mainly via the NMN moiety. The AMP portion of bound NAD^+ is closest to the outside environment, while the NMN portion is located in the interior of the protein and encompassed by both NAD^+ binding and dimerization domains.

The conformation of NAD^+ when bound to DmpF is very similar to the conformation

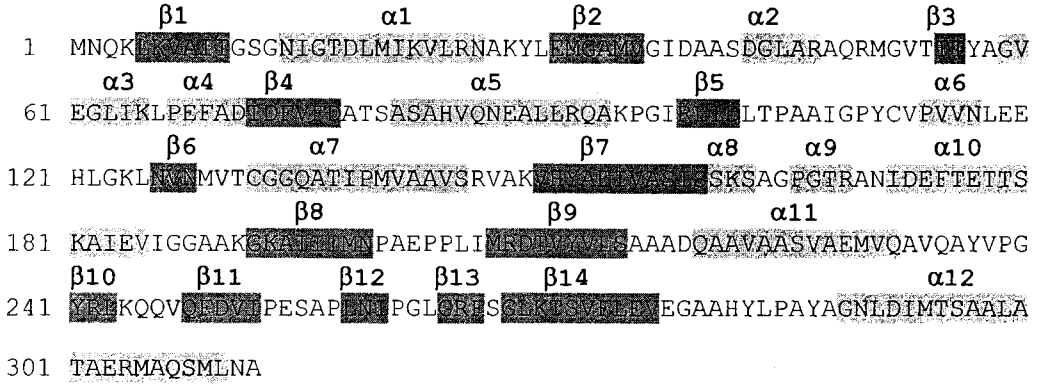

Figure 2.1 Secondary structural elements of DmpF.

Residues shaded dark grey highlight β strands, while residues shaded light gray highlight α-helical regions (derived from PDB entry 1NVM).

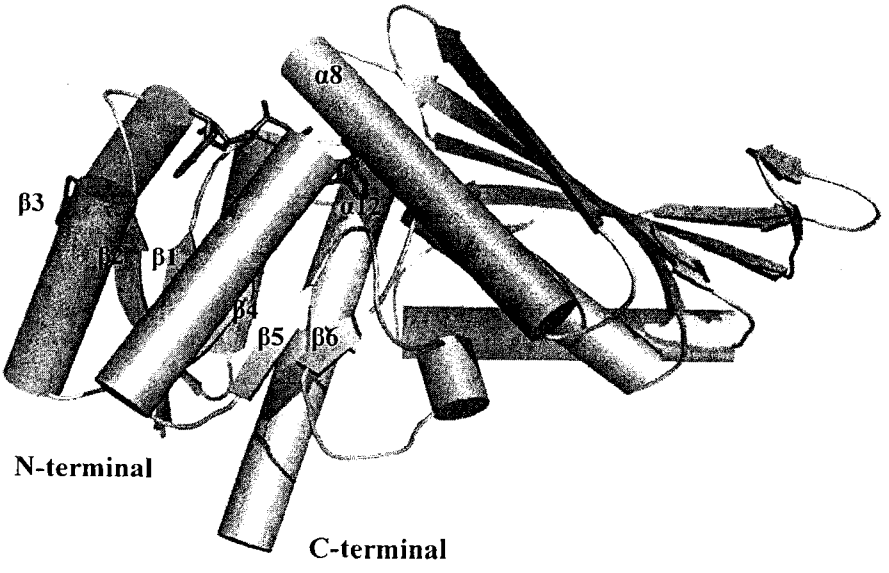

Figure 2.2 Structural overview of the NAD^+–DmpF complex.

β1-β6 represents the six-stranded parallel sheet that comprises the typical Rossman fold mainly involved in AMP binding; α8 and α12 are mainly responsible for the NMN binding together with other structural elements (derived from PDB entry 1NVM).

observed in complex with glyceraldehyde-3-phosphate dehydrogenase from *Bacillus stearothermophilus* (PDB entry 1GD1) (*4, 83*). Thus, both the adenine and nicotinamide rings are in anti conformations and approximately perpendicular to the adjacent ribose rings. The two ribose ring planes are perpendicular to each other. The AMP portion is more elongated than the NMN portion, and both moieties are on the same side relative to the phosphates. The NMN moiety is in the proximity of the rest of the molecule, so it is only half the distance from the nicotinamide group to the closest phosphate as it is in bound NAD^+ on other enzymes such as horse liver alcohol dehydrogenase (PDB entry 2OHX) (*84*).

Although a structure of the NAD^+–DmpF complex has been obtained using X-ray crystallography, the mode of binding of coenzyme A has not been defined. In this study, we have used hydrogen–deuterium exchange experiments to probe the binding of CoASH and have found that this cofactor shares the same binding site as NAD^+.

2.3 Experimental Procedures

Bacterial Strains and Plasmids of Escherichia coli. XL2-Blue was used for DNA and plasmid amplification, and proteins were expressed in *E. coli* C41(DE3) (*85*). DNA manipulations were performed using standard protocols (*86*). A subclone of pVI150, pVI1316Δ (1), was digested with *Xho*II to generate a 3757 bp fragment that was subsequently ligated into the *Bam*HI site of the pT7.5 expression vector (*87*). Orientation was checked by restriction enzyme digestion. The *dmpFG* coding region was thus inserted downstream from the T7 promoter, to give plasmid construct pT7.5-*dmpFG*.

Bacterial Growth. The pT7.5-*dmpFG* plasmid (10 ng) was transformed into *E. coli* C41(DE3) competent cells by incubating the mixture on ice for 15–20 min. Cells (50 μL)

were then spread onto LB agar plates to grow overnight at 37 °C using carbenicillin selection (100 μg/mL). LB medium (10 mL) was added to each plate to suspend the colonies. After transfer of the suspended cells into 1 L of fresh LB medium containing ampicillin (100 μg/mL), cells were grown for ~ 2 h until the OD_{600} reached 0.8–1, at which point IPTG (1 mM) was added to induce protein overexpression. Cells were allowed to grow for an additional 3 h before being harvested. After being washed with 50 mM Na^+ K^+ phosphate buffer (pH 7.5), cell pellets were stored at −80 °C until they were used.

Preparation of Affinity Resin. N^6-carboxymethyl-NAD^+ was synthesized essentially as described by Tynan et al. (*88*). An excess of N^6-carboxymethyl-NAD^+ was coupled at 4 °C to EAH-Sepharose (GE Healthcare) using 1-ethyl-3-[3-(dimethylamino)propyl]carbodiimide, essentially as described by the manufacturer except that pH was maintained between 4.5 and 5.5 by the addition of HCl, as described in reference (*88*). After incubation overnight, the resin was washed thoroughly using several alternating aliquots of 0.1 M sodium acetate (pH 4), containing 0.5 M NaCl, and 0.1 M Tris-HCl (pH 8), containing 0.5 M NaCl. A final wash of 20% ethanol was applied.

Protein Purification. Compared to the previously published method (2), the steps for purifying DmpFG were simplified to DEAE and NAD^+-linked affinity columns, combined with an ammonium sulfate fractionation step. The buffer used for purification was 50 mM Na^+ K^+ phosphate (pH 7.5) containing 1 mM DTT (PD buffer) unless otherwise specified, and all the purification steps were carried out at 4 °C. Approximately 25 g of cell paste from 6 L of culture was resuspended in ~50 mL of PD buffer, and a

spatula tip of DNase I was added. Cell suspensions in a salt/ice bath were sonicated in 30 mL batches with a Branson model Sonifier 250 at an output setting of 60 for 10 × 25 s. The cell debris was removed by ultracentrifugation for 1 h at 62000g. The clear supernatant, termed crude extract, was carefully transferred to a 100 mL cylinder and then applied to a Fast-Flow DEAE-Sepharose column (36.5 cm × 2.6 cm) equilibrated with PD buffer. After the sample had been loaded, the column was washed with PD buffer (100 mL) and then with PD buffer containing 50 mM NaCl (200 mL) at a flow rate of 6 mL/min. A linear gradient of 0.05 to 0.275 M NaCl in PD buffer (750 mL/750 mL) was applied at the rate of 6 mL/min. Fractions (12 mL) were collected, and those with high CoASH-dependent acetaldehyde dehydrogenase specific activity were combined. DmpFG was precipitated with 55% saturated ammonium sulfate and then kept in an ice bath for least 30 min before being collected by centrifugation. The protein precipitate was dissolved in PD buffer to a total volume of 5 mL. After being desalted with a PD-10 column, the protein was applied to an NAD^+ affinity column (3.3 cm × 1.7 cm). The column was washed with 25 mL of PD buffer and then eluted using 0.1 M NaCl in PD buffer. Fractions (2 mL) were collected, and those with high dehydrogenase specific activity were combined. The sample was exchanged with 50 mM Na^+ K^+ phosphate (pH 7.5) containing 0.5 mM TCEP-HCl two to five times and then finally concentrated to ~2 mL. This operation was performed by ultrafiltration using an Amicon concentrator equipped with a YM-30 membrane. The concentrated protein was aliquotted into microfuge tubes (20–50 μL/tube) and then stored at −80 °C. The activity was stable for at least 6 months (2).

Deuterium Exchange Experiments. Deuterium exchange experiments essentially followed previously published methods (*89-91*). The pH measurements were performed with an Orion Micro-Combination pH/Sodium Electrode 98−10. All pH values of D_2O-containing buffers reported here were corrected using the equation pH= pD + 0.3139x + 0.0854x^2 (*92*) , where pD is the pH meter reading of the buffer and x is the fraction of deuterium. Three different samples were equilibrated at 25 ^{0}C for 1 h: (1) 22 μL of DmpFG protein [8.53 mg/mL, 121.8 μM, in 50 mM Na^+ K^+ phosphate buffer (pH 7.5) containing 0.5 mM TCEP-HCl] with 5.5 μL of 50 mM Na^+ K^+ phosphate buffer (pH 7.5) containing 0.5 mM TCEP-HCl; (2) 22 μL of DmpFG protein with 5.5 μL of 10.1 mM NAD^+ in 50 mM Na^+ K^+ phosphate buffer (pH 7.5) containing 0.5 mM TCEP-HCl; and (3) 22 μL of DmpFG protein with 5.5 μL of 11.5 mM CoASH in 50 mM Na^+ K^+ phosphate buffer (pH 7.5) containing 0.5 mM TCEP-HCl.

The H–D exchanges were initiated by transferring the equilibrated samples with multichannel pipettors to aliquots (192.5 μL) of 50 mM Na^+ K^+ phosphate D_2O buffer (pH 7), 25 °C, without cofactors, with NAD^+ (2.05 mM), or with CoASH (2.3 mM). These reaction mixtures were contained in 250 μL thin-walled PCR tubes inserted in a metal heat block kept in a 25 °C water bath. The H–D exchange reactions were thus carried out at 25 °C, at pH 7.09, and with 87.5% D_2O buffer. At various time points, 20 μl of each of the three different samples was transferred to mixtures in PCR tubes containing 110 μL of 0.12% TFA and pellet from 80 μL of immobilized pepsin slurry (on cross-linked 6% agarose beads, 2–3 mg/mL of gel, purchased from Pierce Chemical Co.). Mixing with TFA resulted in a pH of 2.56, effectively quenching the exchange, with the PCR tubes kept at 0 °C by insertion in a metal block which was incubated in an ice/salt

water bath. The immobilized pepsin had been prepared by being washed six times with 0.05% TFA (pH 2.41), and in separate experiments monitored using SDS–PAGE it was established that the pellet from 80 μL of the immobilized pepsin slurry was sufficient to digest completely the DmpFG protein in these samples (data not shown). To facilitate digestion efficiency, up-and-down operation of a multiple-channel pipettor was used to mix the protein and the immobilized pepsin. After 5 min, the digested samples were separated from immobilized pepsin by centrifugation in a microfuge at top speed for 40 s; the supernatants were then aliquoted into thin-wall PCR tubes and frozen in liquid nitrogen. The frozen samples were stored at –80 °C prior to mass spectrometry analysis.

In- and Back-Exchange Controls for Deuterium Incorporation. The extent of deuterium incorporation into each peptic peptide must be adjusted for deuterium gain and loss during quench, peptic digestion, and mass spectrometric analysis. The amount of deuterium lost and gained from a partially deuterated peptide may be estimated from the amount of deuterium lost from a completely exchanged peptide ("back-exchange" or "100% control") and gained from a unexchanged peptide ("in-exchange" or "0% control"), respectively. The in- and back-exchange control experiments were carried out according to methods described previously (*91, 93*). The in-exchange control (0% control) was performed by addition of 2 μL of DmpFG protein to the 0 °C mixture of 110 μL of 0.12% TFA and a pellet from 80 μL of immobilized pepsin slurry, 0.5 μL of 50 mM Na^+ K^+ phosphate H_2O buffer (pH 7.5), and 17.5 μL of 50 mM Na^+ K^+ phosphate D_2O buffer (pH 7). The digestion and associated procedures were the same as those in the deuterium exchange experiments reported above. The back-exchange control (100% control) was started by dissolving the peptic digest of DmpFG dried from the

unexchanged control sample (prepared as described below) in 2.5 μL of H_2O and 17.5 μL of D_2O, producing a mixture containing concentrations of peptides, buffer, and deuterium corresponding to those of the H–D exchange experiments. Samples were then incubated at 25 °C for 2 h to ensure 100% deuterium replacement of the amide hydrogens in the peptides derived from the intact protein. After addition of 110 μL of 0.12% TFA at 0 °C, samples were incubated at 0 °C for the same time period required for sample quenching to pepsin bead isolation, as in the deuterium exchange experiments.

Measurements of Protected Amide Hydrogens, Incorporated Deuterons and Their Exchange Rate Constants for Peptic Digests of DmpFG. The matrix used in the MALDI experiments was α-cyano-4-hydroxycinnamic acid (5 mg/mL) in acetonitrile/99% ethanol/0.07% TFA mixture (1:1:1) (pH 2.5). The matrix solution was kept at 0 °C before use. Frozen sample digests were thawed rapidly, and 10 μl was mixed with an equal volume of matrix; 0.7 μL of the mixture was spotted onto the chilled target plate. The sample spots were dried with a stream of nitrogen gas over ~ 1 min. The spotted and dried target plate was transferred as quickly as possible to the mass spectrometer. The spectra were collected using a Micromass M@LDI-LR TOF mass spectrometer. Spectra were obtained for both deuterium-exchanged samples and unexchanged controls in which the sample was prepared under identical conditions except that buffer prepared with H_2O was substituted for D_2O-containing buffer: these samples were used for sequencing peptides using ESI-Q-TOF MS/MS (details below).

By comparing the spectra of exchanged samples with those of unexchanged controls, we identified the peptides with deuterium incorporation. When masses of peptides from H–D experiments with cofactors shifted at least 0.5 Da lower relative to those incubated

without cofactors, peptides were considered to have undergone amide hydrogen protection by cofactor binding. The number of amide hydrogens protected was estimated by comparing mass differences of the H–D exchange peptides from incubations with and without cofactor. The number of deuterons incorporated into peptic digest peptides of DmpFG was calculated using the equation $D = (m_t - m_{0\%}) \times n/(m_{100\%} - m_{0\%})$, where D is the adjusted number of deuteriums incorporated at time point t; m_t, $m_{0\%}$ and $m_{100\%}$ are the observed masses of a peptide at time point t, time zero (0% control), and fully exchanged (100% control), respectively, and n is the total number of peptide amide hydrogens. The rate constants for deuterium exchange were obtained by fitting the data to a double exponential model using SigmaPlot 9.0 with the equation $D = N_1(1\text{-}e^{-k_1 t}) + N_2(1\text{-}e^{-k_2 t})$, where D is the total number of incorporated deuterons at time t, and N_1 and N_2 are the numbers of deuterons exchanging at rate constants k_1 and k_2, respectively. A mixture of six standards, bradykinin (1060.569 amu), angiotensin I (1296.687 amu), Substance-P (1347.736 amu), Glu-fibrino peptide (1570.677 amu), renin (1758.933 amu) and ACTH (18-39clip, 2465.199 amu), was used to calibrate the instrument. Internal lockmass corrections using ACTH (18-39clip, 2465.199 amu) were used to improve the mass accuracy.

Identification of the Peptic Digests of DmpFG. Using the unexchanged control sample, accurate masses of peptic digests of DmpFG were calculated on the basis of m/z data of ESI-Q-TOF spectra. The peptides were preliminarily identified on the basis of accurate masses by searching DmpFG sequence data with the ExPASy-FindPept tool (*94*). Typically, several possible peptides of DmpFG were indistinguishable since insufficient mass accuracy was obtained in the ESI-Q-TOF measurement, and therefore, peptide

sequencing was carried out using a Waters CapLC system interfaced with an ESI-Q-TOF 2 mass spectrometer. Peptic digests of DmpFG (5 μL) were loaded onto a Symmetry 300 C18 trap column (0.35 mm × 5 mm), for desalting and concentration, followed by elution onto an Atlantis dC C18 NanoEase column, (75 μm × 100 mm). Mobile phase A consisted of formic acid (0.1%) and acetonitrile (3%), while mobile phase B consisted of formic acid (0.1%) and acetonitrile (97%). The CapLC system was equilibrated with a mixture of 95% solvent A and 5% solvent B. The samples were loaded and desalted for 6 min in the trap column (20 μL/min) with the equilibration solvent. Then the flow was switched to the separating column, and a gradient from 5 to 50% mobile phase B was run (6 μL/min) over 50 min, followed by 5 min with 50% B, and then an increase to 95% B over 10 min. After the survey scan had been performed, MS/MS was performed online as peptides eluted from the column, selecting individual peptide precursors: the collision-induced dissociation (CID) energy used for fragmentation was between 25 and 48 eV depending on the mass and charge state of the precursor ion. The peptides picked for MS/MS were mainly those with double and triple charges, and a few with quadruple and quintuple charges.

The raw data from MS/MS of peptic digests of DmpFG were first processed using MaxEnt3 and then loaded into the peptide sequencing program of the BioLynx module of MassLynx version 4.0. The sequence predictions were finally obtained by performing the automated MassSeq approach which often gave a partial sequence of the peptide. A combination of accurate mass and partial sequencing information resulted in the final assignments for peptic digests of DmpFG (*95*). The Q-TOF 2 instrument calibration was

achieved via MS/MS of human [Glu^1]-fibrinopeptide B (1569.6698 Da). The voltage on the capillary probe tip was set to 3.3 kV, and the voltage on the sample cone was 43 V.

Enzyme Kinetic Experiments. Acetaldehyde dehydrogenase activity was monitored by the reduction of NAD^+ at 340 nm in the presence of acetaldehyde and CoASH.

The apparent K_m values for NAD^+ and CoASH were estimated from initial rate measurement in 50 mM HEPES buffer (pH 8.0) containing 1 mM DTT at 25 °C. The reactions were started by addition of DmpFG protein (0.75 μg/mL) to the assay mixture containing substrates NAD^+, CoASH, and 38.4 mM acetaldehyde.

The examination of the effects of coenzyme A on DmpF was performed at pH 7, in 50 mM Na^+ K^+ phosphate buffer at 25 °C. The DmpFG sample was buffer-exchanged with 50 mM Na^+ K^+ phosphate buffer (pH 7), and TCEP-HCl was removed prior to further experiments. The assay mixtures contained 3.0 μg/mL of DmpFG protein, 75.1 μM CoASH 15.5 mM acetaldehyde, and various concentrations of NAD^+. To examine interactions of CoASH with DmpF, the following experiments were performed. The standard assay to which others were compared was initiated by addition of enzyme as the last component of the assay mixture. To test possible inhibition by CoASH, the enzyme was incubated with CoASH before addition of other components, and the reaction was initiated by addition of acetaldehyde. To examine whether NAD^+ could protect against inhibition by CoASH, the enzyme was incubated with NAD^+ prior to CoASH, and then the reaction was started by addition of acetaldehyde. The effects of DTT were tested using the same procedure as the CoASH inhibition assay except that the HEPES buffer already contained 1 mM DTT. Recovery of activity from the CoA-inhibited enzyme by the addition of DTT was examined using the same assay procedure that was used for

CoASH inhibition except that 0.1 M DTT was added to the assay mixture after the incubation of enzyme with CoASH (final DTT concentration of 1 mM).

Automated Docking of CoASH to DmpF. The three-dimensional coordinates for the entire molecule of CoASH (coa_clean.pdb) were obtained from the HIC-Up Server (http://xray.bmc.uu.se/hicup). Atomic coordinates corresponding to the nucleotide portion of CoASH were initially superimposed onto those of the NAD^+ cofactor found in the DmpFG structure (PDB entry 1NVM) using the program LSQMAN (*96*). The atomic coordinates of CoASH corresponding to the pantetheine portion of the cofactor were manually adjusted by general bond torsions using O (*97*) such that all atoms resided within a cavity consisting of the DmpF active site and a tunnel connecting the active site to the protein surface. This model was selected as the candidate ligand for automated docking to DmpF using AUTODOCK (*98*). Eight of the 20 possible torsions in CoASH were active in the docking simulation. The grid of the docking simulation was defined by a 21 Å x 21 Å x 21 Å cube centered on the CoASH molecule within the DmpF active site. The docking simulation was performed using a Lamarckian genetic algorithm search routine with a population of 50 individuals and a maximum of 500000 energy evaluations. In total, 291 generations were analyzed. Molecular graphics were generated using PyMOL (*99*).

2.4 Results

Hydrogen–Deuterium Exchange Experiments. To characterize the binding of NAD^+ and coenzyme A to DmpFG, hydrogen–deuterium exchange experiments were performed by mixing small volumes of DmpFG protein, DmpFG–NAD^+ complex or DmpFG–CoASH complex, with large volumes of D_2O-containing buffer. Cofactor binding sites would be

expected to become inaccessible to D_2O as a result of shielding by any bound cofactors. Comparison of the mass spectra of peptides from pepsin digests of holo-DmpFG to those of apo-DmpFG following quenching at pH 2.5 and 0 °C allowed identification of sites where accessibility to solvent changed upon cofactor binding. In the NAD^+ or CoASH binding experiments, 2 mM NAD^+ or 2.3 mM CoASH permitted observation of reasonable MALDI MS signals. These concentrations also appeared to be saturating, since no significant increase in the number of amide hydrogens protected was observed with 4 mM NAD^+ or CoASH (data not shown). H–D exchange experiments were also performed with either NAD^+ (0.5 and 1 mM) or CoASH, and the same peptides exhibited amide hydrogen protection against H–D exchange although the number of incorporated deuteriums increased (data not shown). Since the accessibility changes were the same at these different concentrations of cofactors, a single binding event was likely measured in these experiments.

To identify the pepsin-generated fragments of DmpFG obtained after quenching, we sequenced peptides using HPLC–ESI-Q-TOF MS/MS. A total of 86 peptides were observed, and 79 were identified (Figure 2.3). Seven peptides could not be characterized because of the weak signal and the interference from strong adjacent peaks. Among the 79 identified peptides, 42 were from DmpF, covering 89% of the sequence (Figure 2.3A) and 37 were from DmpG, covering 85% of the sequence (Figure 2.3B). Fewer identified peptides were observed in the MALDI-TOF spectra: 26 peptides from DmpF were observed, covering 69% of the sequence (Figure 2.3A), and 23 observed DmpG peptides accounted for 66% of the sequence of DmpG (Figure 2.3B). In the in- and back-exchange control experiments, 7–19% (12% average) of in-exchanges and 58–87% (67%) of

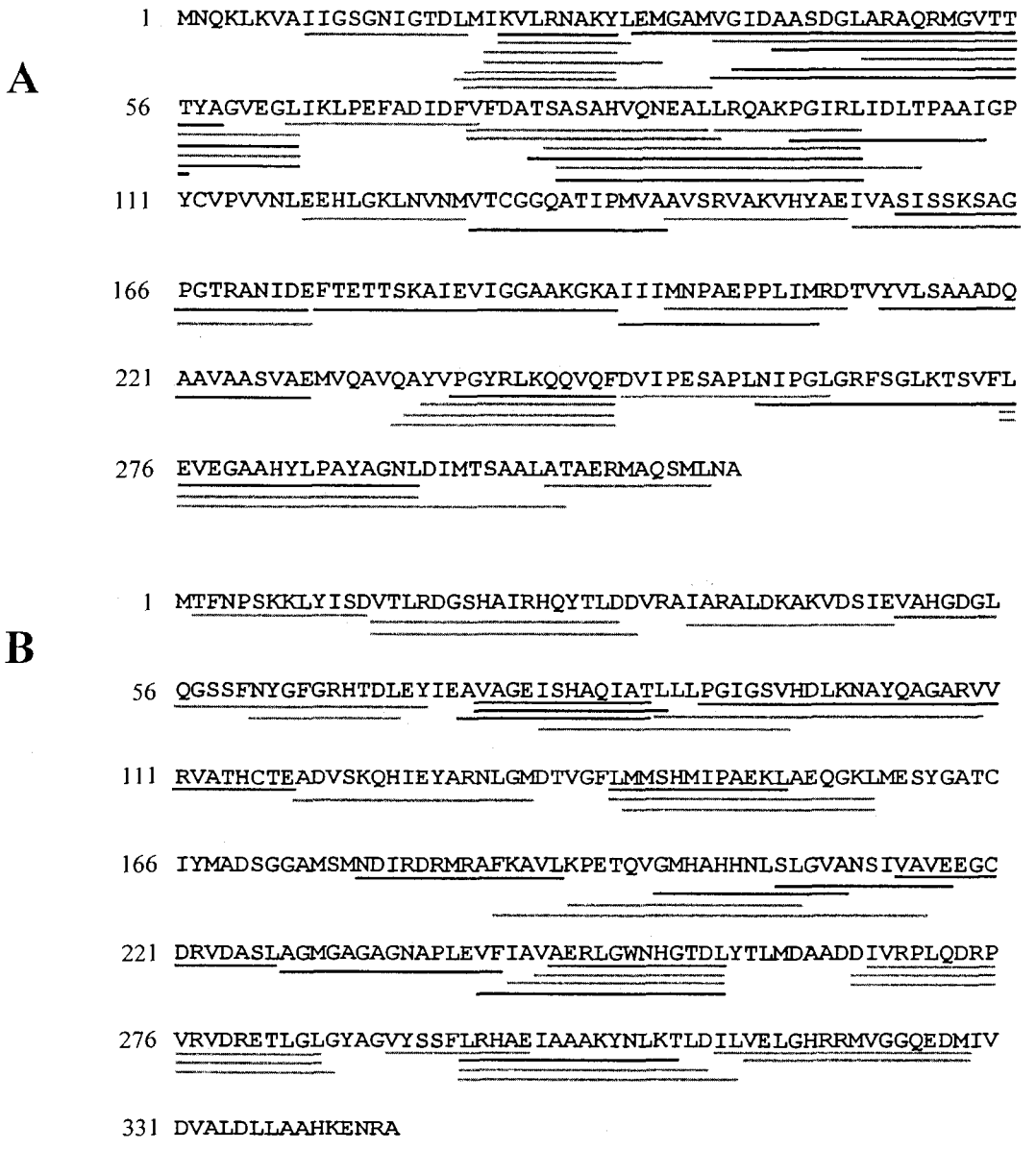

Figure 2.3 Identification of peptides from pepsin digests of DmpFG.

(A) Peptides from DmpF identified using MS/MS are underlined and cover 89% of the sequence; fragments observed in the MALDI-TOF spectrum only are underlined in gray, and cover 69% of the sequence. (B) Peptides from DmpG identified using MS/MS are underlined and cover 85% of the sequence; fragments observed in the MALDI-TOF spectrum only are underlined in gray and cover 66% of the sequence.

back-exchanges were observed among the fragments showing amide hydrogen protection against H–D exchange.

From H–D exchange data, various numbers of amide hydrogens in peptides corresponding to DmpF residues 9–19, 36–63, 46–63, 155–174, 275–291, and 275–301 were found to be involved in protection against H–D exchange in the presence of cofactor (Table 2.1). Incorporation of deuteron into these fragments was biphasic and almost reached the maximum after 10 min (Figure 2.4). Table 2.1 (columns 2 and 3) summarizes the total number of amide hydrogens protected at 15 min, determined directly from the mass shifts of the peptides at this time point. In addition, fitted deuterium incorporation rate constants and amplitudes from kinetics experiments such as those shown in Figure 2.4 are also given in Table 2.1 (columns 4–6). The limited number of data points that could be collected in the early time period means that the fitted rate constants for the faster reaction represent only a lower limit. Nevertheless, the rates and amplitudes of deuterium incorporation in the presence and absence of CoASH and NAD^+, as well as the difference in the total number of deuterons exchanged in the presence and absence of each cofactor, are useful probes of their binding sites.

The rates of hydrogen–deuterium exchange in the presence of CoASH, as well as the numbers of protons exchanged, were, with a few exceptions, indistinguishable from those observed with NAD^+, suggesting that the two cofactors share a single binding site. Furthermore, for all fragments, the number of protons exchanging in the slow phase was relatively constant regardless of the presence or absence of coenzyme, while the number exchanging in the fast phase was significantly decreased in the presence of either NAD^+

Table 2.1 H–D Exchange Parameters of Peptides of DmpF with Amide Hydrogen Protection upon Cofactor Binding.

peptic fragments of DmpF and corresponding masses ([M])	observed total no. of amide H atoms protected against H–D exchange binding at 15 min		no. of exchanged amide H atoms [rate constant (min^{-1})] for fast and slow phases*		
	NAD^+	CoASH	no cofactor	NAD^+	CoASH
residues 9–19 (1058.57)	3.2 ± 0.3	3.2 ± 0.2	4.1 ± 0.1(10.6 ± 3.6) 2.3 ± 0.1(0.3 ± 0.1)	1.7 ± 0.1 (7.4 ± 2.1) 1.5 ± 0.1 (0.4 ± 0.1)	1.5 ± 0.1 (7.2 ± 2.6) 1.8 ± 0.1 (0.4 ± 0.2)
residues 155–174 (1972.03)	3.1 ± 0.1	2.2 ± 0.1	9.7 ± 0.3 (9.0 ± 3.0) 4.4 ± 0.2 (0.4 ± 0.1)	8.3 ± 0.4 (7.6 ± 2.5) 2.7 ± 0.2 (0.4 ± 0.2)	9.0 ± 0.2 (7.6 ± 3.0) 3.1 ± 0.2 (0.4 ± 0.2)
residues 46–63 (1879.97)	3.0 ± 0.1	2.8 ± 0.2	–	–	–
residues 36–63 (2778.40)	4.2 ± 0.1	4.2 ± 0.2	12.6 ± 0.5 (6.1 ± 2.1) 5.9 ± 0.3 (0.3 ± 0.1)	8.8 ± 0.4 (5.7 ± 1.8) 5.4 ± 0.2 (0.3 ± 0.1)	9.0 ± 0.5 (5.7 ± 1.7) 5.4 ± 0.2 (0.3 ± 0.1)
residues 275–291 (1786.90)	1.2 ± 0.1	1.0 ± 0.1	–	–	–
residues 275–301 (2761.37)	4.1 ± 0.2	4.2 ± 0.2	7.8 ± 0.3 (5.5 ± 1.6) 7.8 ± 0.3 (0.4 ± 0.1)	4.5 ± 0.2 (4.3 ± 1.1) 6.9 ± 0.2 (0.3 ± 0.2)	4.4 ± 0.3 (4.3 ± 1.7) 7.2 ± 0.4 (0.3 ± 0.1)

Data shown are averages for three independent experiments.

* From fitting of deuterium exchange data to double exponential as shown in Figure 2.4 and as described in Experimental Procedures.

A

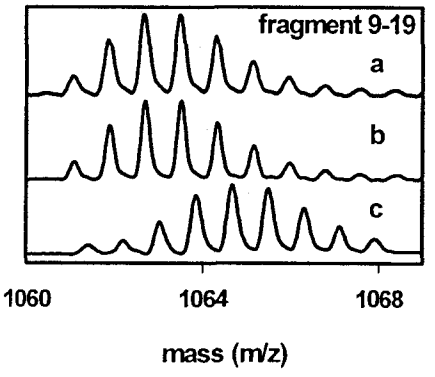
fragment 9-19
a
b
c
1060
1064
1068
mass (m/z)

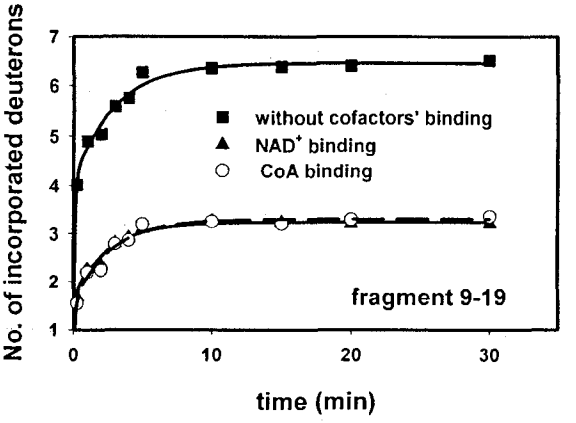
No. of incorporated deuterons
without cofactors' binding
NAD+ binding
CoA binding
fragment 9-19
time (min)

B

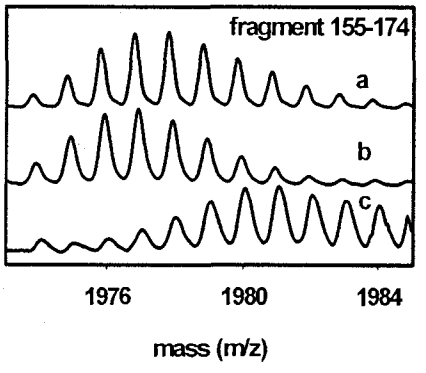
fragment 155-174
a
b
c
1976
1980
1984
mass (m/z)

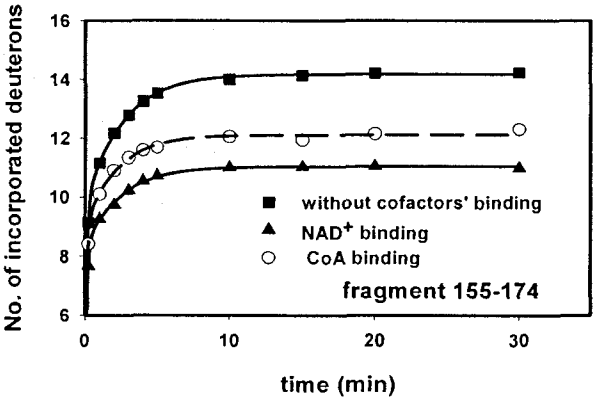
No. of incorporated deuterons
without cofactors' binding
NAD+ binding
CoA binding
fragment 155-174
time (min)

C

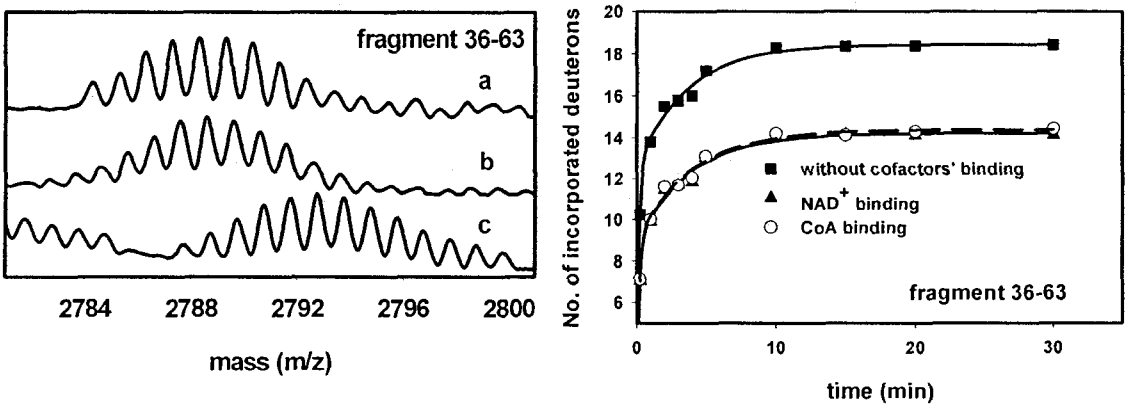
fragment 36-63
a
b
c
2784
2788
2792
2796
2800
mass (m/z)
No. of incorporated deuterons
20
18
16
14
12
10
8
6
without cofactors' binding
NAD+ binding
CoA binding
fragment 36-63
0
10
20
30
time (min)

D

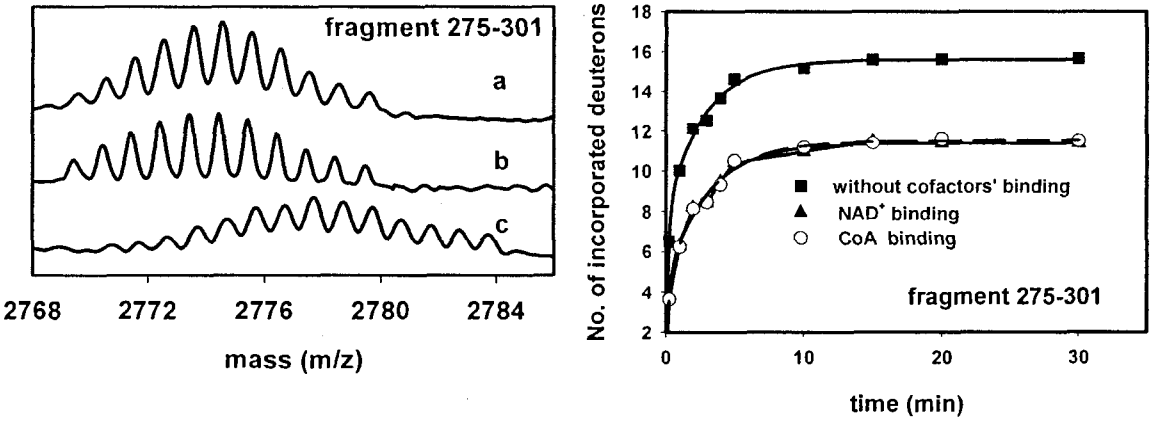
fragment 275-301
a
b
c
2768
2772
2776
2780
2784
mass (m/z)
No. of incorporated deuterons
18
16
14
12
10
8
6
4
2
without cofactors' binding
NAD+ binding
CoA binding
fragment 275-301
0
10
20
30
time (min)

Figure 2.4 Isotopic envelopes of peptides at 10 min (left) and kinetics of incorporation of deuterium into DmpF-derived peptides (right).

Each isotopic envelope indicates peptides from an enzyme that was (a) complexed with CoASH, (b) complexed with NAD^+, and (c) without cofactor binding. Kinetics plots are each fit to a double-exponential equation, as described in Experimental Procedures, with rate constants and amplitudes as in Table 2.1: (A) 1058.57Da peptide (residues 9–19), (B) 1972.03Da peptide (residues 155–174), (C) 2778.40Da peptide (residues 36–63), and (D) 2761.37Da peptide (residues 275–301).

or CoASH. This implies that the more readily accessible backbone protons are blocked by cofactor binding, as one might expect.

Affinity Chromatography and Inhibition by CoASH. Several other experimental observations support the notion that CoASH and NAD^+ share a single cofactor binding site. Thus, either CoASH or NAD^+ was able to elute the enzyme from an NAD^+ affinity column (Table 2.2). Furthermore, preincubation of the enzyme with NAD^+ protected against inhibition by CoASH: inhibition was reversed by the addition of DTT, as one would expect if CoASH inhibition involves a covalent adduct with the enzyme via a disulfide bond at the active site (Figure 2.5). Since DmpF, like other CoASH-linked acetaldehyde dehydrogenases (*48, 52*) catalyzes a ping-pong reaction (Chapter 3) in which NAD^+ and acetaldehyde bind and NADH is released prior to CoASH binding, occupation of the same binding site by the two cofactors is feasible.

Comparison of H–D Exchange Results with NAD^+–DmpF Crystal Structure. Patterns of protection against hydrogen–deuterium exchange in the presence of NAD^+ are consistent with the reported crystal structure of the DmpF–NAD^+ complex (4). This structure indicates that the peptide corresponding to DmpF residues 9–19 contains the dinucleotide-associated binding motif, GXGXXG (residues 11–16) involved in binding to the pyrophosphate, adenine, and ribose ring moieties of NAD^+ (4): in the presence of NAD^+, three amide hydrogens were protected against H–D exchange (Figure 2.4A, traces b and c, and Table 2.1). The peptide corresponding to DmpF residues 155–174, includes a similar GXGXXA motif (sequence 165–170), and mediates binding to pyrophosphate, the nicotinamide and its ribose rings; for this peptide, three amide hydrogens were protected from H–D exchange upon NAD^+ binding (Figure 2.4B, traces b and c, and

Table 2.2 Effectiveness of NAD^+, CoASH, or NaCl in Eluting Native DmpFG Bound to an NAD^+ Affinity Column

apparent K_m for NAD^+ (μM)	apparent K_m for CoASH (μM)	eluted by NAD^+ (mM)	eluted by CoASH (mM)	eluted by NaCl (mM)
156	8.7	2	2.5	100

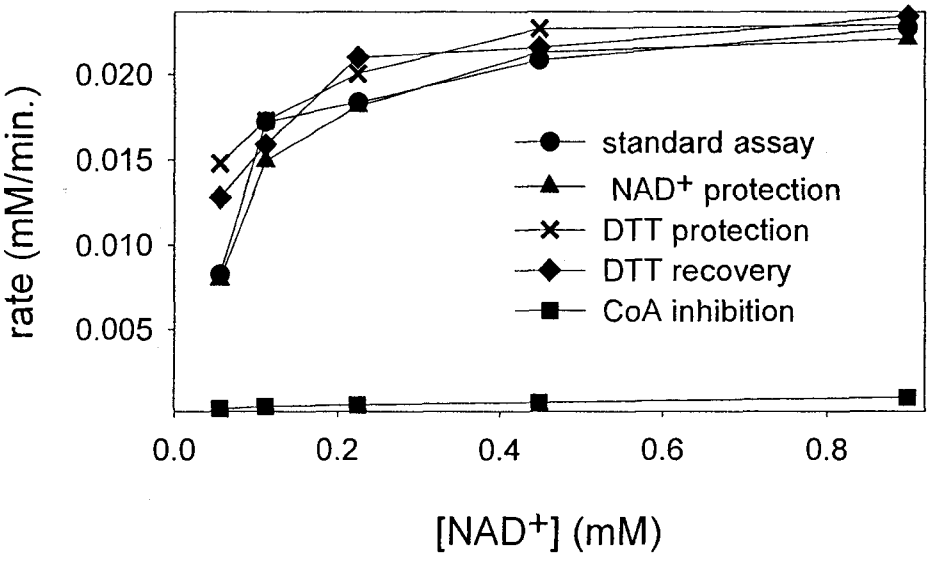

Figure 2.5 Inhibition by preincubation with CoASH and protection by NAD^+ and DTT. Assay conditions are as described in *Experimental Procedures*.

Table 2.1). Peptides corresponding to DmpF residues 36–63 (overlapping with fragment 46–63) and 275–301 (overlapping with 275–291) are involved in binding to the adenine and nicotinamide rings, respectively: in the presence of NAD^+, four amide hydrogens were protected against deuterium replacement for each peptide (Figure 2.4C, traces b and c, and Figure 2.4D, traces b and c, and Table 2.1).

Comparison of H–D Exchange Results with NAD^+ and CoASH. Very similar patterns of protection against H–D exchange were observed in the DmpF subunit upon CoASH binding. Thus, peptides corresponding to DmpF residues 9–19, 155–174, 36–63, 46–63, 275–291 and 275–301 all exhibited amide hydrogen protection against H–D exchange in the presence of either CoASH or NAD^+. Furthermore, in peptides corresponding to DmpF residues 9–19, 36–63 and 275–301 the same total number of hydrogens were protected against exchange as in NAD^+ binding (Figure 2.4A, C, D, traces a and c, respectively, and Table 2.1). However, only two amide hydrogens of the peptide corresponding to DmpF residues 155–174 were protected against deuterium replacement upon CoASH binding (Figure 2.4B, traces a and c, and Table 2.1). Significantly, no differences in H–D exchange upon cofactor binding were observed in the DmpG subunit (data not shown).

These results strongly suggest that the mode of CoASH binding to DmpF is very similar to that of NAD^+, reported for the X-ray structure. The nucleoside moiety of CoASH could interact with regions of peptides corresponding to DmpF residues 9–19, 155–174 and 36–63, all of which interact with the ADP moiety of NAD^+ (Figure 2.6). The segment of DmpF corresponding to residues 275–301 is likely to be associated with the binding of the pantetheine chain, which would need to approach Cys132 in the DmpF

active site in preparation for nucleophilic attack on acetyl-S-Cys132, a postulated intermediate (4). Further insight into the interaction of CoASH with DmpF was obtained by modeling it using AUTODOCK.

Computer-Aided Modelling of the CoASH–DmpF Complex. Of the 50 conformers generated by AUTODOCK, 22 conformers organized into 14 clusters were obtained that exhibited energetically favorable binding to DmpF (energy of docking < –13 kcal/mol; rmsd compared to reference CoASH < 2.0 Å). One of the clusters (cluster 6) contained three CoASH conformers (6_1, 6_2, and 6_3) in which the thiol group is proximal to the thiol group of DmpF Cys132 "B" conformation. The thiol group of conformer 6_1 was observed to be within 2.65 Å of the B thiol group of Cys132. The other two CoASH conformers within this cluster had thiol–thiol distances to the Cys132 B thiol of 2.79 and 3.65 Å, respectively. The 6_1 conformer was estimated by AUTODOCK to bind to DmpF with a ΔG of –11.3 kcal/mol and with a predicted dissociation constant of 5.04×10^{-9} M. Its rmsd compared to the input CoASH reference coordinates was calculated by AUTODOCK to be 1.64 Å. The binding of CoASH conformer 6_1 to DmpF is shown in Figure 2.7A. Extensive hydrogen bonding occurs between the pyrophosphate moiety of the 6_1 conformer and DmpF backbone amide groups. Two hydrogen bonds were observed between the 4'-phosphate of the docked CoASH and DmpF residue Ser12: one to the hydroxyl group of the side chain and one to the backbone carbonyl group of the residue. The 4'-phosphate is further stabilized by hydrogen bonding between its O4 atom and the backbone amide groups of Asn14 and Ile15.

Beyond the potential disulfide formation with CoASH at DmpF Cys132, hydrophilic interactions between the pantetheine moiety of CoASH conformer 6_1 and DmpF are not

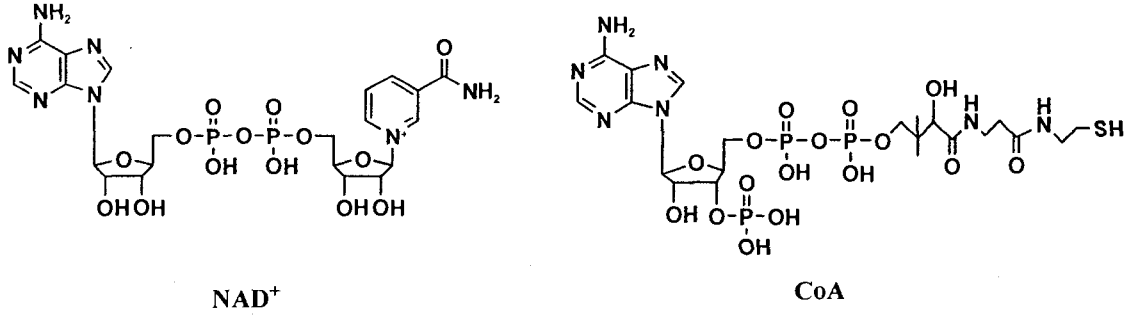

Figure 2.6 Comparison of NAD^+ and coenzyme A structures.

extensive. No hydrogen bonds are observed between the protein and the pantetheine carbonyl groups. A molecular surface projected onto DmpF indicates that the docked conformation of CoASH conformer 6_1 fully occupies the cavity containing the enzyme active site and superimposes with the NAD^+ cofactor observed in the X-ray crystal structure of the holoenzyme (Figure 2.7B).

2.5 Discussion

Our hydrogen–deuterium exchange data establish that CoASH and NAD^+ share a cofactor binding site in the DmpF subunit of DmpFG. The changes in H–D exchange in the presence of the cofactor are consistent with the crystal structure of the enzyme–NAD^+ complex (4), and the model of the enzyme–CoASH complex derived here.

The observation that a single Rossmann fold can alternately bind nicotinamide cofactor and coenzyme A appears to be unique. $NAD(P)^+$-binding Rossmann folds have been characterized in many different dehydrogenases (*100*), and Rossmann folds that bind coenzyme A have also been characterized (*101*); to the best of our knowledge, a single Rossmann fold that binds both cofactors has not been described previously. Interestingly, the sequence of DmpF clusters in the Pfam database with the NAD^+-binding Rossmann fold of phosphorylating dehydrogenases such as aspartate semialdehyde dehydrogenase (79), rather than the CoASH-binding fold of succinyl-CoA synthetase (*101*). Furthermore, a three-dimensional structure-based search of the PDB archive using Secondary Structure Matching (SSM) (14) revealed the closest match to structures of glyceraldehyde-3-phosphate dehydrogenases, rather that CoA-binding Rossmann fold-based proteins (data not shown). Nevertheless, the NAD^+ and CoA-binding Rossmann folds are quite similar to one another (*100*).

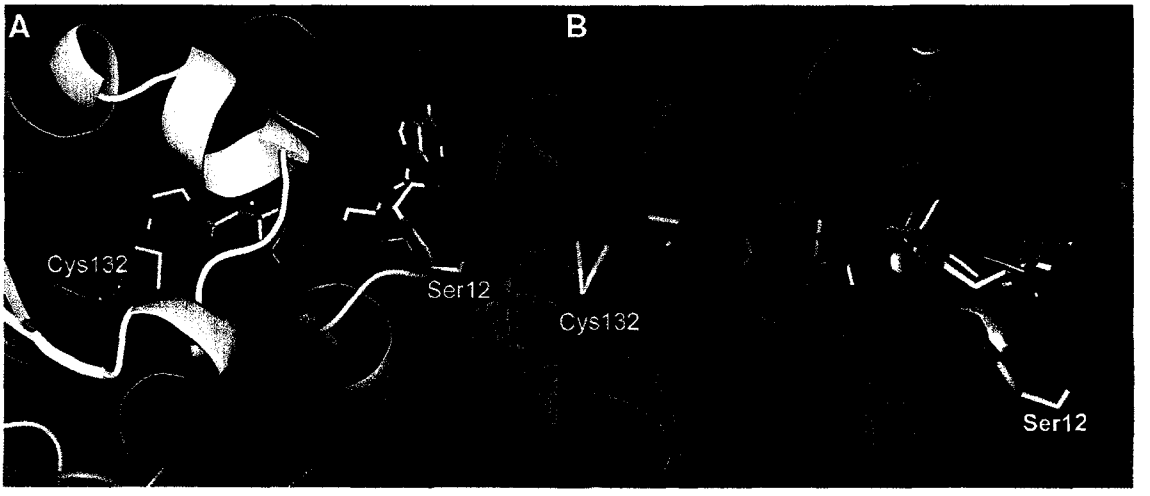

Figure 2.7 Models generated using AUTODOCK.

(A) Binding of CoASH docked conformer 6_1 to DmpF. The CoASH cofactor is shown as sticks and colored according to element (blue for nitrogen, orange for phosphate, red for oxygen, white for carbon, and yellow for sulfur). The DmpF protein is shown in a cartoon representation (flat coils: helices). DmpF residues protected against H–D exchange are shaded as follows: residues 9–19, light orange; residues 36–63, green; residues 155–174, yellow; and residues 275–301, pink. The remaining DmpF residues are colored light blue. The two conformations of the Cys132 side chain are shown as sticks (white for carbon and yellow for sulfur). The residue Ser12, colored by elements, is also shown. (B) Superposition of CoASH conformer 6_1 with NAD^+ in the DmpF active site. A molecular surface, colored light blue, generated on DmpF shows the extent of the cavity containing the DmpF active site. The rest of the DmpF protein is shown in cartoon representation as in Figure 2.7A. Docked CoASH conformer 6_1 is shown as sticks (colored as in Figure 2.7A). The NAD^+ cofactor found in the crystal structure of the holoenzyme (PDB entry 1NVM) is shown as sticks and is colored light pink. These models were generated using Pymol.

Cofactor Binding Site Characterization. In DmpF, the observation that three amide hydrogens of the fragment of residues 9–19 were protected by NAD^+ against deuterium replacement (Table 2.1) is in agreement with the crystal structure data. The AO3* oxygen atom of the adenine ribose of NAD^+ forms a hydrogen bond to the main chain nitrogen atom and the side chain hydroxyl oxygen atom of Ser12. The main chain nitrogens of Asn14 and Ile15 bind to the pyrophosphate through hydrogen bond interaction with AO2 and NO2 oxygen atoms, respectively. Meanwhile, the side chain of Ile15 and the nicotinamide ring of NAD^+ are involved in a van der Waals interaction.

Homologous interactions are observed in the modeled complex with CoASH. The $O3^*$ atom of the adenine ribose of CoASH H-bonds with the main chain nitrogen of Gly13 instead of that of Ser12 in the NAD^+–DmpF complex, while the main chain nitrogens of Asn14 and Ile15 hydrogen bond to O4 of CoASH. Furthermore, the side chain of Ile15 interacts with C12 of the pantetheine chain of CoASH, in place of the nicotinamide ring of NAD^+. The observation that three amide hydrogens in this region were protected against H–D exchange upon CoASH binding is thus consistent with the AUTODOCK model, although it should be noted that protection from H–D exchange need not necessarily correlate with the number of amide hydrogen bonds.

When NAD^+ and CoASH bind, three amide hydrogens and two amide hydrogens, respectively, of a peptide corresponding to DmpF residues 155–174 were protected from H–D exchange (Table 2.1). Two amide hydrogens may be protected by the hydrogen bonding interaction between the amide nitrogens of Gly165 and Gly167 and the pyrophosphate oxygen of NAD^+ (NO1 and AO1) (4) or CoASH (O5 and O1) in the modeled complex. The origin of the extra amide protected against exchange by NAD^+

may be the H-bonding interactions between the side chain nitrogen and carbonyl oxygen of Asn171 and NO3* and NO2* of the nicotinamide ribose. In the modeled CoASH complex, the side chain nitrogen and carbonyl oxygen of Asn171 appear to be involved in weaker van der Waals contacts with C6 and C7 of the pantetheine chain.

The labeling patterns of overlapping DmpF peptides corresponding to residues 46–63 and 36–63 indicate that within the shorter peptide (residues 46–63), three amide hydrogens are protected from H–D exchange, while in the longer peptide one additional proton is protected (Table 2.1). While crystal structure data show that three residues, Val36, Gly37, and Ile38, within the DmpF sequence of residues 36–45 are involved in van der Waals interactions with NAD^+, no residue within the sequence of residues 46–63 is in direct contact with bound NAD^+. In this case, the observed protection against H–D exchange may result from protein conformational change that makes some amino acid residues less accessible and other residues more exposed to the solvent. In fact, a significant conformational change was observed upon cofactor binding to DmpFG in the crystal structure (4), as summarized in Figure 2.8A. The structural differences observed upon NAD^+ binding affect not only residues which directly interact with cofactor but also other regions which are located near the binding site or even farther from it (Figure 2.8B). Residues in positions 36–45 undergo a large movement upon NAD^+ binding, especially Asp39 and Ala40: these residues could not be matched with the corresponding residues in the apo structure. Residues 46–63 also shift considerably such that Thr54, Thr55, Thr56, and Tyr57 in the apo and holo structures do not overlap (Figure 2.8B). Thus, protection of the three amide hydrogens observed in the peptide corresponding to DmpF residues 46–63 is likely due to the conformational change caused by NAD^+

binding. Essentially identical H–D exchange behavior in peptides corresponding to DmpF residues 46–63 and 36–63 was observed upon CoASH binding (Table 2.1), in which three amide hydrogens were protected in the shorter peptide (residues 46–63), and one additional proton was protected in the longer peptide, suggesting that CoASH stimulates a conformational change in DmpF similar to that which occurs when NAD^+ binds.

Comparison of another pair of overlapping peptides, corresponding to DmpF residues 275–291 and 275–301, indicates that one and four amide hydrogens are protected upon NAD^+ binding, respectively (Table 2.1). In the DmpFG crystal structure, the side chain amide nitrogen of Asn290 contacts the carboxamide nitrogen of the bound NAD^+. One side chain carbon of Leu291 contacts the carboxamide oxygen of NAD^+, and the side chain CG and CE atoms of Met 294 interact with NC5 and NC6 in the nicotinamide ring. In addition, alignment of the holo and apo structures indicates that residues 285–294 undergo a large displacement upon NAD^+ binding (Figure 2.8B). We propose that protection of the four amide hydrogens in the peptide corresponding to residues 275–301 is due to the direct interaction of three residues, Asn290, Leu291, and Met 294, with the nicotinamide ring or to the conformational change associated with NAD^+ binding. The same H–D exchange events were observed in peptides corresponding to residues 275–291 and 275–301 upon CoASH binding as observed upon NAD^+ binding. The fact that no interaction occurred between residues 275–301 and CoASH in the model of the complex supports our hypothesis that protection of the four amide hydrogens is likely due to a conformational change similar to that observed upon NAD^+ binding.

In the crystal structure of DmpFG, Cys132 of DmpF is 3.4 Å from the nicotinamide ring of NAD^+. The covalent modification of an enzyme-based thiol group by CoASH, suggested by the results shown in Figure 2.5, could be explained by the close approach of the thiol group of bound CoASH to the thiol group of Cys132. In the CoASH–DmpF model, the 2.65 Å distance between the sulfur atom of Cys132 and the thiol group of CoASH is, given a reasonable degree of error in the model, potentially short enough for formation of a disulfide bond. Interestingly, the atoms at the end of the pantetheine chain, including atoms S1, C2, C3, N4, C5, and O5 of the carbonyl oxygen, are all proximal to atoms of Cys132, Thr131, or Val130 residues, which may help position the thiol group, allowing it to form the disulfide bond. Although formation of a disulfide bond appears to occur when CoASH is incubated with enzyme in the absence of other substrates, a close approach of the CoASH thiol would also be required for attack on a Cys132–thioacetyl intermediate in the proposed catalytic cycle (4).

Comparison with Other CoASH-Binding Proteins. More 100 structures of CoASH-binding proteins in complex with the cofactor have been determined. The CoASH-binding folds for these proteins include a large variety of different topologies. Some folds are not exclusive to CoASH binding (the four-helical up-and-down bundle, the Rossmann fold, and the TIM barrel fold) while others have been reported in only CoASH-binding proteins to date (*102*). Only succinyl-CoA synthetase (*101, 103*), formyl-CoA transferase from *Oxalobacter formigenes* (*104*) and, a protein of unknown function, Pfu-723267-001 from *Pyrococcus furiosus* (PDB ID entry 1Y81), have been shown to bind CoASH at a Rossmann fold, which appears to be the case with DmpF. However, none of these proteins has been reported to bind $NAD(P)^+$ also. The identification of structural features

A

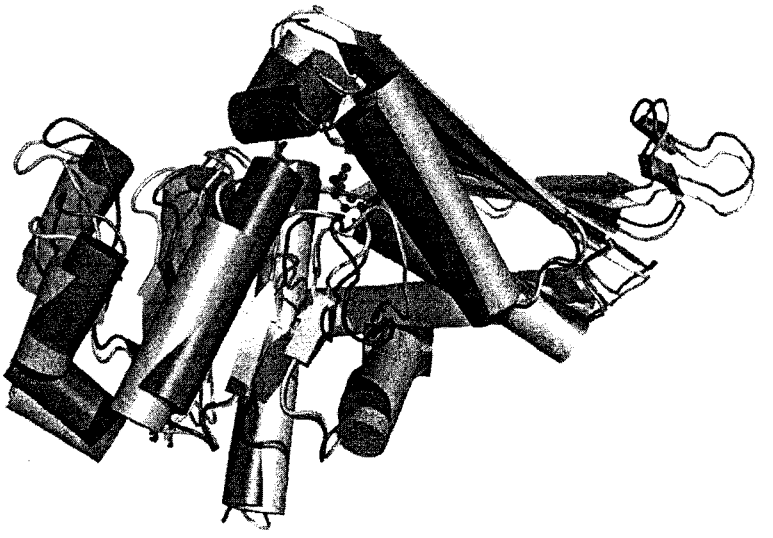

B

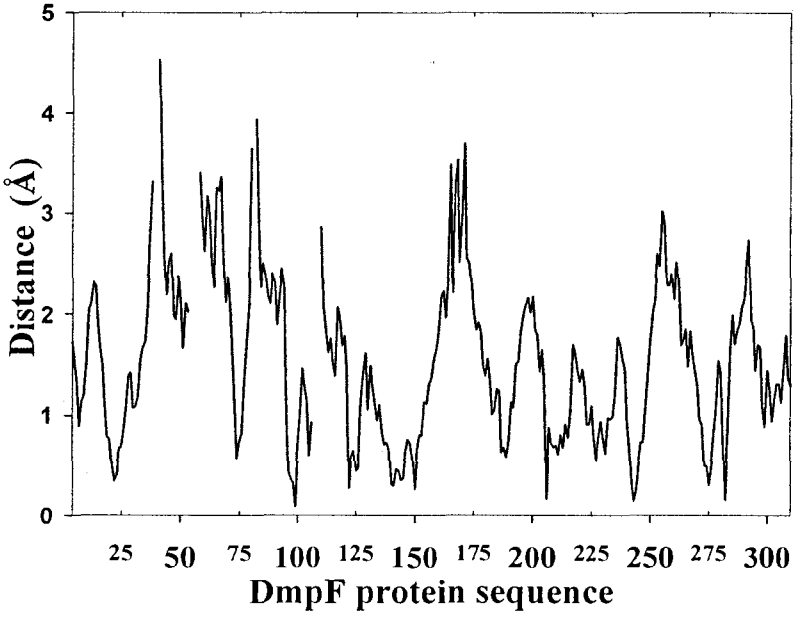

Figure 2.8 Comparison of DmpF (apo) and DmpF–NAD^+ (holo) structures based on PDB entry 1NVM.

(A) Superimposition of Holo-DmpF (chain H, dark gray) and apo-DmpF (chain F, light gray) backbones. Active site residue Cys132 is denoted by ball and stick. (B) Cα distances of the aligned residues between holo- and apo-DmpF. The space gaps represent nonaligned residues. Three-dimentional structures of chains H (holo) and F (apo) of DmpF were aligned using SSM (http://www.ebi.ac.uk/msd-srv/ssm/cgi-bin/ssmserver). Cα distances of the corresponding residues were obtained for drawing the plot.

that allow the Rossmann fold of DmpF to bind either cofactor must await determination of the crystal structure of a complex with CoASH.

Conformations of the cofactors in the experimentally observed CoASH complexes of succinyl-CoA synthetase (SCS) and formyl-CoA transferase (FCT), and the NAD^+ complex of DmpF, are remarkably similar. The bound CoASH in succinyl-CoA synthetase and formyl-CoA transferase adopts an extended conformation. The distance between AC6 and PS1 is 17.3 Å in the CoASH of SCS, while it measures 16.5 Å in FCT: this is comparable with the 16.5 Å distance between AC6 and NC4 of NAD^+ bound in DmpF. The adenine rings of CoASH in both SCS and FCT, as well as the NAD^+ in DmpF, all are positioned in the anti conformation relative to the ribose group. The ribose ring of CoASH in SCS exhibits a 1'-exo conformation, not the more common 2'-endo conformation observed in CoASH of FCT and NAD^+ bound to DmpF, but the difference between the two conformations is not believed to be large (*103*). In the CoASH–SCS and NAD^+–DmpF complexes, the planes of the adenine ring and the axis connecting pyrophosphate are almost perpendicular to each other, whereas the adenine ring of CoASH in FCT and the axis are coplanar. These experimentally observed similarities support our observations that CoASH and NAD^+ share a binding site in DmpF.

Comparison to Other Proteins with Overlapping Ligand Binding Sites. Our finding that the two cofactors of DmpF share a binding site is an enzymatic property not without precedent in the literature, although reviews on this topic are scarce. Recently reported structures of enzymes with overlapping ligand binding sites include three reductases [methylenetetrahydrofolate reductase (*105, 106*), flavin reductase PheA2 (*107, 108*), and

quinone reductase type1 (*109, 110*)], and two other enzymes [chalcone synthase (*111*) and biosynthetic thiolase (*112*)].

These enzymes exhibit a diverse range of folds but share some common features. First, the substrates binding to the overlapping site often possess common structural elements; local conformational changes may also promote the recognition and binding of substrates. Second, these examples have in common ping-pong reaction mechanisms in which one of the substrates binds first and then a product is released to vacate the site for binding the next substrate. During catalysis, the formation of a covalently bound intermediate enzyme complex may be involved, e.g., a polyketide-S-Cys64 intermediate in chalcone synthase, acetyl-S-Cys89 intermediates in biosynthetic thiolase, and an acetyl-S-Cys132 intermediate in DmpF (Chapter 3). Third, in the examples cited, van der Waals forces dominate the interaction between the enzyme active site and substrates; limited numbers of H-bonds and the absence of electrostatic interactions lead to weak affinity, which favors the alternate binding and release of substrates and minimizes the strong interactions required for distinct recognition of structurally different substrates. These features are consistent with the data on DmpF that we report here.

As is apparently the case with DmpF, overlapping ligand binding sites are also associated with the Rossmann fold in a number of other enzymes. Malate dehydrogenase (decarboxylating) binds NAD^+, a substrate, and ATP, a regulator of catalytic activity, at a Rossmann fold with common binding interactions around their ADP moieties (*113-115*). Glyceraldehyde-3-phosphate dehydrogenase, the protein structurally most similar to DmpF, binds RNA and DNA competitively with NAD^+/NADH at a common site in the Rossmann fold (*116*). Furthermore, other dehydrogenases with Rossmann folds, such as

alcohol dehydrogenase and lactate dehydrogenase, appear to bind RNA at the pyridine nucleotide cofactor binding site (*116*). The data presented here establish that DmpF is a member of a class of proteins that can bind multiple substrates at a single Rossmann fold. However, to best of our knowledge this is the only example thus far which binds NAD^+ and CoASH, two cofactors involved in the catalytic cycle of an enzyme.

2.6 Acknowledgements

We thank Alain Tessier and Bernard Gibbs for help and advice with the mass spectrometry experiments.

Chapter 3 Covalent Reactions at the Essential Active Site Cysteine of a CoA-Dependent Aldehyde Dehydrogenase: Insights into Mechanism and Inhibition

3.1 Abstract

DmpFG, a bifunctional aldolase/dehydrogenase from *Pseudomonas* sp. strain CF600, catalyzes the last two reactions of the degradation pathway for phenol and methyl-substituted phenols. This heterotetrameric enzyme cleaves the substrate, 4-hydroxy-2-ketovalerate, into pyruvate and acetaldehyde in the active site of the DmpG subunit, while at the active site of the DmpF subunit, acetaldehyde is oxidized to acetyl-coenzyme A. Here we examine the reactivity of the active-site cysteine of DmpF, Cys-132, in catalysis and substrate-induced inactivation. Substitution of Cys-132 by Ser resulted in an enzyme that exhibited 5,000-fold lower activity relative to WT. Mass spectrometry was used to identify a trapped acetyl-Cys132 adduct formed during turnover. Preincubation of DmpFG with acetaldehyde in the presence of oxygen led to inactivation of the dehydrogenase, where Cys-132 was shown using mass spectrometry to be oxidized to cysteine sulfinic acid. Unhydrated acetaldehyde appeared to be the preferred substrate for the enzyme: during turnover of 4-hydroxy-2-ketovalerate by DmpG it may be transferred to DmpF via the hydrophobic tunnel shown to bridge the two active sites [Manjasetty, B. A., et al. (2003) *Proc. Natl. Acad. Sci. U.S.A*, *100*, 6992-6997], thus avoiding hydration. Structural parameters potentially responsible for activation of Cys-132 were also examined and compared with other aldehyde dehydrogenases.

3.2 Introduction

Pseudomonas sp. strain CF600 uses the *dmp*-operon encoded *meta*-cleavage pathway to catabolize phenol, cresols and dimethylphenols (1). The last two enzymes in this

pathway are the gene products of *dmpF* (32.7 kDa) and *dmpG* (37.3 kDa), which copurify as a heterotetramer ($DmpF_2DmpG_2$) (2). DmpG is a metal-dependent aldolase (E.C. 1.2.1.10) and DmpF is a CoA-dependent aldehyde dehydrogenase (E.C. 4.1.3.39), which together convert 4-hydroxy-2-ketovalerate to pyruvate and acetyl-CoA. The toxic intermediate in this reaction, acetaldehyde, is oxidized by DmpF in an NAD^+- and CoA-dependent reaction to acetyl-CoA. Channeling of acetaldehyde from the active site of DmpG to that of DmpF via a 29 Å long connecting hydrophobic tunnel has been postulated on the basis of the crystal structure (*4*). The tertiary structure of DmpF is most similar to the aldehyde dehydrogenase superfamily member, glyceraldehyde-3-phosphate dehydrogenase.

Aldehyde dehydrogenases may be subdivided into two sub-families distinguished on the basis of cofactor dependence: $NAD(P)^+$ -dependent aldehyde dehydrogenase, and $NAD(P)^+$- and CoA-dependent aldehyde dehydrogenase. The former sub-family can be further sub-divided into: 1) phosphorylating $NAD(P)^+$-dependent aldehyde dehydrogenases, which reversibly oxidize the aldehyde substrate to phosphoester with the involvement of inorganic phosphate; and 2) non-phosphorylating $NAD(P)^+$-dependent aldehyde dehydrogenases, which irreversibly catalyze aldehyde oxidation to produce the corresponding acid. The CoA-dependent enzymes reversibly oxidize the aldehyde substrate using $NAD(P)^+$, and transfer it to coenzyme A to make the acyl-CoA product. Although unrelated in primary structure, the aldehyde dehydrogenases resemble each other in some aspects of catalysis (*36*).

Previously-published work has shown that both CoA-dependent aldehyde dehydrogenases and phosphorylating $NAD(P)^+$-dependent enzymes follow ping-pong

reaction mechanisms during catalysis (*38, 48-50, 52*). Aldehyde and nicotinamide cofactor bind, and NAD(P)H is released prior to the binding of the third substrate, either inorganic phosphate or coenzyme A. By contrast, non-phosphorylating $NAD(P)^+$-dependent aldehyde dehydrogenases have been shown to follow an ordered sequential kinetic mechanism, with NAD(P)H dissociating last (*34, 45*)

Relatively little mechanistic work has been done on the $NAD(P)^+$ and CoA-dependent aldehyde dehydrogenases compared to phosphorylating and non–phosphorylating $NAD(P)^+$-dependent enzymes. It has been shown that both phosphorylating (*42, 43*) and non-phosphorylating $NAD(P)^+$-dependent aldehyde dehydrogenases (*45*) share a similar two-step reaction that involves the acylation and deacylation of a conserved cysteine residue at the active site. In the first step, the carbonyl carbon of the substrate aldehyde undergoes nucleophilic attack by the cysteine thiolate, to form a thiohemiacetal enzyme complex, followed by hydride transfer to $NAD(P)^+$ to generate an acylenzyme intermediate. In the second step, the acyl group undergoes nucleophilic attack by phosphate or water to produce a phospho-ester or an organic acid, respectively.

Recently, some of the covalent intermediates involved in these reactions have been characterized structurally. The architectures of thiohemiacetal and acylenzyme intermediates were determined in two recently-solved crystal structures of aspartate-β-semialdehyde dehydrogenase, a representative of the phosphorylating $NAD(P)^+$-dependent aldehyde dehydrogenase sub-family (*35, 47*). Insights into the catalytic intermediates of non-phosphorylating $NAD(P)^+$-dependent aldehyde dehydrogenases

were gained by characterization of the thioacylenzyme intermediate of E268A-glyceraldehyde 3-phosphate dehydrogenase from *Streptococcus mutans* (*36*).

Although the reaction mechanisms of phosphorylating and non-phosphorylating $NAD(P)^+$-dependent aldehyde dehydrogenases both involve thiolenzyme intermediates, the catalytic details of acylation and deacylation differ. The mechanism of phosphorylating $NAD(P)^+$-dependent aldehyde dehydrogenases appears to involve a catalytic triad, in which a histidine residue deprotonates and activates the active site cysteine for nucleophilic attack on the aldehydic carbon to form a thiohemiacetal intermediate (*35, 38, 117*). For the non-phosphorylating $NAD(P)^+$-dependent aldehyde dehydrogenases, the positively-charged nicotinamide ring of the bound $NAD(P)^+$, accompanied by conformational rearrangement within the active site concomitant with $NAD(P)^+$ binding, both play roles in stabilizing the cysteine thiolate (*41*). Additional evidence suggests that backbone amide nitrogens from the cysteine residue itself, and the adjacent residue, may also contribute to stabilization of the thiolate (*39*). By analogy with serine proteases (*118*), for both phosphorylating and non-phosphorylating $NAD(P)^+$-dependent aldehyde dehydrogenases, oxyanion holes have been proposed to stabilize the thiohemiacetal oxyanion, as well as facilitate hydride transfer to $NAD(P)^+$ to generate acylenzyme intermediate (*33, 47*). In the last step of the mechanism for phosphorylating aldehyde dehydrogenases, phosphate attacks the carbonyl carbon of the acylenzyme to generate a tetrahedral intermediate, followed by the release of phosphoester upon the collapse of this intermediate (*47*). In the case of non-phosphorylating $NAD(P)^+$-dependent aldehyde dehydrogenases, an invariant Glu participates in the deacylation step

by orienting and activating a bound H_2O molecule for nucleophilic attack on the acylenzyme intermediate (*34*).

CoA-dependent aldehyde dehydrogenases have been studied much less intensively than the other aldehyde dehydrogenase subfamilies. As these enzymes share the ping-pong reaction mechanism of phosphorylating $NAD(P)^+$-dependent aldehyde dehydrogenases, possess conserved active site cysteine residues, and often require sulfhydryl reagents for enzyme activity or stability, catalysis has been proposed to involve covalent acyl-S-enzyme intermediates (*3, 4, 48, 49, 52, 54*). However, no direct evidence for an acylenzyme intermediate has been reported previously for a CoA-dependent aldehyde dehydrogenase.

Here we report on the kinetics of DmpF, the identification of an acylenzyme intermediate during catalysis, and covalent reactions of the active site thiol with oxygen and coenzyme A that lead to inactivation.

3.3 Materials and Methods

Materials. For expression of recombinant wild-type (WT) and variant DmpFG proteins, *E. coli* C41 (DE3) cells were used (*85*). The plasmid for expression of WT DmpFG was constructed previously using the pT7.5 vector (*119*). Mutagenic oligonucleotides were synthesized by BioCorp Inc., Montreal, Quebec, Canada. The following oligonucleotides were used for mutagenesis:

5'-GCTGATCAT**GCGCGC**CACCGTGTATGTGC-3' (D209A),

5'-GCACATACACGGTG**GCGCGC**ATGATCAGC-3' (D209A) and

5'-CGTCAACATGGTTAC**CTCGGG**CGGCCAGGCGACC-3' (C132S),

5'-GGTCGCCTGGCCG**CCCGAG**GTAACCATGTTGACG-3' (C132S)

Silent restriction sites (*BsePI* for D209A and *AvaI* for C132S) were introduced into the primers for subsequent identification of successfully introduced mutations in plasmid DNA. The bases highlighted in bold denote the recognition sequence of the restriction endonuclease in the primers, while underlined bases are those that have been changed for site-directed mutagenesis and/or silent mutation to create restriction sites. *E. coli* XL2-Blue cells were used for DNA and plasmid amplification. Plasmids were purified using the Wizard miniprep kit (Promega).

Sequencing Grade Modified Trypsin (porcine) from Promega was used for protein digestion. CoA, acetyl-CoA and anhydrous acetaldehyde were purchased from Sigma-Aldrich; dimethylformamide (DMF) was from Honeywell Burdick & Jackson. NAD^+ was bought from Roche Diagnostics Corporation. 4-Hydroxy-2-ketovalerate (4H2KV) was synthesized from the corresponding lactone, as described in a previous report (*120*). Chromatography resins were purchased from GE Healthcare.

Site-Directed Mutagenesis. DNA manipulations were according to standard methods (*121*). Site-directed mutagenesis to produce D209A and C132S variants of DmpF was carried out using the Quickchange method (Stratagene), essentially as described by the manufacturer. The template, pCR®2.1*(dmpFG)*, was prepared by inserting the *EcoR*I-*Not*I fragment from the *dmpFG* coding region of a subclone of pVI150, pVI1316Δ into the same sites of the pCR®2.1 vector (Invitrogen®) (*1*). Mutagenized plasmid DNA was prepared from several individual colonies and screened for the presence of the appropriate introduced silent restriction site. A small DNA fragment containing the mutation was then excised with appropriate restriction endonucleases (*Bpu1102I/Bsu36I*, generating a 334 bp fragment for D209A and *PmaCI/Bpu1102I*, generating a 350 bp

fragment, for C132S) and subsequently inserted into these sites in the WT pT7.5 DmpFG protein expression plasmid. Successful incorporation of the mutated fragment was again confirmed by the silent restriction site analysis. Expression plasmids for each variant were sequenced over the mutagenized insert region to insure that no unexpected mutations were introduced into the fragment derived from the Quickchange procedure. Each purified WT and variant DmpFG protein was further verified by accurate mass measurement of intact protein using an ESI-Q-TOF mass spectrometer. The experimental masses were as expected for the introduced substitution.

Protein Purifications. WT and the variant DmpFG proteins were overexpressed in *E. coli* C41 (DE3) cells as described for WT DmpFG (*119*). Variant D209A was purified by the method previously reported for WT protein (*119*). Variant C132S did not bind efficiently to the NAD^+ affinity column, so phenyl-Sepharose chromatography was used for further purification after the DEAE chromatography step. The pool of DEAE column fractions, which had been pre-adjusted to 10% $(NH_4)_2SO_4$ saturation, was loaded onto a phenyl-Sepharose column (36 cm × 2.6 cm) equilibrated with 50 mM Na^+ K^+ phosphate buffer containing 1 mM DTT ("PD buffer") and 10% saturated $(NH_4)_2SO_4$. The column was then washed with this buffer (200 mL), followed by a gradient (200 mL/200 mL) of 10% saturated $(NH_4)_2SO_4$ in PD buffer to 50mM PD buffer at a flow rate of 2 mL/min, collecting 6 mL fractions. Based on SDS-PAGE analysis (*122*), the fractions with purified DmpFG protein exclusively were combined, subjected to buffer exchange and then concentrated and stored, as described previously (*119*).

Protein concentrations were determined by combination of the modified BCA (Pierce) method (*123*) and 280 nm absorbance detection where one unit of absorption at 280 nm was estimated to correspond to a 0.62 mg/mL of protein concentration (*124*).

Estimation of Steady-State Kinetic Constants. Acetaldehyde dehydrogenase activity of DmpFG is defined as the rate of NAD^+ reduction (measured at 340 nm) in the presence of acetaldehyde and coenzyme A. The kinetic constants were estimated using initial velocities at different substrate concentrations, and fitting the data to the Michaelis-Menten equation using GraFit 5 (*125*). The assays were initiated by the addition of the enzyme (210 μg/mL C132S or 0.75 μg/mL WT and D209A) to 50 mM HEPES buffer (pH 8, 25 °C) containing 1 mM DDT, varying concentrations of each of the three substrates and fixed concentrations of the other two substrates (568.5 μM NAD^+, 128.2 μM CoA and 38.7 mM acetaldehyde). To investigate the aldehyde dehydrogenase kinetic mechanism, both initial velocity and product inhibition experiments were performed. In the initial velocity experiments each of the three substrates, NAD^+, acetaldehyde and coenzyme A, was varied while the other two substrates were maintained in the general concentration range of their Michaelis constants. In the product inhibition experiments initial velocity measurements were conducted where the concentration of substrate, CoA or NAD^+, was varied at several fixed concentrations of product, either NADH or acetyl-CoA. Product inhibition patterns were examined using Lineweaver-Burk plots.

NAD^+, CoA and NADH concentrations were determined spectrophotometrically using molar extinction coefficients of ε_{260} = 18,000 $cm^{-1}M^{-1}$, ε_{260} = 16,800 $cm^{-1}M^{-1}$ and ε_{340} = 6,220 $cm^{-1}M^{-1}$, respectively (*126*). Acetaldehyde concentration was estimated with alcohol dehydrogenase (*127*). The concentration of L(S)-4H2KV (1) was taken as

identical to that of the NADH generated by coupling DmpG with DmpF under conditions where all 4H2KV was depleted.

Generation of Acylenzyme Intermediate. Acetyl-enzyme intermediate from the back reaction was produced by incubating 0.17 nmol of WT DmpFG protein (or 0.19 nmol of C132S) with 0.27 nmol of acetyl-CoA for 1 min (10 min for C132S) at 22 °C in 50 mM HEPES buffer (pH 8). Then, samples were analyzed by mass spectrometry or immediately digested with trypsin (1:12 ratio, w/w with protein) for 2 h at 37 °C. Digestion was quenched by adding TFA (final pH~2) followed by storage at –80 °C until mass spectrometric analysis.

Sample preparation from the forward reaction was carried out by incubating 0.17 nmol of WT DmpFG protein (or 0.19 nmol of C132S) with 20.5 nmol of NAD^+ and 4 μmol of acetaldehyde prepared in H_2O (or, alternatively, 59.4 nmol of DmpG substrate, 4-hydroxy-2-ketovalerate) for 30 sec (3 min for C132S) at 22 °C in 20 mM HEPES buffer (pH 6.5). Samples were subsequently dried using a SpeedVac at room temperature to remove the unreacted acetaldehyde. After being dissolved in 50 mM HEPES buffer (pH 8), the dried samples were either subjected to intact protein mass analysis or to trypsin digestion as detailed above.

Acylenzyme Intermediate Identification with Mass Spectrometry. The tryptic peptide analyses of DmpFG by either MALDI or ESI-Q-TOF mass spectrometry were performed as described previously (*119*), as was full-length sequencing of targeted peptides using HPLC–ESI-Q-TOF. Protein mass measurement was done using a Waters CapLC system coupled to an ESI-Q-TOF 2 mass spectrometer. The CapLC system was equilibrated with a mixture of 90% solvent A (97% H_2O: 3% acetonitrile: 0.1% formic acid) and 10%

solvent B (97% acetonitrile : 3% H_2O : 0.1% formic acid). The samples were loaded and desalted in the Symmetry 300 C18 trap column (0.35 mm × 5mm) with the equilibration solvent. Then the proteins were eluted into the mass spectrometer with a gradient of 10% to 90% solvent B over 30 min.

Unhydrated Acetaldehyde as a Substrate for DmpF. Preliminary experiments with the organic solvents acetonitrile, acetone, dimethoxyethane, dimethylforamide and tetramethylurea showed that no alteration of DmpF activity was observed in the presence of 1% dimethylforamide or tetramethylurea (v/v) in the reaction buffer. Thus, dimethylforamide (DMF) was used for the preparation of acetaldehyde in non-aqueous solvent.

Two sets of experiments were executed to investigate whether hydrated or unhydrated acetaldehyde is a preferred substrate in the DmpF reaction. In the first set of experiments, all three assays were performed in 50 mM HEPES buffer (pH 8) at 22 °C containing 1 mM DTT, 284.2 μM NAD^+, 67 μM CoA, 39 nM DmpF and 5.9 mM total acetaldehyde concentration. Acetaldehyde was delivered to the assay in different ways. One assay was initiated by addition of acetaldehyde prepared in DMF. A second assay was started by addition of DmpFG as the last component to the assay mixture: acetaldehyde prepared in DMF had been allowed to pre-equilibrate in the assay buffer for 5 min. A third assay with anhydrous acetaldehyde in DMF and carbonic anhydrase was performed as for the assay initiated with acetaldehyde from DMF, except that carbonic anhydrase (0.2 mg/mL) was included in the assay mixture.

The second set of experiments consisted of two assays, done at pH 7.5 in either 50 mM Na^+ K^+ phosphate or 50 mM HEPES buffer at 22 °C, with identical substrate

concentrations to the experiments described in the previous paragraph. However, these assays were each started by addition of acetaldehyde in DMF to the assay mixture as the last component.

To estimate the half-life of acetaldehyde hydration in 50 mM Na^+ K^+ phosphate or 50 mM HEPES buffer (pH 7.5) at 22 °C, 100 µL of 1.2 M acetaldehyde in DMF was mixed with 900 µl of either buffer, and the absorbance decrease at 280 nm was recorded, representing the carbonyl signal disappearance during its hydration (*128*). The equations $Abs = 0.909 + 0.6067e^{-9.031t}$ and $Abs = 0.882 + 0.6456e^{-0.7982t}$ perfectly fit the data with 50 mM Na^+ K^+ phosphate and 50mM HEPES buffers, respectively. The half-life values of acetaldehyde hydration in both buffers were calculated based on these equations.

Acetaldehyde-Mediated DmpF Inactivation. Acetaldehyde-mediated DmpF inactivation, and the effects of NAD^+ and DTT on the inactivation, were carried out in a series of related experiments. These assays were performed in 50 mM HEPES buffer (pH 8.0), with 492.5 µM NAD^+, 130.3 µM CoA, 60 mM acetaldehyde and 10.8 nM WT enzyme. The DTT concentration, when present, was 1 mM. The standard assay was started by adding the enzyme to the DTT-containing reaction mixture. The acetaldehyde-mediated inactivation in the presence of DTT was performed by pre-mixing acetaldehyde with the enzyme in the DTT-containing buffer prior to addition of the other reactants. Acetaldehyde-mediated inactivation without DTT was carried out similarly except buffer without DTT was used instead. To examine NAD^+ protection against inactivation, NAD^+ was incubated with the enzyme in assay buffer lacking DTT followed by addition of acetaldehyde, then other assay components. Similar experiments were applied to the

variant C132S enzyme using 468.5 μM NAD^+, 128. μM CoA, 3.84 M acetaldehyde and 3 μM C132S.

To study which form of acetaldehyde more efficiently mediates DmpF inactivation, two comparison experiments were performed. In one, the aldehyde in DMF was added to the DmpFG-containing assay mixture to incur the inactivation, while in the other acetaldehyde was hydrated by pre-equilibrating an identical aliquot of acetaldehyde prepared in DMF in the assay buffer before mixing with the enzyme to start the inactivation. The other reactants were added in the same order for the two experiments. Both experiments were performed at 22 °C in 50 mM HEPES buffer (pH 8), containing 284.2 μM NAD^+, 67 μM CoA, 39 nM enzyme and 43.9 mM acetaldehyde.

Calculation of Solvent Accessible Surfaces. The atomic solvent accessibility of residue Cys-132 of DmpF was estimated using CSU software (*129*) (http://bip.weizmann.ac.il/oca-bin/lpccsu).

3.4 Results

Site-Directed Mutagenesis of Cys-132 and Asp-209 in DmpF. In common with other aldehyde dehydrogenses, a conserved cysteine residue in DmpF has been postulated to be essential for catalysis. Chemical modification studies indicated that the dehydrogenase activity of DmpFG was inactivated by thiol-directed reagents (*3*): sequence analysis and crystal structure data suggested that Cys-132 is an active site residue (*4*). Substitution of Cys-132 by serine incurred no changes of fluorescent and far-UV CD spectra (data not shown), however, decreased k_{cat} approximately 5000-fold (Table 3.1), indicating an important role for this residue in catalysis.

On the basis of the crystal structure, and by comparison with related dehydrogenases,

Table 3.1 Enzyme kinetic parameters for WT DmpF and variants

DmpF protein	apparent K_m (mM)			apparent k_{cat} (sec^{-1})
	NAD^+	CoA	acetaldehyde	
WT	0.156 ± 0.011[a]	0.0087 ± 0.001[a]	38.9 ± 3.4	32.2 ± 0.91
C132S	0.05 ± 0.006	0.043 ± 0.004	13 ± 1.2	0.0066 ± 0.001
D209A	0.203 ± 0.015	0.0091 ± 0.003	41.3 ± 4.1	30.4 ± 1.13

[a] adapted from reference (*119*).

Asp-209 in DmpF was proposed to function as a general base to activate the thiol group of Cys-132 (*4*). The side chain oxygen of Asp-209 is 5.9Å away from the sulfur atom of Cys-132, locating it in a position to activate the Cys-132 thiol group via a bound H_2O molecule. However, for the variant where Asp-209 was replaced by Ala, kinetic parameters were very similar to WT DmpF (Table 3.1). This excludes the possibility that Asp-209 is required to act as a general base to activate Cys-132.

Evidence for Acylenzyme Intermediate Formation at Cys-132 of DmpF. In common with other $NAD(P)^+$ and CoA–dependent aldehyde dehydrogenases (*48, 51, 52, 54*), DmpF follows a bi uni uni uni ping-pong mechanism (Figure 3.1) on the basis of initial velocity and product inhibition studies. In initial velocity experiments where either the NAD^+ or acetaldehyde concentration was varied, with the other two substrate concentrations at a constant ratio, a set of intersecting lines was obtained in Lineweaver-Burk plots (Figure 3.2A and 3.2B). When CoA concentration was varied, a set of parallel lines was obtained instead (Figure 3.2C). In product inhibition experiments both products NADH and acetyl-CoA exhibited competitive inhibition relative to CoA and NAD^+ (Figure 3.3), respectively. These data are consistent with the kinetic mechanism shown in Figure 3.1.

For enzymes catalyzing ping-pong reactions, a covalent intermediate is often, but not always, observed. A covalent acylenzyme intermediate, symbolized F in the kinetic mechanism shown in Figure 3.1, would be formed during either the forward or backward reaction. Thus, it may be possible to capture acylenzyme forms of DmpF either by: incubating with the substrates NAD^+ and acetaldehyde; incubating with the substrates NAD^+ and 4-hydroxy-2-ketovalerate, which is cleaved to acetaldehyde and pyruvate by the associated DmpG; or by reaction with the product, acetyl-CoA.

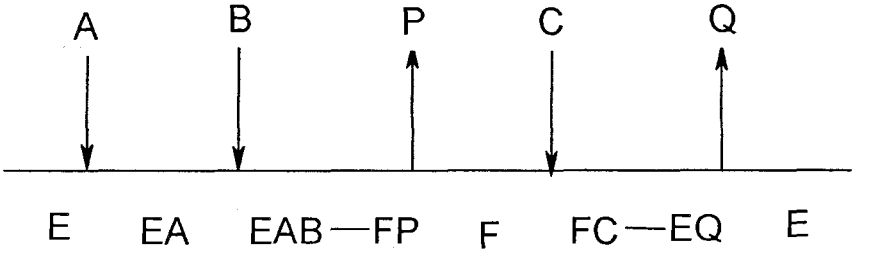

Figure 3.1 Bi uni uni uni ping-pong reaction mechanism scheme for DmF.

E, DmpF; A and B, NAD^+ or acetaldehyde; C, coenzyme A; P, NADH; Q, acetyl-CoA

A

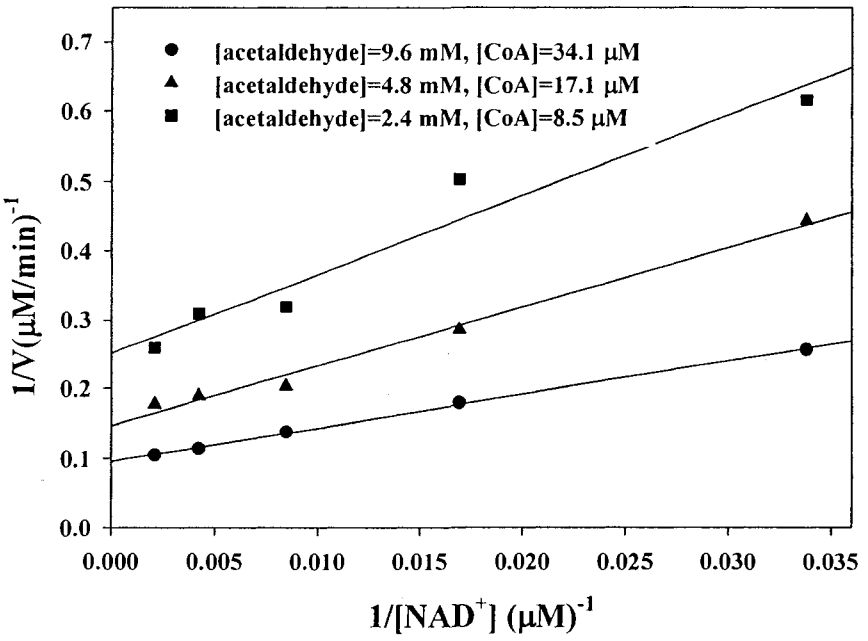
[acetaldehyde]=9.6 mM, [CoA]=34.1 μM
[acetaldehyde]=4.8 mM, [CoA]=17.1 μM
[acetaldehyde]=2.4 mM, [CoA]=8.5 μM
1/V(μM/min)-1
1/[NAD+] (μM)-1
0.0
0.1
0.2
0.3
0.4
0.5
0.6
0.7
0.000
0.005
0.010
0.015
0.020
0.025
0.030
0.035

B

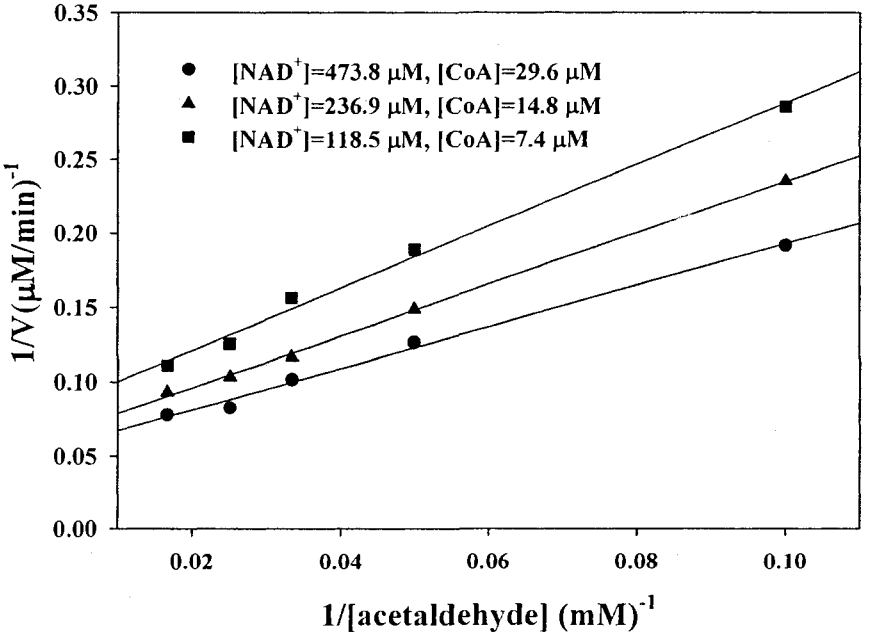
[NAD+]=473.8 μM, [CoA]=29.6 μM
[NAD+]=236.9 μM, [CoA]=14.8 μM
[NAD+]=118.5 μM, [CoA]=7.4 μM
1/V(μM/min)-1
1/[acetaldehyde] (mM)-1
0.00
0.05
0.10
0.15
0.20
0.25
0.30
0.35
0.02
0.04
0.06
0.08
0.10

C

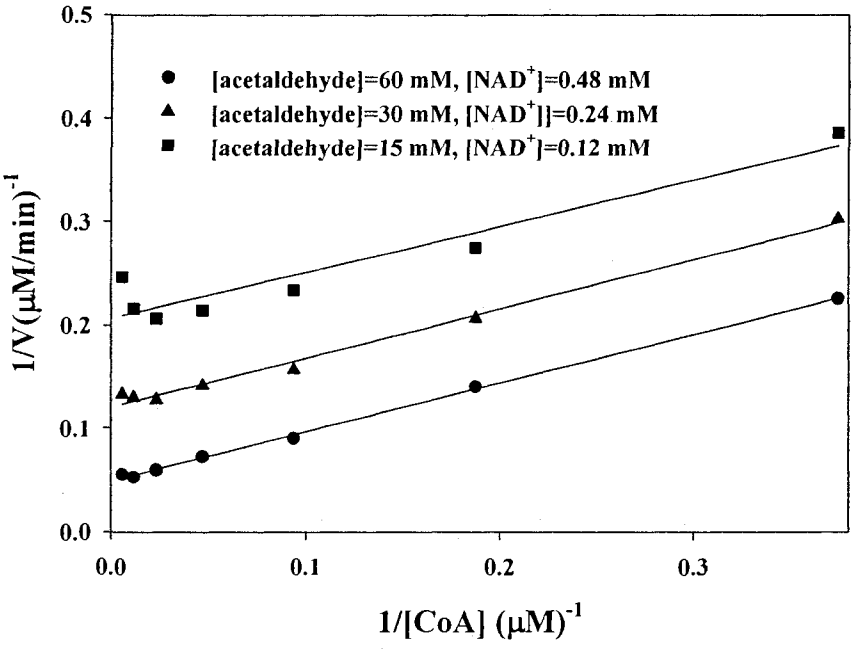

Figure 3.2 DmpF initial velocity patterns with varying concentrations of each of the three substrates and the other two substrates in constant ratio as indicated in the insets.

(A) With NAD^+ as the varied substrate and the concentrations of acetaldehyde and CoA in constant ratio.

(B) With acetaldehyde as the varied substrate and the concentrations of NAD^+ and CoA in constant ratio.

(C) With CoA as the varied substrate and the concentrations of NAD^+ and acetaldehyde in constant ratio.

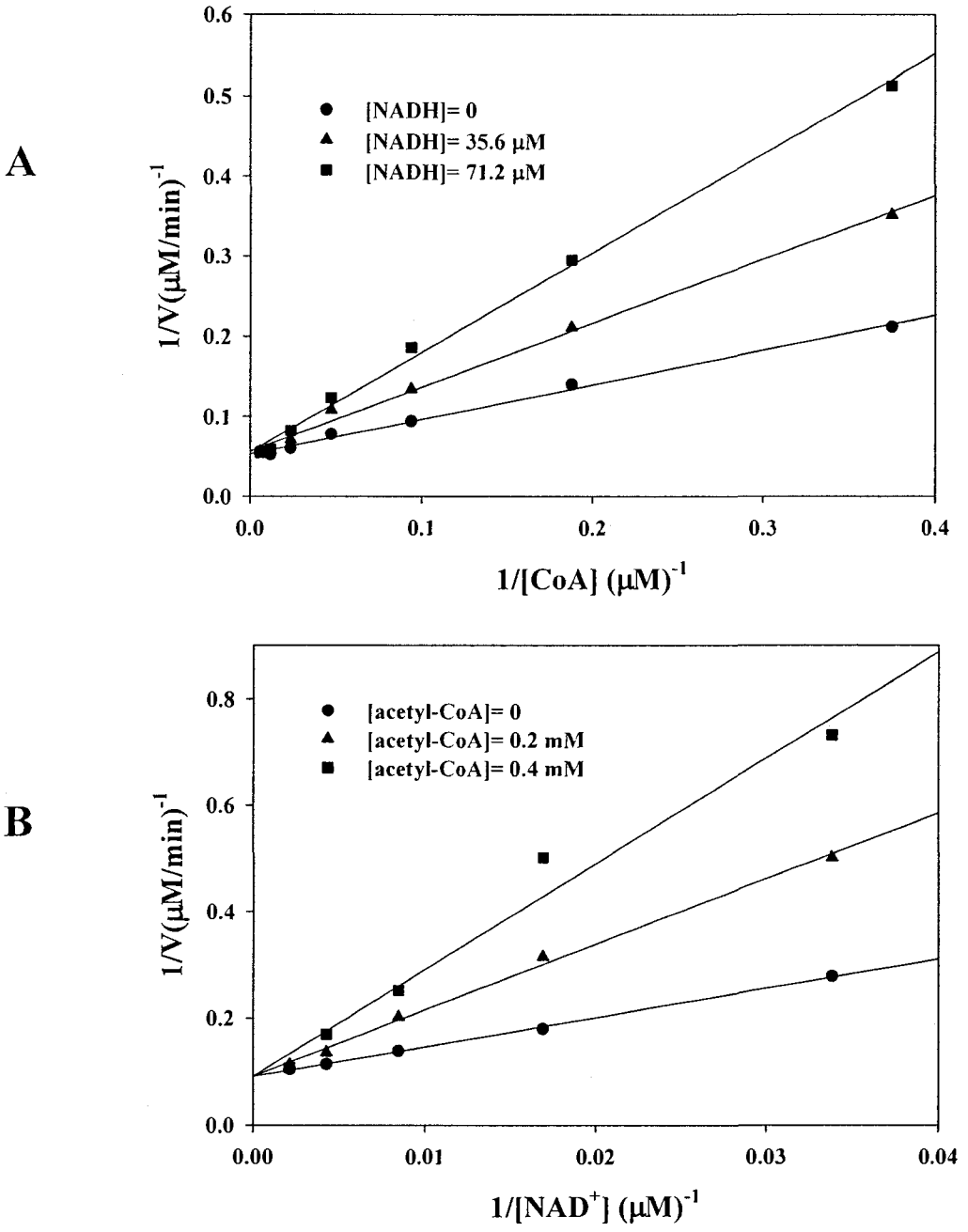

Figure 3.3 Product inhibition of DmpF by NADH or acetyl-CoA.

(A) Inhibition by NADH relative to CoA. The concentrations of NAD^+ and acetaldehyde were held at 492 μM and 65 mM, respectively. The NADH concentrations are indicated in the inset. (B) Inhibition by acetyl-CoA relative to NAD^+. The concentrations of acetaldehyde and CoA were held at 10.6 mM and 45.1 μM, respectively. The acetyl-CoA concentrations are indicated in the inset.

ESI-Q-TOF spectra showed that a 42 Da adduct of intact DmpF was obtained under all three conditions, (Figure 3.4A and data not shown), consistent with the formation of a covalent acetyl-DmpF complex. MALDI-TOF spectra of tryptic digests of modified enzyme generated by either forward or backward reactions demonstrated an extra peptide of 2274.17 Da ($[M+H]^+$), which represents modification of the 2232.17 Da peptide ($[M+H]^+$) by 42 Da, corresponding to an acetyl group (compare Figure 3.5A with 3.5B, and data not shown). This modified peptide, not present in control experiments lacking substrates or product (Figure 3.5A), was tentatively assigned as the fragment comprising residues 125–146 of DmpF, based on its predicted molecular mass of 2232.13 Da ($[M+H]^+$).

In the ESI-Q-TOF spectra of peptides from tryptic digests of the intermediate enzyme complex, a doubly-charged species at m/z 1137.56 Th corresponds to a 2274.12 Da peptide, while a doubly-charged ion at m/z 1116.56 Th corresponds to the unmodified peptide, with a mass 42 Da lower (Figure 3.6A, 3.6B and data not shown). HPLC–ESI-MS/MS was performed to sequence the doubly-charged peptides with m/z 1116.56 Th and 1137.56 Th. The results show that the species with m/z 1116.56 Th represents the doubly charged peptide corresponding to residues 125–146 of DmpF (Figure 3.7, Table 3.2), while the peptide with m/z 1137.56 Th corresponds to the modification of peptide 125–146 of DmpF with an acetyl group (42 Da) addition on Cys-132 of the sequence (Figure 3.8, Table 3.2). Thus, the acetyl-S-Cys132 DmpF intermediate can be generated from both catalytic directions, and is stable enough under the experimental conditions used to be identified by sequencing the modified peptide and comparing those results to the unmodified peptide.

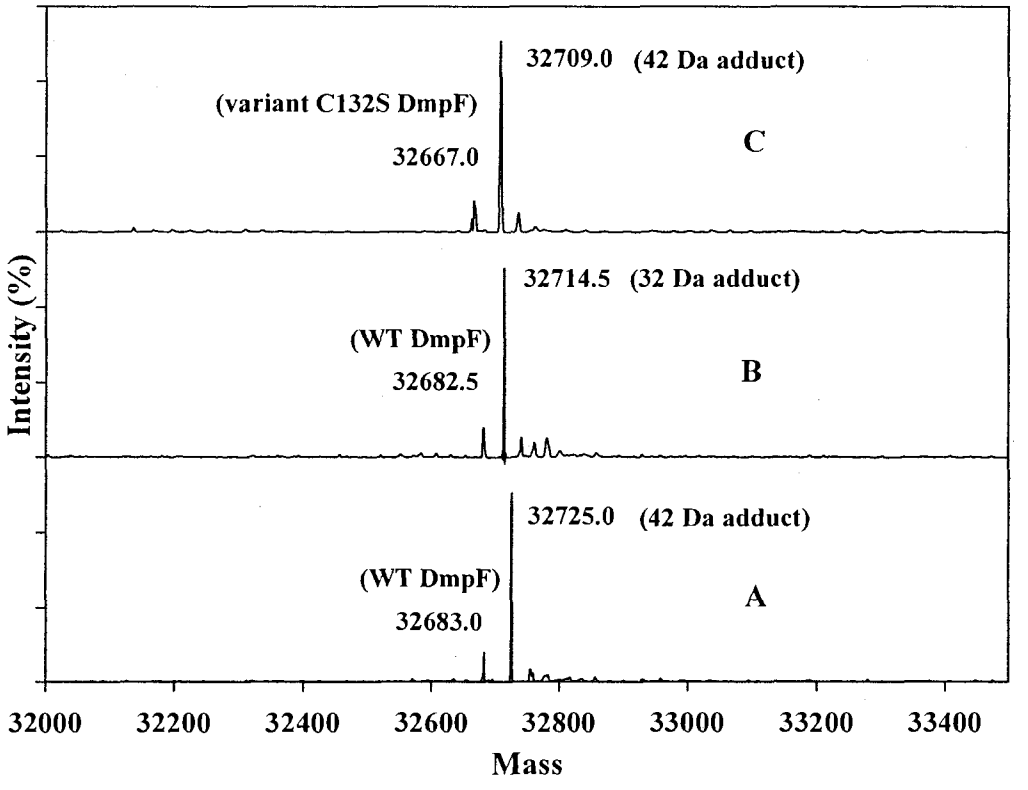

Figure 3.4 DmpF intact protein masses determined by ESI-Q-TOF:

(A) WT DmpFG incubated with acetyl-CoA; similar results were obtained by incubating WT DmpFG with NAD^+ and acetaldehyde or with NAD^+ and 4-hydroxy-2-ketovalerate (data not shown). (B) WT DmpFG incubated with acetaldehyde and (C) the C132S variant incubated with acetyl-CoA; similar results were obtained by incubating the C132S variant with NAD^+ and acetaldehyde or with NAD^+ and 4-hydroxy-2-ketovalerate (data not shown).

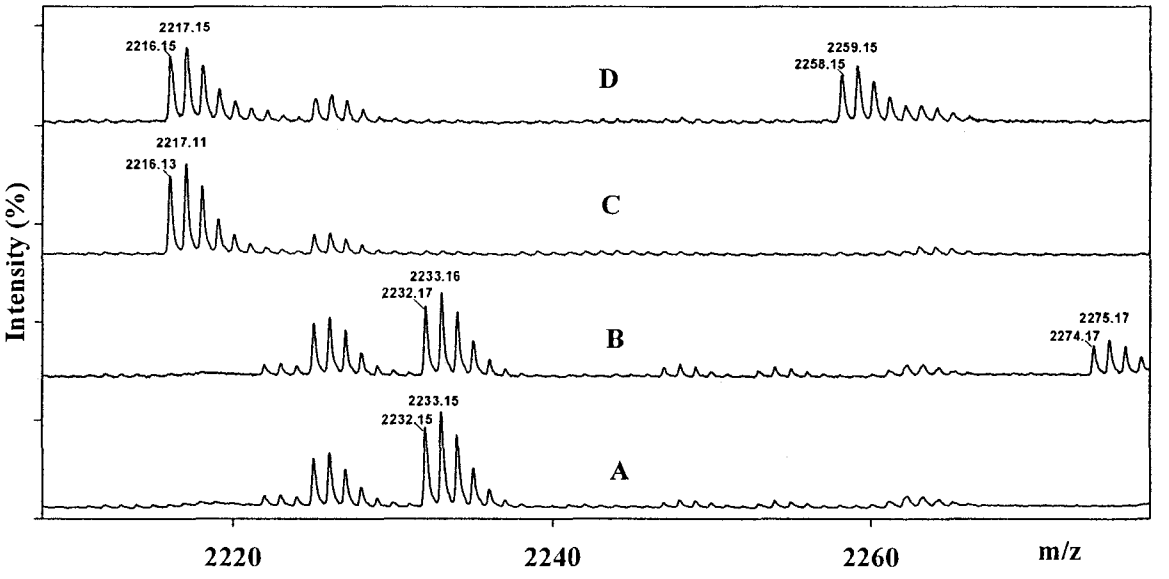

Figure 3.5 Partial range of isotopic envelopes of MALDI-TOF spectra of tryptic digests of (A) WT DmpFG or (B) WT DmpFG incubated with acetyl-CoA. Similar spectra were observed for the tryptic digests of samples obtained by incubating WT DmpFG with NAD^+ and acetaldehyde or with NAD^+ and 4-hydroxy-2-ketovalerate (data not shown). Partial range of isotopic envelopes of MALDI-TOF spectra of tryptic digests of the (C) C132S variant or (D) C132S variant incubated with acetyl-CoA. Similar spectra were observed for the tryptic digests of samples obtained by incubating C132S with NAD^+ and acetaldehyde or with NAD^+ and 4-hydroxy-2-ketovalerate (data not shown).

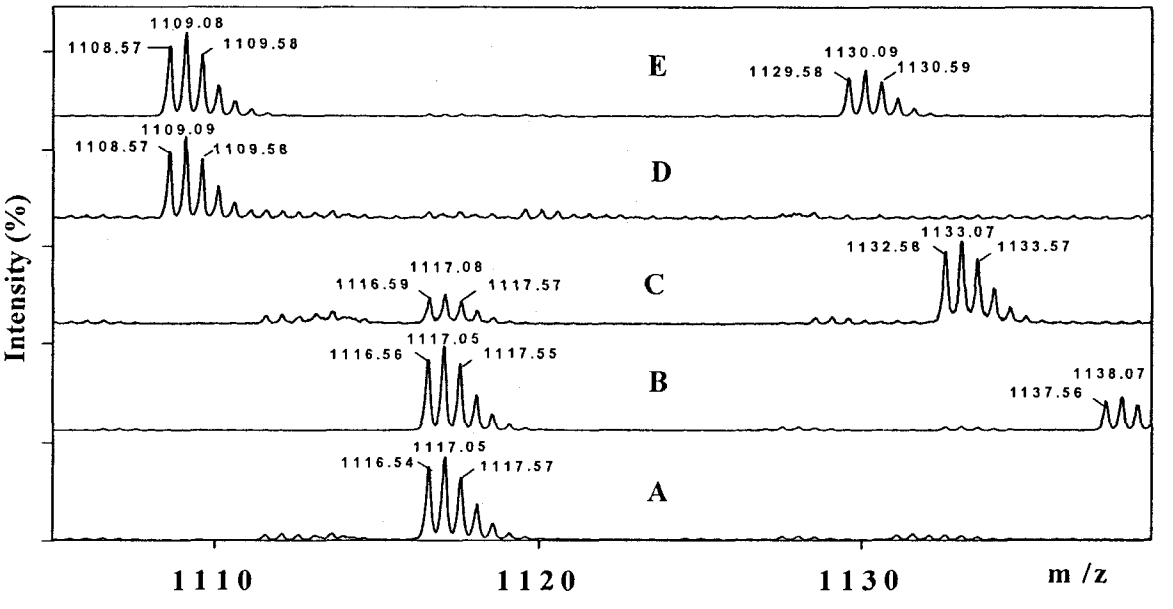

Figure 3.6 Partial range of isotopic envelopes of ESI-Q-TOF spectra of tryptic digests of (A) WT DmpFG and (B) tryptic digest of WT DmpFG incubated with acetyl-CoA. Similar spectra were obtained for tryptic digests of samples prepared by incubating WT DmpFG with NAD^+ and acetaldehyde or with NAD^+ and 4-hydroxy-2-ketovalerate (data not shown). Partial range of isotopic envelopes of ESI-Q-TOF spectra for (C) tryptic digest of WT DmpFG incubated with acetaldehyde, (D) tryptic digest of C132S variant and (E) tryptic digest of C132S variant incubated with acetyl-CoA. Similar spectra were obtained for the tryptic digests of samples obtained by incubating the C132S variant with NAD^+ and acetaldehyde or with NAD^+ and 4-hydroxy-2-ketovalerate.

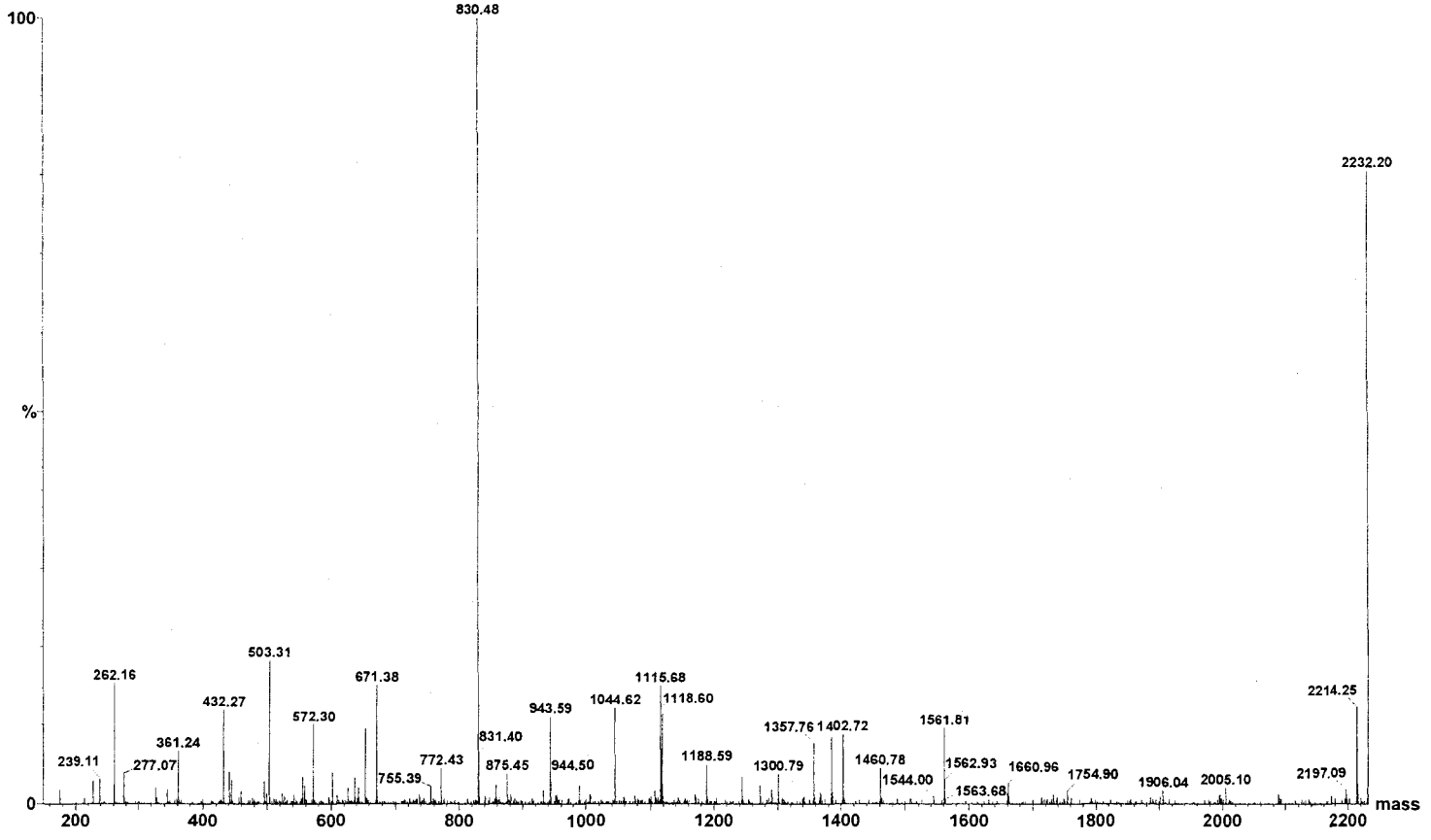

Figure 3.7 Deconvoluted ESI-MS/MS spectrum for the 1116.56 Th ($[M+2H]^{2+}$) peptide of WT DmpFG. The peptide was identified as the sequence corresponding to residues 125–146 of WT DmpF.

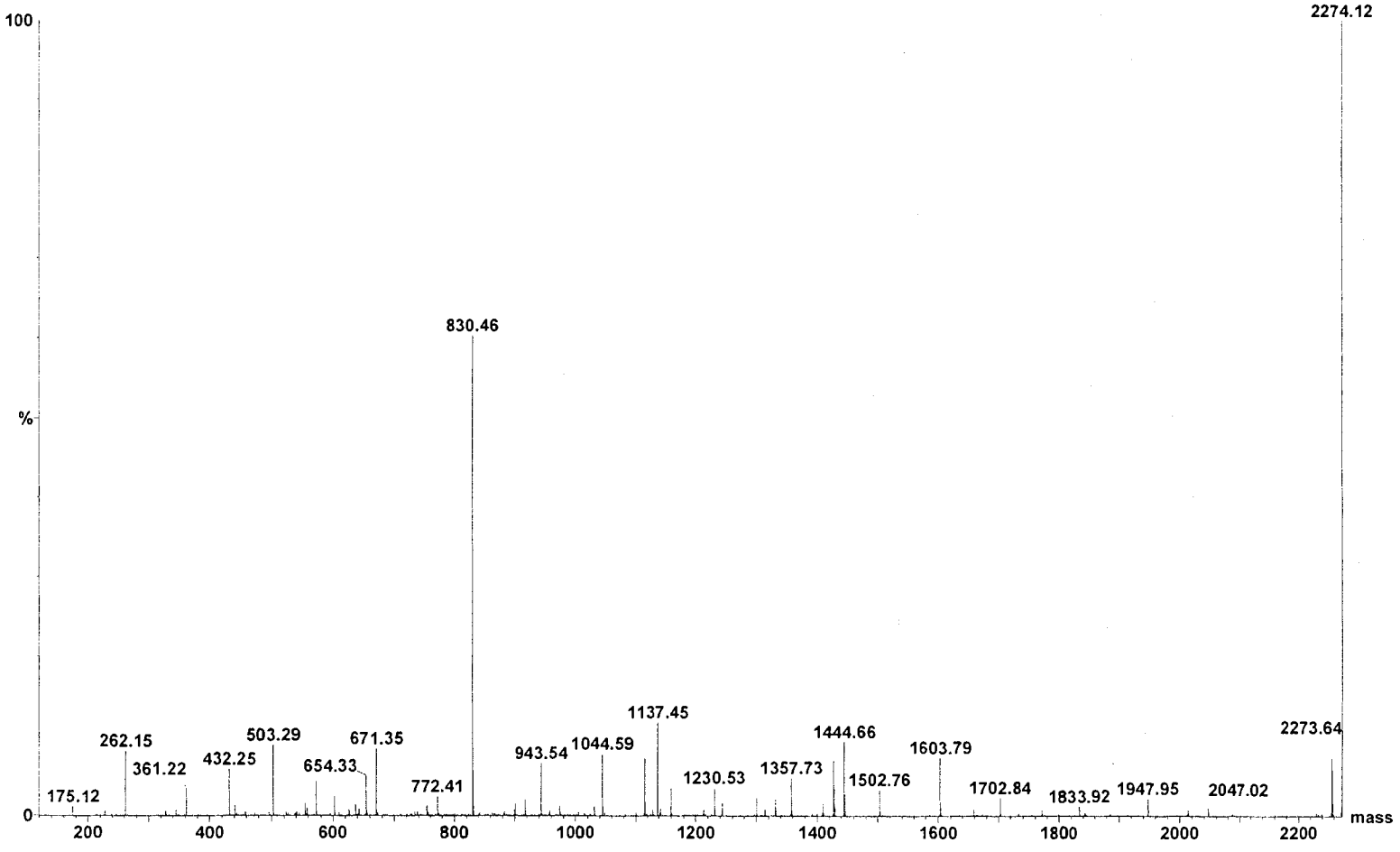

Figure 3.8 Deconvoluted ESI-MS/MS spectrum for the 1137.56 Th ($[M+2H]^{2+}$) peptide of WT DmpFG

This peptide was identified as the sequence corresponding to residues 125–146 with 42Da modification on Cys-132.

Table 3.2 Deconvoluted Fragment Ions from MS/MS Analysis of the 1116.56 Th and 1137.56 Th ($[M+2H]^{2+}$) Peptides of WT DmpFG

	y ion	y ion adduct	b ion	b ion adduct		y ion	y ion adduct	b ion	b ion adduct
Leu_{125}	2232.20	2274.12	-	-	Ala_{136}	1115.68	1115.63	1188.59	1230.53
Asn	-	2160.90	228.14	228.13	Thr	1044.62	1044.59	1289.64	1331.57
Val	2005.10	2047.02	327.22	327.20	Leu	943.59	943.54	1402.72	1446.54
Asn	1906.04	1947.95	441.26	441.25	Pro	830.48	830.46	1499.77	1541.72
Met	1791.98	1833.92	572.30	572.28	Met	733.47	733.40	1630.80	1672.76
Val	1660.96	1702.84	671.38	671.35	Val	602.38	602.36	1729.97	1771.90
Thr	1561.81	1603.79	772.43	772.41	Ala	503.31	503.29	1800.94	1842.85
Cys	1460.78	1502.76	875.45	917.40	Ala	432.27	432.25	1871.98	1913.97
Gly	1357.76	1357.73	932.47	974.40	Val	361.24	361.22	1971.07	2012.96
Gly	1300.79	1300.70	989.48	1031.45	Ser	262.16	262.15	-	-
Gln_{135}	1243.73	1243.70	-	1159.56	Arg_{146}	175.12	175.12	2214.25	2256.06

Active Site Reactivity of the Cys132Ser Variant of DmpF. The data shown in Table 3.1 indicate that the C132S variant of DmpF is still active, albeit with a greatly depressed k_{cat}. To investigate whether a covalent adduct was formed by this variant, mass spectrometry experiments were applied to it in parallel with the WT. In analogy with those experiments, described above, interpretation of these data are consistent with the presence of an acetyl-O-Ser132 DmpF intermediate (Figure 3.4C, 3.5C, 3.5D, 3.6D, 3.6E, 3.9, 3.10 and Table 3.3).

Optimization of Conditions for Observation of Acylenzyme Intermediates. Conditions required to observe acylenzyme intermediates had to be determined empirically. The rate of formation of acetyl-DmpF appeared to depend on pH, in the range of pH 6 to 9: the higher the pH, the faster the formation of acetyl-DmpF as judged by mass spectrometry (data not shown). At pH 8, under the conditions indicated in *Material and Methods*, almost all WT DmpF reacted to form acetyl-S-DmpF within one min at room temperature, as judged by the relative intensities of peaks of modified and unmodified intact protein in ESI mass spectra (for example the data shown in Figure 3.4 A were obtained after one min incubation). The C132S variant took a much longer time to be converted into acetyl-O-DmpF (data not shown). However, the acetyl-S-DmpF intermediate was not stable past one min at pH 8 as indicated by the observation that the relative intensity of modified DmpF decreased, and that of unmodified DmpF grew stronger, with increased incubation times (data not shown). The acetyl-O-DmpF intermediate was more stable than its acetyl-S-DmpF counterpart, which is similar to the case of β-ketoacyl thiolase from *Zoogloea ramigera* (*130*). However, when DmpF acylation reactions were quenched by denaturing the protein or decreasing to low pH

after a short reaction time, the relative intensities of modified and unmodified proteins did not change over time, suggesting that the acetyl-DmpF complex was stable when unfolded or under acidic conditions.

Conditions for the preparation of trypsinized samples also had to be optimized for observation of the acylenzyme intermediates. To trap the acetyl-DmpF intermediate from the backward reaction, acetyl-CoA was incubated with DmpFG for one min at pH 8 and room temperature, and then a high concentration of trypsin was added to digest the acetyl-DmpF as soon as possible before more acetyl-DmpF could hydrolyze to free DmpF. In the forward reactions, DmpFG was incubated with either NAD^+ and acetaldehyde or with NAD^+ and 4-hydroxy-2-ketovalerate, and the unreacted acetaldehyde was removed prior to trypsin digest, otherwise the unreacted acetaldehyde modified the free amino group at the N-terminal of the digest peptides and some exposed amino groups after protein denaturation (data not shown). Low pH buffer (6–6.5) was used for the forward reaction to keep the formed acetyl-DmpF more stable during removal of the unreacted acetaldehyde with the Speedvac. The dried sample was then dissolved and adjusted to pH ~ 8 for optimal digestion by trypsin.

Unhydrated Acetaldehyde as a Substrate for DmpF. The results in the previous section showed that Cys-132 at the active site of DmpF is capable of forming an acetyl-enzyme intermediate consistent with the kinetic mechanism shown in Figure 3.1. Attack of the active site thiol on the aldehyde of the substrate would be facilitated if the functional group were not hydrated. In fact, the very high K_m (38.9 mM, Table 3.1) for acetaldehyde suggests that exogenous acetaldehyde equilibrated in water may be a very poor substratefor DmpF. Therefore, the ability of unhydrated acetaldehyde to function as

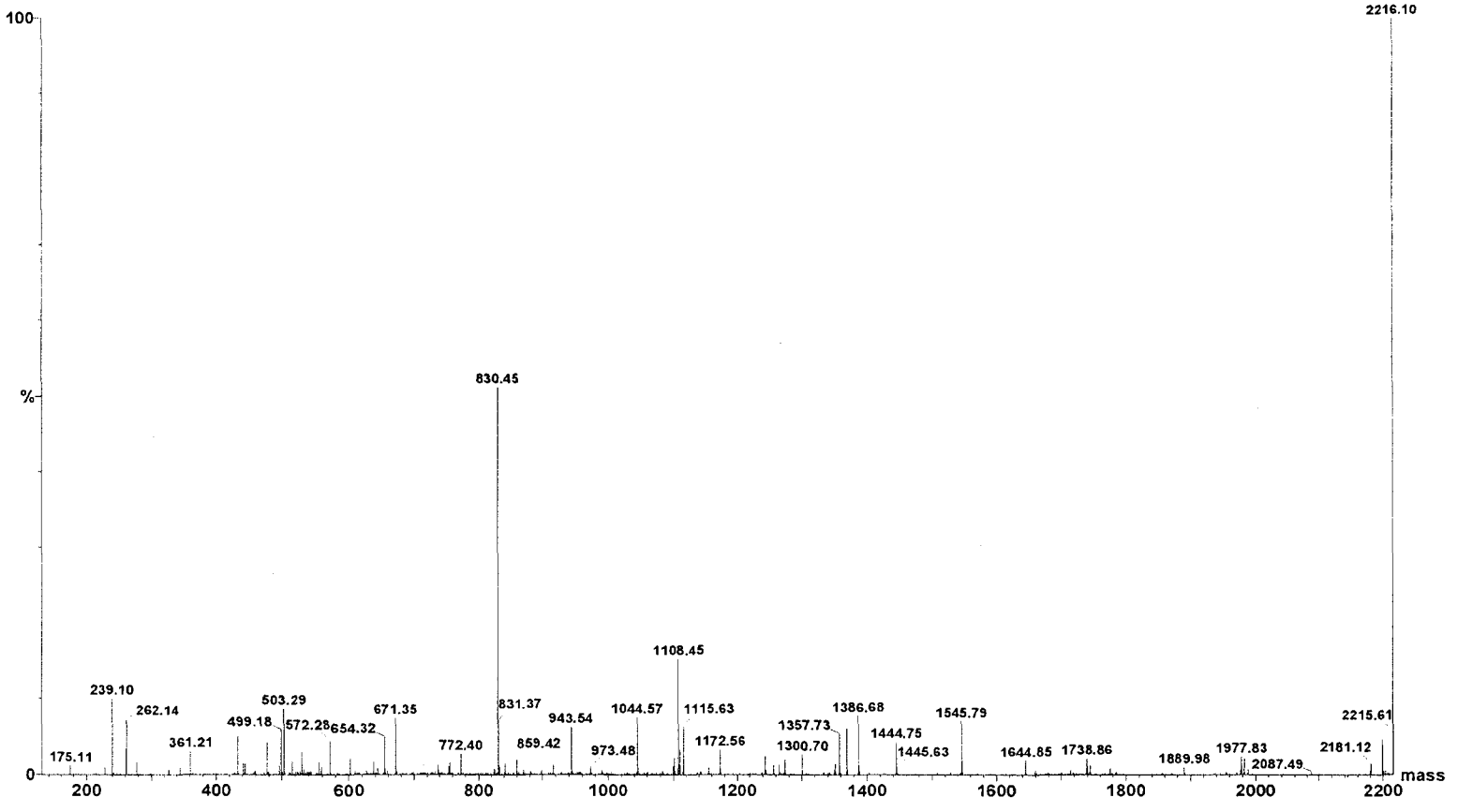

Figure 3.9 Deconvoluted ESI-MS/MS spectrum for the 1108.57 Th ($[M+2H]^{2+}$) peptide of the C132S variant. This peptide was identified as the sequence corresponding to residues 125–146 of C132S DmpF.

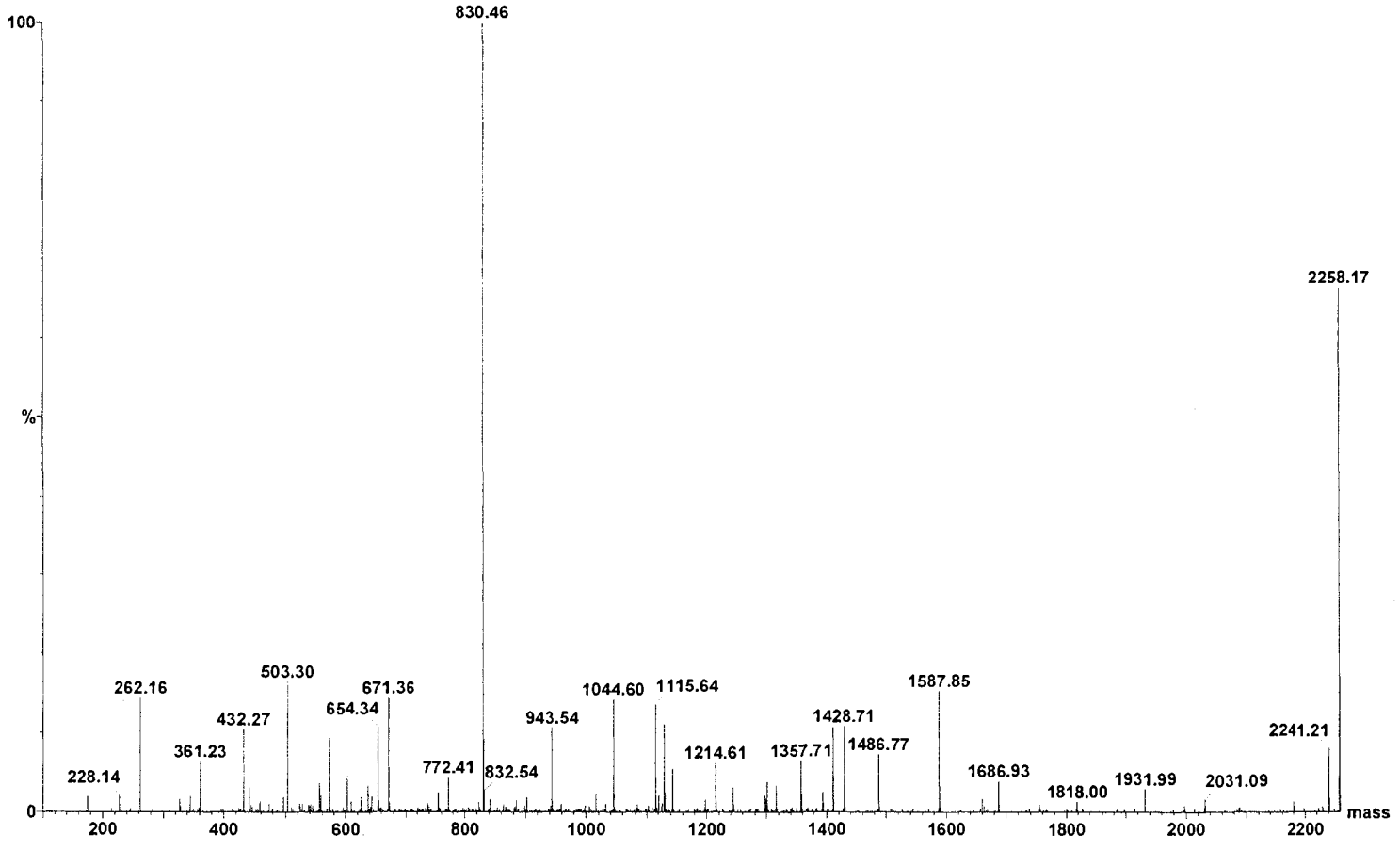

Figure 3.10 Deconvoluted ESI-MS/MS spectrum for the 1129.58 Th ($[M+2H]^{2+}$) peptide of the C132S variant. The peptide was identified as the sequence corresponding to residues 125–146, with a 42Da modification on Ser-132, of C132S DmpF.

Table 3.3 Deconvoluted Fragment Ions from MS/MS Analysis of the 1108.57 Th and 1129.58 Th ($[M+2H]^{2+}$) Peptides of the C132S Variant

	y ion	y ion adduct	b ion	b ion adduct		y ion	y ion adduct	b ion	b ion adduct
Leu_{125}	2216.10	2258.17	-	-	Ala_{136}	1115.63	1115.64	1172.56	1214.61
Asn	-	-	228.13	228.14	Thr	1044.57	1044.60	1273.60	1315.63
Val	1988.99	2031.09	327.19	327.21	Leu	943.54	943.54	1386.68	1428.71
Asn	1889.98	1931.99	441.24	441.25	Pro	830.45	830.46	1483.75	1525.72
Met	1775.85	1818.00	572.28	572.29	Met	733.39	733.42	1614.75	1656.86
Val	1644.85	1686.93	671.35	671.36	Val	602.35	602.37	1713.85	1755.94
Thr	1545.79	1587.85	772.40	772.41	Ala	503.29	503.30	1784.88	1826.93
Ser	1444.75	1486.77	859.42	901.47	Ala	432.25	432.27	1855.83	1897.94
Gly	1357.73	1357.71	916.46	958.47	Val	361.21	-	1955.02	1997.07
Gly	1300.70	1300.73	973.48	1015.50	Ser	262.14	262.16	2042.03	2084.10
Gln_{135}	1243.65	1243.73	1101.49	1143.57	Arg_{146}	175.11	175.12	-	-

substrate was examined by initiating the reaction with acetaldehyde from organic solvent, as has been done previously with other dehydrogenases (*131-133*).

When the DmpF activity assay was initiated by addition of acetaldehyde in dimethylforamide (DMF) to 50 mM HEPES buffer (pH 8) containing 284 μM NAD^+ and 67 μM CoA, as well as DmpFG and 1 mM DTT, the initial rate was clearly faster than in the reaction where acetaldehyde in DMF was allowed to equilibrate in the assay buffer for five min and DmpFG was added last (Figure 3.11A). An identical result was obtained when acetaldehyde prepared in HEPES buffer was added as the last component (data not shown), showing that the initial rate increase could not be explained by preincubation of DmpFG with NAD^+, CoA and DTT. Furthermore, when carbonic anhydrase, which promotes the hydration of acetaldehyde (*134*), was included in assays initiated by addition of acetaldehyde from DMF, the initial rapid reaction period was drastically shortened (Figure 3.11A). The activity burst became shorter with higher concentrations of carbonic anhydrase (data not shown). Finally, the initial rate of DmpF activity when acetaldehyde in DMF was added last varied, depending on whether the assay was done in HEPES or phosphate buffers (Figure 3.11B), This correlates with the hydration half-life of acetaldehyde, which was observed to be 0.87 min in 50 mM HEPES buffer (pH 7.5) and only 0.077 min in 50 mM phosphate buffer (pH 7.5) at 22 °C. Together, these results indicate that higher DmpF activity is associated with a higher effective concentration of unhydrated acetaldehyde.

Acetaldehyde-Mediated DmpF Inactivation. Preincubation of enzyme with CoA or acetaldehyde resulted in loss of DmpF activity (*119*) (Figure 3.12). Protection against

A

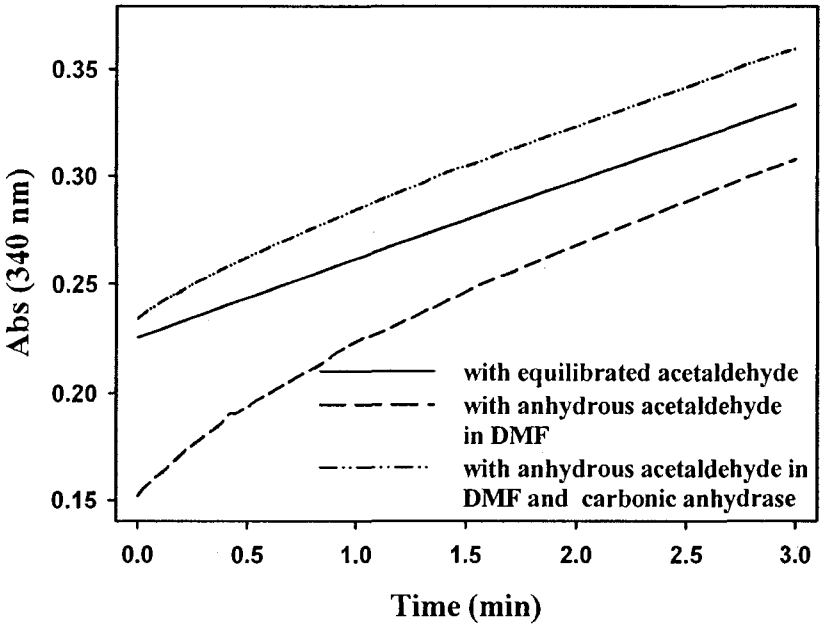
0.35
0.30
0.25
0.20
0.15
Abs (340 nm)
0.0
0.5
1.0
1.5
2.0
2.5
3.0
Time (min)
with equilibrated acetaldehyde
with anhydrous acetaldehyde in DMF
with anhydrous acetaldehyde in DMF and carbonic anhydrase

B

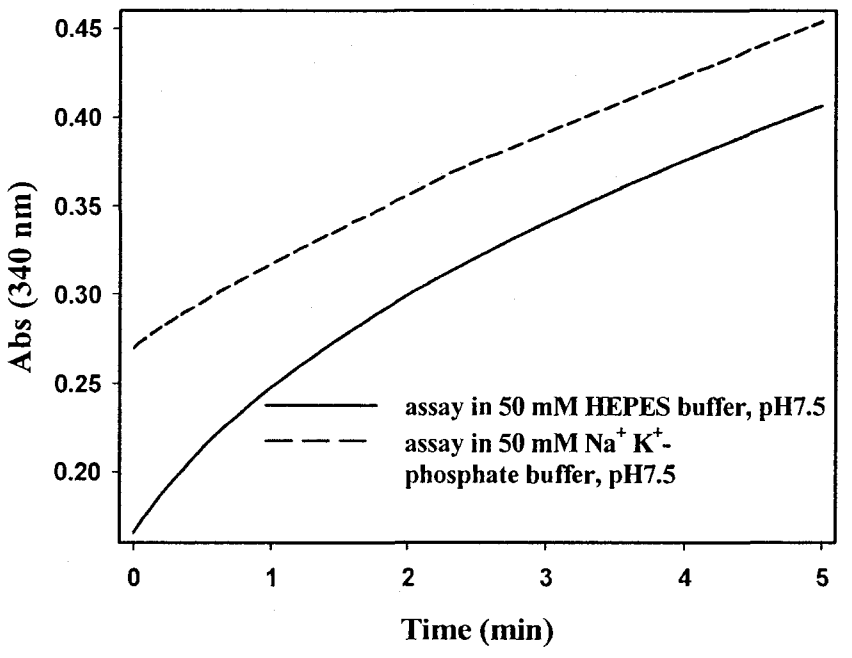
0.45
0.40
0.35
0.30
0.25
0.20
Abs (340 nm)
0
1
2
3
4
5
Time (min)
assay in 50 mM HEPES buffer, pH7.5
assay in 50 mM Na+ K+-phosphate buffer, pH7.5

Figure 3.11 The effect of acetaldehyde hydration on the initial rate of DmpF.

The reaction buffers contained 1 mM DTT, 284 μM NAD^+, 67 μM CoA, 39 nM enzyme and 5.9 mM acetaldehyde prepared in DMF. Note that traces are offset for clarity.

(A) Assays were performed in 50 mM HEPES buffer (pH 8) at room temperature (ca. 22 ^{o}C). The assay with anhydrous acetaldehyde was initiated by the addition of acetaldehyde in DMF. The assay with equilibrated acetaldehyde was started by the addition of DmpFG enzyme, so that acetaldehyde delivered from DMF was preequilibrated in the assay buffer. The assay with anhydrous acetaldehyde and carbonic anhydrase was performed as the assay with anhydrous acetaldehyde in DMF except that 0.2 mg/mL of carbonic anhydrase was included in the reaction buffer.

(B) Assays were carried out in 50 mM Na^+ K^+ phosphate or HEPES buffer (pH 7.5) at room temperature. The reactions were started by addition of acetaldehyde in DMF to the assay mixture as the last component.

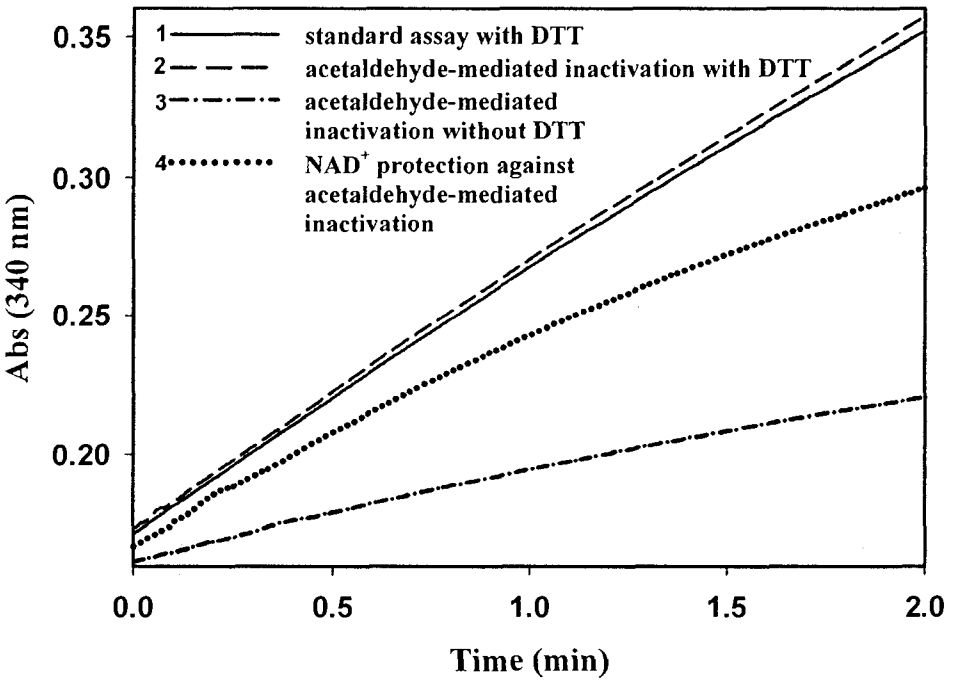

Figure 3.12 Acetaldehyde-mediated inactivation of DmpF, and protection by NAD^+.

The assays were performed in 50 mM HEPES buffer (pH 8) with 493 μM NAD^+, 130 μM CoA, 60 mM acetaldehyde and 10.8 nM enzyme: when present, the DTT concentration was 1mM. Enzyme was added as the last component to the standard assay mixture containing DTT (1). Acetaldehyde–mediated inactivation was performed by mixing acetaldehyde with the enzyme in the DTT-containing buffer before addition of other reactants, and the reaction was started by adding CoA last (2); this experiment was repeated using buffer without DTT (3). NAD^+ protection against acetaldehyde–mediated inactivation was carried out by mixing NAD^+ with the enzyme in the absence of DTT and the reaction was initiated by addition of CoA last (4).

inhibition by 1 mM DTT (*119*) (Figure 3.12) suggests that inhibition by these substrates resulted from the oxidation of a thiol group on the enzyme. Essentially no inhibition by pre-incubation with CoA or acetaldehyde was observed in the C132S variant of DmpF indicating that the active site thiol of DmpF is the residue susceptible to oxidation (Figure 3.13). As previously reported, 1 mM DTT rescued CoA-mediated inactivation, consistent with disulfide formation between the thiol groups of CoA and Cys-132 (*119*). However, although the presence of DTT protected against inactivation by acetaldehyde (Figure 3.12), it could not recover acetaldehyde-inactivated DmpF after it had been generated (data not shown). These results suggest that more than one oxidized form of Cys-132 may be formed by incubating acetaldehyde with the enzyme.

Mass spectrometry was employed to further examine the nature of acetaldehyde-mediated DmpF inactivation and the oxidation state of Cys-132. Upon incubation with acetaldehyde alone, DmpF underwent a 32 Da modification (Figure 3.4 B). Formation of acetaldehyde adducts with α-amino groups (*30*), ε-amino groups (*31*), or thiol groups (*32*) of proteins has been reported previously. These acetaldehyde-protein adducts were identified to be imidazolidinone or thiazolidine derivatives, which give mass increments of 26 Da (*135, 136*). Although 26 Da adducts were observed when DmpF was digested with trypsin in the presence of excess acetaldehyde (data not shown), removal of acetaldehyde using the Speedvac prior to digestion resulted in only the 32 Da adduct being observed.

Information about the position of modification was obtained by tryptic digestion and sequencing of the modified peptides. ESI-MS analysis of tryptic digests revealed an additional doubly-charged peptide of m/z 1132.58 Th present in tryptic digests of

DmpFG incubated with acetaldehyde, compared to enzyme that had never been incubated with acetaldehyde (compare Figure 3.6A with 3.6C). The doubly-charged ion with m/z 1132.58 Th was sequenced using MS/MS and found to correspond to residues 125–146 of DmpF, with a 32 Da modification on Cys-132 (Figure 3.14, Table 3.4). The $[M+H]^{2+}$ ion at m/z 1132.58 Th was not observed when DmpFG was incubated with acetaldehyde in an oxygen-free glove box (data not shown). Together, these data are consistent with the addition of two oxygen atoms to Cys-132 to form cysteine sulfinic acid ($-SO_2H$), resulting in inactivation of DmpF activity.

In order to establish whether acetaldehyde and oxygen-mediated DmpF inactivation was catalyzed by metal ions, acetaldehyde was mixed with DmpFG prior to addition of the other reactants as in Figure 3.12, but in the presence of 0.2 mM diethylenetriaminepentaacetic acid (DTPA) or 5 mM ethylenedinitrilotetraacetic acid (EDTA), respectively. No effect was incurred by DTPA or EDTA on the inactivation of DmpF (data not shown), suggesting that metal ions are not required for acetaldehyde-mediated inactivation of DmpF.

Since the anhydrous form of acetaldehyde was observed to support faster initial rates of DmpF turnover (Figure 3.11), acetaldehyde-mediated inactivation of DmpF was also investigated by inactivating DmpF with acetaldehyde prepared in DMF vs. acetaldehyde equilibrated in water. Acetaldehyde delivered from DMF incurred more extensive inactivation of DmpF than acetaldehyde in DMF equilibrated in buffer first (Figure 3.15). Furthermore, inactivation in the former case appeared to produce more Cys-132 sulfinic acid than in the latter case, as judged by relative peak heights of modified and unmodified peptides in mass spectra of tryptic digests (data not shown).

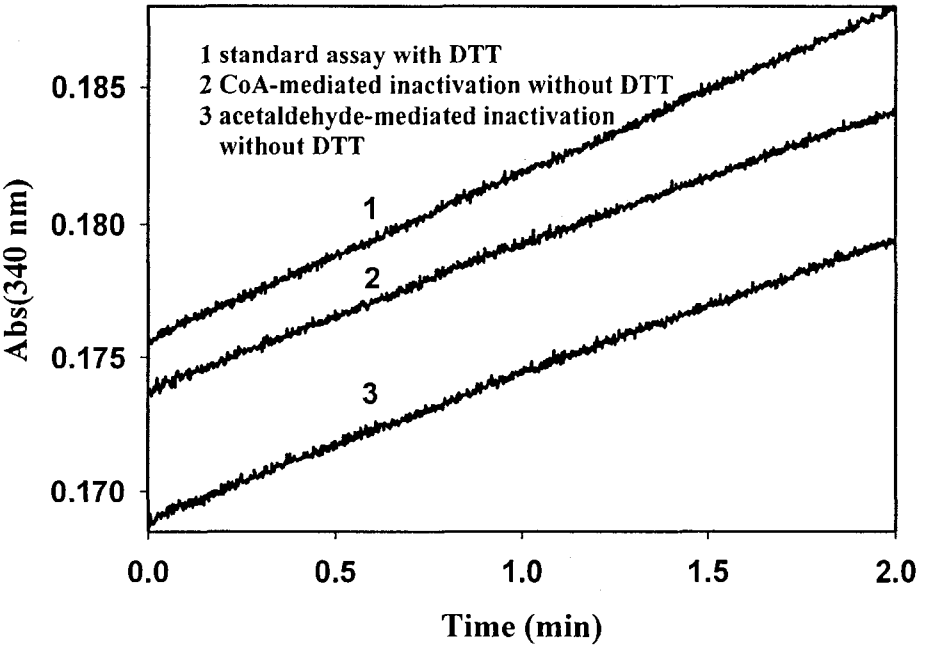

Figure 3.13 Effects of preincubation with acetaldehyde or CoA on activity of C132S DmpF.

Assays were performed in 50 mM HEPES buffer (pH 8) with 469 μM NAD^+, 128 μM CoA, 3.84 M acetaldehyde and 3 μM enzyme: when present, the DTT concentration was 1 mM. CoA-mediated inacativation without DTT was carried out by pre-mixing CoA with the enzyme in the buffer in the absence of DTT prior to addition of the other reactants, and the reaction was started by adding acetaldehyde last. The other assays were done as described for the corresponding ones for WT in Figure 3.12 except that no NAD^+ protection experiment was run in this case.

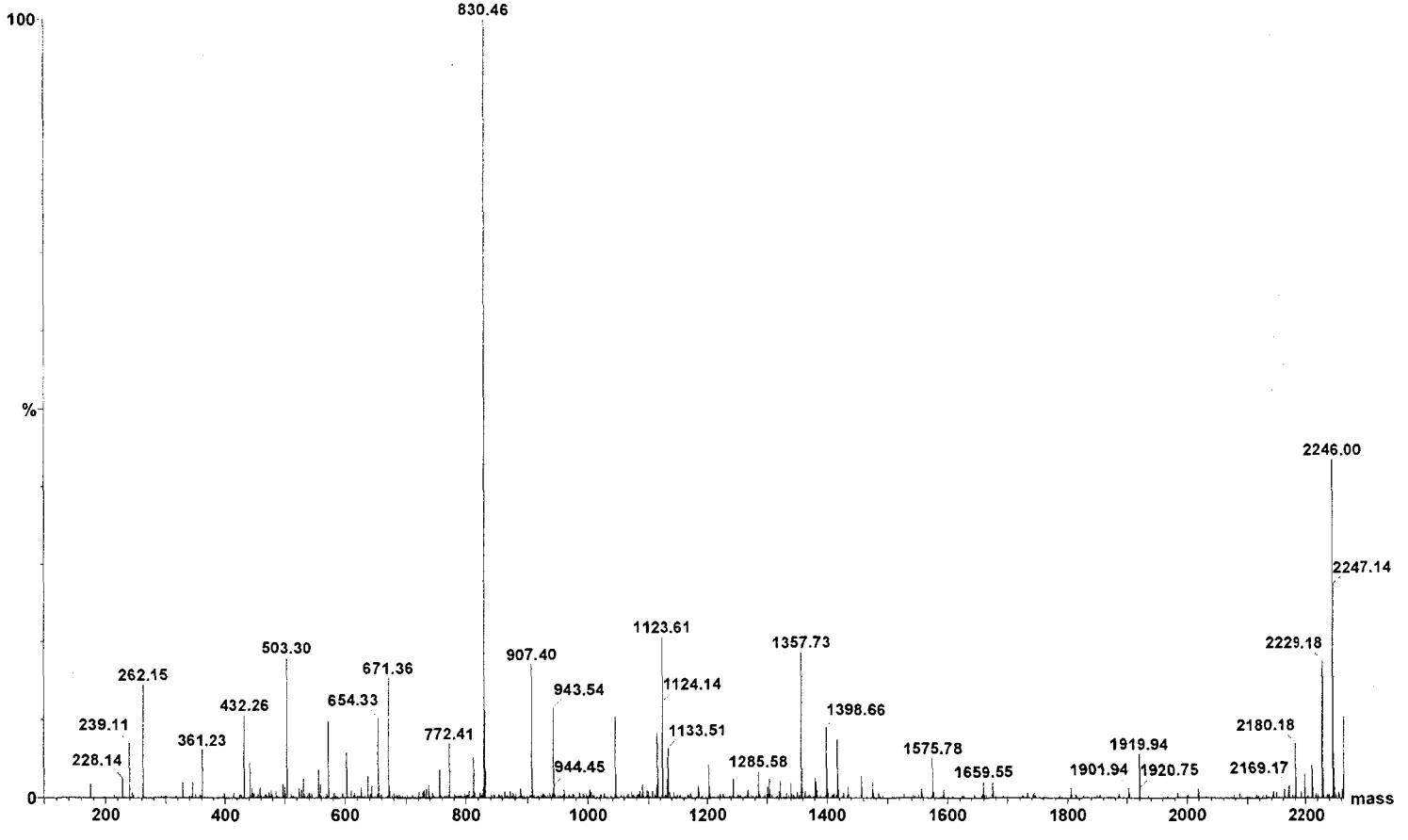

Figure 3.14 Deconvoluted ESI-MS/MS spectrum for the 1132.58 Th ($[M+2H]^{2+}$) peptide of WT DmpFG. The peptide was identified as the sequence corresponding to residues 125–146, with a 32 Da modification on Cys-132 of WT DmpF upon being incubated with acetaldehyde

Table 3.4 Deconvoluted Fragment Ions from MS/MS Analysis of the 1132.58 Th Peptide ($[M+2H]^{2+}$) of WT DmpFG upon incubation with acetaldehyde

	y ion adduct	b ion adduct		y ion adduct	b ion adduct
Leu_{125}	2264.10	-	Ala_{136}	1115.68	1220.57
Asn	-	228.14	Thr	1044.62	1321.75
Val	-	327.21	Leu	943.54	1434.66
Asn	-	441.25	Pro	830.46	-
Met	1823.94	572.30	Met	733.41	-
Val	1692.86	671.36	Val	602.36	1761.86
Thr	1593.79	772.41	Ala	503.30	1832.80
Cys	1492.74	907.40	Ala	432.26	1904.01
Gly	1357.73	964.48	Val	361.23	2003.08
Gly	1300.71	1021.52	Ser	262.15	-
Gln_{135}	1243.68	1149.49	Arg_{146}	175.12	2246.00

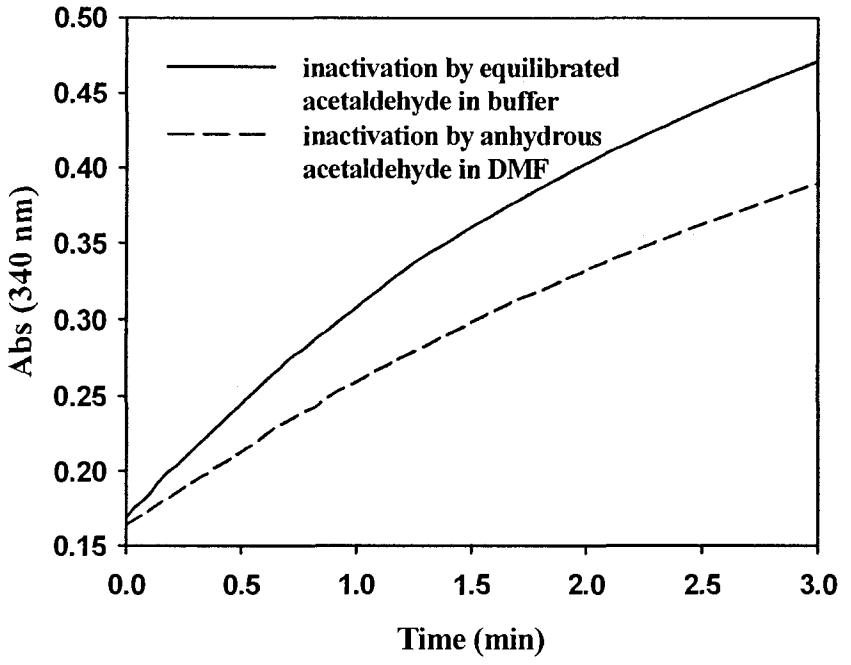

Figure 3.15 The effect of acetaldehyde hydration on acetaldehyde-mediated inactivation of DmpF.

The reaction buffer (pH 8) contained 284 μM NAD^+, 67 μM CoA, 39 nM enzyme, 1 mM DTT and 44 mM acetaldehyde. DmpF reaction in the presence of anhydrous acetaldehyde (- - - - -) was carried out by adding acetaldehyde in DMF to the enzyme-containing buffer, followed by inclusion of DTT, acetaldehyde in H_2O, CoA and NAD^+ (added last). DmpF inactivation in the presence of equilibrated acetaldehyde (———) was performed by preincubating acetaldehyde in DMF with buffer for 5 min, followed by addition of DmpFG enzyme, DTT, acetaldehyde in H_2O, CoA and NAD^+ added last.

3.5 Discussion

The reactivity of the active site cysteine residue of DmpF, a CoA and NAD^+ dependent dehydrogenase, has been probed under a variety of conditions that shed light on its involvement in catalysis and inhibition. Site-directed mutagenesis established that replacement of Cys-132 by serine resulted in a 5,000-fold decrease in apparent k_{cat}. Structural features that would favour deprotonation of the thiol group of Cys-132 would make it a more effective nucleophile for attack on the carbonyl carbon of the substrate, acetaldehyde. However, unlike the structurally similar phosphorylating glyceraldehyde-3-phosphate dehydrogenase (*117*) no residues, such as histidine, which could act as a catalytic general base are evident within a 5Å radius of the sulfur atom of Cys-132 (*4*). We have previously speculated that Asp-209 might activate a water molecule for deprotonation of the Cys-132 thiol (*4*), but site-directed mutagenesis results reported here showed that this residue is not essential.

It is therefore evident that thiol group activation would have to be induced by other elements of the microenvironment around the Cys-132 side chain. By inspection, in the X-ray structure of the DmpFG-NAD^+ complex (PDB entry: 1NVM), the nicotinamide ring is approximately 4 Å away from the sulfur atom of Cys-132: its positive charge would favor the formation of the thiolate. Furthermore, Cys-132 is located at the N-terminal of helix H7 (residues 132-154), and the Cys-132 thiol group is near the N-terminal of helix H12 (residues 289-310), where N-terminal helix dipoles would assist in stabilizing the thiolate anion of the side chain [as has been postulated for other proteins, e.g. (*137*)]. It should also be noted that the amide NHs of both Cys-132 and Gly-133 are close enough to potentially hydrogen bond to the thiol group of Cys-132, which would

also favor the formation of thiolate. All of these structural features that could help stabilize the thiolate form of the Cys-132 side chain may also facilitate deprotonation of the thiol group of coenzyme A in the active site to attack the acyl-DmpF intermediate and generate the product, acetyl-CoA.

Instability of the acetyl-DmpF intermediate in the folded protein and under alkaline conditions was an obstacle that had to be overcome for characterization of this complex. Several different methods were tried in order to capture the acetyl-DmpF from the backward reaction, where the enzyme was incubated with the product, acetyl-CoA. Acetone with HCl (0.5% w/v) or TCA (10% w/v) were used to denature and precipitate any protein-bound intermediates as described in a procedure for β-ketoacyl thiolase (*130*); however, the precipitated protein failed to dissolve properly in buffer suitable for the subsequent trypsin digest. Immobilized pepsin worked well for acetyl-DmpF digestion at pH 2.5 and 4 °C, conditions under which the acetyl-enzyme complex was stable. However, overlapping digestion by pepsin led to generation of more peptides than trypsin digestion, and none of the peptides containing the modified Cys-132 residue was observed in MALDI spectra, although the peptide of residues 130–142, including Cys-132, was well-identified as a doubly-charged ion (m/z 624.29Da) in ESI-Q-TOF spectra (data not shown). The unpredictability of cutting sites during pepsin digest also added more complications to full-length peptide sequencing. In the simple and successful method of sample preparation that is described in *Materials and Methods*, porcine trypsin was selected to digest the intermediate complex since bovine trypsin can autolyze a 2273.16Da peptide ($[M+H]^+$) which would overlap with the acetyl adduct of peptide

125–146 of DmpF (2274.13Da in $[M+H]^+$) in both MALDI and ESI spectra, causing identification difficulties.

Mass spectrometry showed that formation of acyl enzyme at Cys-132 occurs from either direction (Figure 3.1), as would be expected if it is involved in catalysis. Covalent acyl-enzyme intermediates have been detected previously in both phosphorylating and non-phosphorylating $NAD(P)^+$-dependent aldehyde dehydrogenases (*35, 36, 47*). This is the first time that an acyl-enzyme intermediate has been experimentally shown to be formed in a CoA-dependent aldehyde dehydrogenase. Attack of the cysteine thiolate on the carbonyl group of acetaldehyde should involve the non-hydrated form of the substrate, which hydrates in pure water at 25 °C to form a 1.06 : 1 mixture of hydrated and non-hydrated forms (*138*). Therefore it was of interest to assay DmpF activity using hydrated and non-hydrated forms of acetaldehyde.

All of the evidence collected was consistent with non-hydrated acetaldehyde being a better substrate for DmpF than the hydrated form. It has been previously shown that the anhydrous form of aldehyde is a more effective substrate for such enzymes as yeast aldehyde dehydrogenase (*132*), and yeast and human liver alcohol dehydrogenases (*132, 133, 139*). DmpF exhibited a high K_m value for substrate aldehyde prepared in H_2O, a feature common to many other $NAD(P)^+$ -and CoA- dependent aldehyde dehydrogenases. Thus, K_m values for the aldehyde substrate ranged from 2.2 to 10 mM for the following enzymes: CoA-linked aldehyde dehydrogenase from *Escherichia coli* (*49*); CoA-dependent succinate-semialdehyde dehydrogenase from *Clostridium kluyveri* (*51*); CoA-acylating aldehyde dehydrogenase from *Clostridium beijerinckii* NRRL B592 (*50*); CoA-linked acetaldehyde dehydrogenase from *Clostridium acetobutylicum* (*53*); CoA-linked

acetaldehyde dehydrogenase from *Leuconostoc mesenteroides* (*140*); and CoA-linked acetaldehyde dehydrogenase from *Acetobacterium woodii* (*54*). Some others exhibited lower K_m values, in the range 0.15 mM to 0.45 mM, including CoA-linked acetaldehyde dehydrogenases from *Clostridium kluyveri* (*52, 141*), aldehyde dehydrogenase (CoA-acetylating) from *Giardia lamblia* (*76*) and the NAD^+- and CoA dependent acetaldehyde/alcohol dehydrogenase from *Entamoeba histolytica* (*142*). The high K_m value measurements for aldehyde substrate suggest that, for the $NAD(P)^+$ and CoA-dependent aldehyde dehydrogenases, the aldehyde substrate may equilibrate with the hydrated form, which is not an effective substrate.

The observation that DmpF appears to be more active with the non-hydrated form of acetaldehyde may be significant in the context of the bifunctional nature of the enzyme. The X-ray structure of the tightly-associated DmpFG heterotetramer revealed that a hydrophobic tunnel connects the active site of DmpF with DmpG, which is where acetaldehyde is generated from 4-hydroxy-2-ketovalerate (*4*). If acetaldehyde travels through this tunnel to the active site of DmpF, it may remain unhydrated until it is attacked by the thiolate of Cys-132. The tunnel in this case may help to improve the efficiency of the enzyme by maintaining the substrate in a more reactive form by keeping it sequestered from the bulk solvent.

Interestingly, many CoA–dependent aldehyde dehydrogenases that are involved in alcohol fermentation have aldehyde/alcohol bifunctionality (*48, 76, 140, 142-144*). Thus, both acetaldehyde dehydrogenase and alcohol dehydrogenase activities are incorporated in a single protein molecule which reversibly catalyzes the reduction of acetyl-CoA to alcohol via acetaldehyde as an intermediate. It would be interesting to know if there are

special architectural features in these bifunctional aldehyde dehydrogenases, such as the hydrophobic tunnel in DmpFG, which would allow anhydrous transport of acetaldehyde to the alcohol dehydrogenase catalytic site.

Oxygen sensitivity has previously been investigated in some CoA-dependent aldehyde dehydrogenases. CoA-dependent aldehyde dehydrogenase from *Clostridium beijerinckii* NRRL B592 was found to be significantly sensitive to O_2, and DTT was required to protect against inactivation during protein purification and activity assay (*50*). Incubation of O_2-inactivated enzyme with CoA or CoA plus DTT was found to restore activity. Coenzyme A-linked acetaldehyde dehydrogenase from *Acetobacterium woodii* (*54*) and the coenzyme A-dependent succinate-semialdehyde dehydrogenase from *Clostridium kluyveri* (*51*) were also reported to be susceptible to O_2-inactivation. The observation that sulfhydryl reagents such as DTT could protect against inactivation in these enzymes suggested involvement of one or more essential cysteine residues. However, the nature of the oxidation reactions was not determined.

The results reported here indicate that in the presence of acetaldehyde, particularly the non-hydrated form, Cys-132 of DmpF becomes particularly susceptible to oxidation. Mass spectrometry showed that Cys-132, in the proposed active site of DmpF, was the target for oxidation, undergoing conversion to a form whose mass spectrum is consistent with the sulfinic acid. Although DmpF was not very sensitive to oxidation in the absence of acetaldehyde, it was still slowly inactivated during long-term storage, with the production of detectable amounts of Cys-132 sulfinic acid even when kept at –80 °C. Interestingly, in the structure of phosphorylating glyceraldehyde-3-phosphate dehydrogenase from *Bacillus stearothermophilus*, only the reactive glyceraldehyde 3-

phosphate (non-hydrated form) was found to be bound within the active site of the protein despite the favored existence of the hydrated form in equilibrated solutions (*64*). It thus appears that the binding of non-hydrated acetaldehyde to the active site of DmpF promotes the sensitivity of Cys-132 to oxidation.

Protection against inactivation by the continuous presence of DTT, which was ineffective after inactivation had occurred, is consistent with previous observations that initial thiol oxidation products such as disulfides are reduced by DTT, whereas sulfinic acids are not (*145*). Phosphorylating glyceraldehyde-3-phosphate dehydrogenase (GAPDH), the structurally most similar aldehyde dehydrogenase to DmpF, has also been identified as an oxidant-sensitive enzyme. Loss of enzyme activity was correlated with oxidation of the essential cysteine thiol into distinct products depending on the oxidant applied. An intramolecular disulfide was generated by iodosobenzoate oxidation (*146*), cysteine sulfonic acid was produced in the presence of H_2O_2 (*147*) and a mixture of cysteine sulfinic and sulfonic acids, as well as disulfide, was produced by peroxynitrite oxidation (*145*). Furthermore, oxidation of cysteine to sulfinic acid by oxidants such as hydrogen peroxide and hypochlorous acid (HOCl) has been reported to occur in many other proteins containing an essential cysteine residue (*148-151*)

The facile oxidation of active site cysteines in proteins such as GAPDH and peroxiredoxins, which are thiol-dependent peroxidases responsible for detoxification of reactive oxygen species (*152-155*), has been proposed to be due to low pK_a values for their active site cysteine thiol groups (pK_a = 5.5 and 4.6 for GAPDH and peroxiredoxin, respectively) (*156, 157*). These low pK_a values appear to be a result of stabilization of the thiolate by surrounding positive charges. The anion form of a cysteine thiol group is more

susceptible to oxidation by peroxides than its protonated form (*158*). Increased sensitivity of Cys-132 to O_2 could be explained if acetaldehyde binding to DmpF lowered the thiol group pK_a of Cys-132, making it more susceptible to oxidation.

Assay data also showed that pre-binding of the NAD^+ cofactor could protect against the acetaldehyde-mediated inactivation of DmpF (Figure 3.12). In the case of GAPDH, NAD^+ binding promoted the reactivity of the essential thiol group with peroxides (*147*) by supplying additional positive charge (*156, 159*) or altering the local conformation within the active site (*41*) that depressed the pK_a of the active site cysteine thiol. Accordingly, it is possible that the pK_a would decrease as a result of NAD^+ binding to DmpF, but another possibility is that NAD^+ binding would also physically block solvent accessibility to Cys-132. Comparison of the solvent accessibility between apo DmpF and NAD^+-bound DmpF shows that the solvent accessible surfaces for the sulfur atom of Cys-132 are 9.2 $Å^2$ and 1.6 $Å^2$, respectively. The significantly different solvent accessibilities would mean that O_2 dissolved in buffer becomes much less accessible to the thiolate group of Cys-132 upon NAD^+ binding to DmpF, leading to the observed NAD^+ protection against the acetaldehyde-mediated inactivation. Similarly, for GAPDH in the presence of substrate, glyceraldehyde-3-phosphate, inactivation by H_2O_2 was greatly decreased compared to uncomplexed enzyme. This may be due to the formation of hemithiolacetyl ester between the substrate and the essential cysteine thiol group, which resulted in the protection of the thiol group (*147*). However, in the case of DmpF, the acetaldehyde-mediated oxidation might have occurred prior to the formation of hemithiolacetyl ester.

3.6 Acknowledgements

This work was supported by a Discovery grant from the Natural Sciences and Engineering Research Council of Canada.

Chapter 4 Active Site Studies and Metal Ion Requirements of DmpG, an Aldolase Involved in Bacterial Degradation of Aromatic Compounds

4.1 Abstract

DmpFG, a bifunctional aldolase/dehydrogenase, catalyzes cleavage of 4-hydroxy-2-ketovalerate, a catabolic intermediate in phenol degradation, into pyruvate and acetyl-CoA via acetaldehyde. DmpG is a divalent cation-dependent class II aldolase belonging to the HMGL-like family. In this study, purified DmpFG was shown by ICP-MS to contain a total of one equivalent of a mixture of Fe, Mn, Zn and Cu, with Fe and Mn predominating. Site-directed mutagenesis combined with ICP-MS and kinetics studies were used to probe the roles of amino acid residues observed in the crystal structure to coordinate the metal ion at the active site of DmpG. Substitution of any of the three metal-binding ligands, D18, H200 or H202, resulted in almost complete loss of Fe and Mn, and of activity. Addition of Mn^{2+}, Co^{2+}, Ni^{2+} or Cd^{2+} to the assay increased aldolase activity of WT up to approximately 26-fold, and stimulated the activity of the metal ligand variants to different degrees. In the presence of Mn^{2+} or Co^{2+}, H202A aldolase activity was restored to activity levels similar to WT, H200A activity was partially restored, and D18N activity remained at trace levels. The H200A variant exhibited a perturbed fluorescence emission spectrum, suggesting a structural change resulting specifically from that substitution. Urea-induced unfolding experiments and analytical ultracentifugation experiments indicated that H202A had destabilized secondary and quaternary structures in the absence of added metal ion. Although a number of divalent metal ions were activating, Zn^{2+} was not, and it inhibited the activation by Mn^{2+}, Co^{2+}, Ni^{2+} or Cd^{2+}. Taken together, these results indicate that DmpG contains a tightly bound metal ion that plays a structural role, and apparently requires a second metal ion for activity.

4.2 Introduction

Pseudomonas sp. strain CF600 is able to grow efficiently using phenol and methyl-substituted phenols via the *dmp*-operon encoded *meta*-cleavage pathway which comprises nine enzyme activities (*160*). The end products of this pathway are pyruvate and acetyl-CoA, which feed into central metabolism. The last two enzymes in this pathway are the gene products of *dmpF* (32.7 kDa) and *dmpG* (37.3 kDa) (2). DmpG, a divalent cation-dependent aldolase, converts 4-hydroxy-2-ketovalerate (4H2KV) into pyruvate and acetaldehyde while DmpF, an NAD^+–, and CoA–dependent acetaldehyde dehydrogenase, oxidizes acetaldehyde to acetyl-CoA. These proteins are purified as an active heterotetramer (F2G2) complex, and thus constitute a bifunctional enzyme. Interestingly, the aldolase (DmpG) of DmpFG could not be successfully expressed in an active form separately from the acetaldehyde dehydrogenase (DmpF) (3).

Aldolase enzymes may be classified according to metal cation requirement (*161*). Class I aldolases are metal-independent and catalysis involves an intermediate Schiff-base complex between substrate and an active site Lys within an $(\alpha/\beta)_8$ TIM barrel structural framework. Class II aldolases absolutely require divalent metal cations for catalysis, and are further sub-classified based on the type of protein fold (*26*). Both classes of aldolase are exemplified by fructose-1,6-bisphosphate aldolases (FBPA), which catalyze the reversible cleavage of fructose-1,6-bisphosphate to dihydroxyacetone phosphate and glyceraldehyde 3-phosphate (*162*). Class I FBPAs from eukaryotes (*163-166*) have been well characterized, while less is known about class II FBPAs from microorganisms (*25-27, 29, 167*).

In Class II FBPA, catalysis occurs in the metal-containing active site of a $(\alpha/\beta)_8$ TIM barrel (*25, 28, 168*), which is also a structural feature of DmpG (*4*). The reaction involves general base and acid catalysis, and formation of a carbanionic intermediate (*25, 169, 170*). The catalytic divalent cation coordinates with the side chains of three histidine residues as well as, by inference from a structure of a complex with a transition state analogue, the hydroxyl and carbonyl oxygens of the substrate, dihydroxyacetone phosphate (DHAP) (*25, 28*). The metal ion is proposed to polarize the carbonyl bond to facilitate C-C bond cleavage. Besides the requirement for divalent cation, either firmly bound or dissociable, monovalent cations such as K^+ or NH_4^+ must be present for optimal class II FBPA activity (*24, 162*). The monovalent cation binding site was identified in the structures of *E. coli* FBPA (*26, 27*), where it was supposed to coordinate substrate (DHAP) binding and alignment for efficient catalysis (*25*).

The HMGL-like family is a recently-recognized group of class II aldolases which comprises 3-hydroxy-3-methylglutaryl-CoA (HMG-CoA) lyase, α-isopropylmalate synthase (α-IPMS), transcarboxylase (TC) 5S subunit and DmpG (*5*). Structures of the four proteins of the family have been solved recently (*4, 6-9*). Members of this family feature a conserved active site located in the $(\alpha/\beta)_8$ TIM barrel catalytic domain, and thus are likely to use similar reaction mechanisms to catalyze divalent cation-dependent C-C bond cleavage or condensation. Similar to class II FBPA, the mechanism of HMGL-like enzymes has been proposed to involve general base and /or acid catalysis and carbanion intermediate formation (*6*).

HMGL-like family members have been crystallized for structure determination either with or without added metal ions. DmpFG was crystallized in the absence of added

divalent cation as a tetrameric dimer in which two DmpG subunits associate with one another, and DmpF subunits stack at either end of the DmpG dimer (*4*). The DmpG subunit was observed to have bound metal ion coordinated in octahedral geometry with the side chains of Asp-18, His-200 and His-202, together with one ordered H_2O oxygen and two carbonyl oxygens from a unidentified ligand that was proposed to be oxalate (PDB entry: 1NVM). Human 3-hydroxy-3-methylglutaryl-CoA lyase was crystallized in buffer containing Mg^{2+}, which is essential for enzyme activity. In this case, a single metal ion was observed in the crystal structure ligated in octahedral geometry to side chains of Asp-42 , His-233 and His-235, Asn-275 and two H_2O oxygens (PDB entry: 2CW6) (*7*). Bacterial 3-hydroxy-3-methylglutaryl-CoA lyases were crystallized from solutions with high concentrations of Ca^{2+}, which has no effect on the enzyme activity but likely mimics the catalytic metal ion (PDB entries: 1YDO and 1YDN) (*6*). The Ca^{2+} ion was observed to have similar coordination as Mg^{2+} in the human homologue. α-Isopropylmalate synthase from *Mycobacterium tuberculosis* was crystallized from solution containing Zn^{2+}, which is an inhibitor of the enzyme (PDB entry: 1SR9) (*8, 21*). The metal ion was observed to be bound to Asp-81, His-285, His-287, one H_2O oxygen and two carbonyl oxygens of the substrate, α-ketoisovalerate. Finally, transcarboxylase 5S subunit from *Propionibacterium shermanii* (PDB entries: 1S3H, 1U5J, 1RQB, 1RQE, 1RR2 and 1RQH) (*9*), was expressed in medium containing Co^{2+} and Zn^{2+}, and one Co^{2+} was observed in the active site of the protein. The Co^{2+} was coordinated by the side chains of Asp-23, His-215, His-217, as well as one H_2O oxygen and two carboxyl group oxygens from bound substrate.

Although proteins of the HMGL-like family share only 12% - 23% primary sequence identity, they demonstrate significant similarity in the active site stereo arrangement based on the three dimensional structural alignments (*14, 171*). As detailed above, a divalent cation is ligated by the side chains of one aspartate and two histidine residues [in the conserved motif of HXH (*172*)], with one additional Asn ligand in HMG-CoA lyase, together with one ordered H_2O oxygen and at least one oxygen from substrate with overall octahedral geometry. Furthermore, inspection of the structures indicates that the metal ligand residues in each family member are precisely aligned and stabilized by similar hydrogen bond networks.

Interestingly, in all HMGL-like family members a conserved arginine residue (R17 in DmpG) interacts with a conserved glutamate residue near the metal-binding ligands. The arginine side chain was proposed to be involved in neutralization of the negative charge generated on the enolate catalytic intermediate, according to the structural analysis of pyruvate- and oxaloacetate-transcarboxylase 5S complexes (1RQH and 1RQE) (*6*). The conserved divalent cation was observed to interact with two carbonyl groups of the substrate in the substrate-protein complex of either α-isopropylmalate synthase or transcarboxylase 5S subunit (1SR9 and 1RQE), supporting the notion that the metal ion of HMGL-like proteins participates in catalysis by polarizing the carbonyl bond of the substrate.

The catalytic general acid/base appears to be unique for each HMGL-like family member. A conserved cysteine residue of HMG-CoA lyase was assigned to be the general base, based on its position in the structure and enzyme kinetic data for a variant (*6, 15*). In α-IPMS, two conserved residues, His-379 and Glu-218, are potential general

bases, and an ordered H_2O molecule is the candidate for general acid (*8*). In DmpG, a pair of residues, His-21 and Tyr-291, was proposed to deprotonate the substrate, 4H2KV, and protonate the pyruvate enolate intermediate, respectively, during catalysis (*4*).

The active site residues of DmpG were investigated here, to better define the role of the metal ion using a variety of metal ions and metal-binding variants, and to investigate the proposed involvement of active site residues in aldolase activity.

4.3 Materials and Methods

Materials. In ICP-MS experiments, the single-element standards Fe, Mn, Zn, Ni, Cd and multi-element standard containing Al, As, Co, Cr, Cu, K, Na, P and Pb were purchased from SPEX CertiPrep®, Inc.

Construction of plasmid DNA for expression of the DmpG variants H200A, H202A and H203A was described previously (*173*). The following primer pairs (Biocorp Inc., Montreal) were used for site-directed mutagenesis to generate the DmpG variants R17Q, D18N, H21A, H21Q, Y291A and Y291F:

5' CGTAACC**CTGCAG**GACGGCAGCCATGCC 3' and

5' GGCATGGCTGCCGTC**CTGCAG**GGTTACG 3' **(R17Q)**

5' CGTAACCC**TGCGCA**ACGGCAGCCATGCC 3' and

5' GGCATGGCTGCCGT**TGCGCA**GGGTTACG 3' **(D18N)**

5' CTGCGTGACGGCAGCGCTGC**GATTC**GCCACCAGTACAC 3' and

5' GTGTACTGGTGGC**GAATC**GCAGCGCTGCCGTCACGAAG 3' **(H21A)**

5' CTGCGTGACGGCAGCCAAGC**GATTC**GCCACCAGTACAC 3' and

5' GTGTACTGGTGGC**GAATC**GC**T**TGGCTGCCGTCACGCAG 3' **(H21Q)**

5' GGATATGCCGGTGTCTTTTCA**A**GCTTCCTGC 3' and

5' GCAGG**AAGCTT**GAAAAGACACCGGCATATCC 3' **(Y291F)**

5' CTCGGATATGCCGGTGTCGCTTC**A**AGCTTCCTGCGTCACGCC 3' and

5' GGCGTGACGCAGG**AAGCTT**GAAGCGACACCGGCATATCCGAG 3' **(Y291A)**

Silent restriction sites (*PstI* for R17Q, *AviII* for D18N, *TfiI* for H21A and H21Q, *HindIII* for Y291A and Y291F) were introduced into the primers for subsequent identification of successfully introduced mutations in plasmid DNA. The bases highlighted in bold denote the restriction enzyme recognition sites in the primers, while underlined bases are those that have been changed for site-directed mutagenesis and/or silent mutation to create restriction sites.

Site-Directed Mutagenesis. pCR®2.1*(dmpFG)* (Chapter 3) was used as a template in the Quickchange mutagenesis method (Stratagene) for preparation of DmpG site-directed variants. Mutagenized plasmids were amplified in *E. coli* XL2-Blue and subsequently purified using the Wizard miniprep kit (Promega). Mutagenized regions of the expression plasmid encompassing R17Q, D18N, H21A or H21Q were excised on a 566 bp *Bsu36*I-*Sph*I fragment. For the variants Y291A or Y291F, the mutagenized DNA was excised on a 350 bp *Sph*I-*Not*I fragment. These fragments were inserted into the corresponding restriction sites in the WT pT7.5 based DmpFG expression plasmid (*119*). Subsequently, each plasmid DNA was checked by sequencing over the insert region, to insure that only the expected mutation had been introduced. Furthermore, exact mass measurement of purified intact proteins (with the exception of D18N) using ESI-Q-Tof

MS showed that the experimental mass difference between variant and WT proteins was consistent with only the introduced substitution (data not shown). Since the D18N protein has only a one Da mass difference compared to WT, the intact protein was digested with immobilized pepsin, and MS/MS sequencing of peptic peptide 14-31 (*119*) showed that Asp-18 of DmpG was replaced by Asn in the variant protein (data not shown).

Protein Expression and Purification. All the variant DmpFG proteins, R17Q, D18N, H21A, H21Q, H200A, H202A, Y291A and Y291F, were expressed and purified as previously described for WT (*119*). However, the D18N, H21A and H21Q proteins were eluted from the NAD^+ affinity column with 0.5 M NaCl in 50 mM Na^+ K^+ phosphate buffer (pH 7.5) instead of 0.1 M NaCl, which was sufficient to elute WT and the other variant DmpFG proteins.

Kinetics Experiments for DmpFG. Acetaldehyde dehydrogenase activity was estimated using the procedure described previously (Chapter 3). Kinetic constants for acetaldehyde dehydrogenase activity were estimated using initial velocities of reactions that were carried out in 50 mM HEPES buffer (pH 8, 25 °C) at varying concentrations of NAD^+ or CoA with fixed concentrations of the other two substrates: acetaldehyde (38 mM), NAD^+ (570 μM) or CoA (120 μM). Aldolase activity was estimated by monitoring the rate of NAD^+ reduction through coupling with the acetaldehyde dehydrogenase reaction of DmpFG. The assay was initiated by addition of DmpFG to metal-free 50 mM HEPES buffer mixture (pH 8) containing the substrate, 4H2KV, and experimentally saturating concentrations of NAD^+ (554 μM) and CoA (107 μM), in the presence or in the absence of added divalent cation. Apparent kinetic parameters for aldolase activity were estimated using initial velocities at varying divalent cation or 4H2KV concentrations, respectively,

at fixed concentration of substrate, 4H2KV (132.7 μM for the assays of metal ligand variants in the presence of Mn^{2+}, and 75.8 μM for all the other assays with WT and metal ligand variant enzymes), or divalent cation (10 mM Mn^{2+}, 5mM Co^{2+}, 2.5mM Ni^{2+} or 125 μM Cd^{2+}). Specific activities of either WT or variant enzymes were calculated using initial rates observed in metal-free 50 mM HEPES buffer (pH 8, 25 °C) containing 554 μM NAD^+, 107 μM CoA, 133 μM 4H2KV and, if present, 10 mM Mn^{2+} or 5 mM Co^{2+}. Preparation of 4H2KV and concentration determination for the substrates, 4H2KV, acetaldehyde, NAD^+ and CoA, were as described previously (Chapter 3).

Preparation of samples to measure the effects of Fe^{2+} on the aldolase activity of DmpFG was carried out under anaerobic conditions. Stock solutions of ferrous ion were prepared by dissolving ferrous chloride or ferrous ammonium sulfate in anaerobic Milli-Q H_2O in a glove box (M. Braun) where the O_2 concentration was under 5 ppm at 22 °C. The metal-free 50 mM HEPES assay buffer (pH 8), and substrate-containing solutions were all bubbled with N_2 and then moved into the glove box. Enzyme samples were prepared in the glove box as well. All reaction components except enzyme were premixed in a septum-sealed cuvette in the glove box. The enzyme was loaded into an airtight syringe in the glove box and then the septum-sealed cuvette and syringe were moved out of the glove box. The reaction was initiated by injecting the enzyme through the septum into the cuvette, followed by mixing. Progress of the reaction was monitored at 340 nm.

Zn^{2+} inhibition of divalent cation–stimulated DmpG activity. Zn^{2+} inhibition of Mn^{2+} (or Co^{2+}) stimulated DmpG activity was investigated by measuring initial velocities of the acetaldehyde dehydrogenase through coupling DmpG with DmpF assays: at the

concentrations used, Zn^{2+} showed no effect on the acetaldehyde dehydrogenase activity. The assays were performed in 50 mM HEPES buffer (pH 8, 25 °C) containing various Mn^{2+} (or Co^{2+}) concentrations, 554 μM NAD^+, 107 μM CoA and 133 μM 4H2KV at several fixed Zn^{2+} concentrations ranging from 0 to 125 μM. The inhibition pattern was analyzed using the program of Cleland (*174*) to fit the assay data points, and the inhibitor dissociation constant, K_i, was calculated. Assays were also carried out in the presence of varying Zn^{2+} concentrations and fixed Mn^{2+} or Co^{2+} concentrations (10 mM or 5 mM, respectively), in 50 mM HEPES buffer (pH 8, 25 °C), 554 μM NAD^+, 107 μM CoA and 133 μM 4H2KV. Activity in the absence of Zn^{2+} was considered to be 100%, and assay data were plotted using the IC50 model in GraFit 5 (Erithacus Software) to give an estimate of the concentration of Zn^{2+} which inhibits 50% activity.

Oxalate inhibition of aldolase activity. Oxalate inhibition of aldolase activity was investigated by measuring aldehyde dehydrogenase initial velocities through coupling DmpG with DmpF reactions since oxalate showed no effect on the acetaldehyde dehydrogenase activity. The assays were carried out in metal-free 50 mM HEPES buffer (pH 8, 25 °C) with vaying concentrations of 4H2KV, 554 μM NAD^+ and 107 μM CoA, at several fixed oxalate concentrations. The oxalate inhibition pattern was analyzed using the program of Cleland (*174*) and the oxalate dissociation constant, K_i, was calculated. The coupled DmpFG assays were also carried out with a fixed concentration of 4H2KV (133 μM) and varying concentrations of oxalate in 50 mM HEPES buffer (pH 8, 25 °C) with 554 μM NAD^+ and 107 μM CoA. Activity in the absence of oxalate was considered to be 100%, and assay data were plotted using the IC50 model in GraFit 5

(Erithacus Software) to give an estimate of the concentration of oxalate which inhibits 50% activity.

Sample Preparation for ICP-MS Experiments. All of the containers, tips and tubes used for sample preparation for ICP-MS experiments were polypropylene and soaked in 7% HNO_3 (w/w, trace metal grade) at least overnight, then rinsed thoroughly with Milli-Q H_2O (18.2MΩ) and dried in a 37 °C incubator prior to use. Metal-free 50 mM HEPES buffer (pH 8.0), was prepared by passing the buffer through a column of Chelex®100 resin (biotechnology grade, 100-200 mesh, sodium form, Bio-Rad Laboratories) which was previously washed with 7% HNO_3 and Milli-Q H_2O. Then the metal-free 50 mM HEPES buffer was adjusted to pH 8 with 6N semiconductor grade NaOH solution.

All protein samples used for metal detection were digested in 10% HNO_3 at 50 °C overnight, then diluted with Milli-Q H_2O prior to analysis. Flowthrough which was collected at the end of buffer exchange during protein purification procedures was subjected to the same treatment as the sample for use as a control in ICP-MS experiments. For samples used to estimate metal ion stoichiometry after incubation with excess metal ion, 250 μL of WT DmpFG (in 50 mM HEPES buffer, pH 8) (113 μM) was mixed with 2.5 μL of 1 M $MnCl_2$ (10 mM Mn^{2+} final concentration) or 0.5 M $CoCl_2$ (5 mM Co^{2+} final concentration) and incubated at 22 °C for 10 min. To remove the excess metal ion, the mixture was loaded onto a NAP-5 column (GE Healthcare) which was previously washed with 200 mM EDTA and equilibrated with metal-free 50 mM HEPES buffer (pH 8). Next, 250 μL of 50 mM HEPES buffer (pH 8), was applied to the column and the eluate was discarded. Finally the enzyme was eluted with 500 μL of 50 mM HEPES buffer (pH 8), followed by collection of an equal volume of flowthrough.

Controls were prepared in parallel following the same procedure as above, except that 250 μL of flowthrough collected at the end of the last step of the protein purification procedure was used instead of 250 μL DmpFG.

ICP-MS Analysis. Metals associated with WT DmpFG and its variants were evaluated using an Agilent Technologies 7500ce collision/reaction cell ICP-MS system which could be run in three distinct gas modes: hydrogen, helium or no-gas mode. First, semi-quantitative analysis was conducted to identify the metals present, and their approximate amounts. Metal contents were then accurately quantified by using an external calibration technique in He mode. To achieve optimal performance, the following ICP-MS conditions were used: peristaltic pump speed was 0.1 rps; sampling depth was 8 mm; RF power was 1,500 W; and the carrier gas and makeup gas were supplied at flow rates of 0.8 and 0.2 L/min, respectively. Helium gas was applied to the reaction cell at 5 mL/min.

Circular Dichroism (CD) Spectroscopy. Far-UV CD experiments were conducted at 22 °C using a JASCO J-815 CD spectrometer. The scans were made between 210–260 nm with a step resolution of 0.2 nm, response time of 0.25 s, and bandwidth of 1 nm. Protein samples were diluted to 0.5 mg/mL in 50 mM HEPES buffer (pH 8.0) for analysis.

Fluorescence Spectroscopy. Fluorescence measurements were carried out on an Aminco Bowman series 2 Fluorimeter. DmpFG at a concentration of 0.2 mg/mL in 50 mM HEPES buffer (pH 8.0) was excited at λ_{ex} = 280 nm or 295 nm. The fluorescence emission spectra were monitored at 22 °C from 285–400 nm for 280 nm excitation, and from 300–400 nm for 295 nm excitation, with a scan rate of 1.0 nm/sec. Samples were

contained in a 1.0 cm quartz cuvette. The spectrum of the buffer blank was subtracted from all protein spectra.

Urea-Induced DmpFG Unfolding Experiments. In either the absence or the presence of added 1 mM Mn^{2+}, DmpFG samples (0.2 mg/mL) were incubated with urea in increasing concentration from 0 to 5 M at 22 °C for 16 h. The buffer used was metal-free 50 mM HEPES (pH 8.0). Spectra were then acquired between 210 and 260nm at 22 °C: the CD signal at 222nm was used to monitor the α-helical content remaining. Before fitting a dose-response curve to obtain the $[urea]_{50\% \text{ unfolding}}$, which represents the concentration of urea that induces 50% unfolding of protein, the CD signal at 222 nm was converted to percent intensity with respect to the sample lacking urea. The following equation was employed to fit the experimental data using SigmaPlot 9.0:

$$y = \min + \frac{\max - \min}{1 + (x / EC50)^{Hillslope}}$$

where y is the percent signal intensity, x is the corresponding urea concentration, and EC50 represents the urea concentration that incurred 50% protein unfolding.

Analytical Ultracentrifugation. Sedimentation velocity experiments were performed using a Beckman Optima XL-I analytical ultracentrifuge. The sedimentation behaviour of DmpFG was examined by centrifuging 400 μL of 0.5 mg/mL samples at 42,000 rpm in a 60-Ti rotor at 20 °C. Sedimentation runs were scanned at 280 nm. The sedimentation coefficients, S, were obtained by analyzing the data using DCDT+ software (version 1.14) (*175*). Reference samples with buffer only were centrifuged side-by-side with the protein samples. Sedimentation coefficients were corrected for buffer density and

viscosity at different temperatures, which were calculated using the Sednterp (Sedimentation Interpretation) program version 1.08 (*176*).

4.4 Results

Aldehyde Dehydrogenase (Acylating) Kinetics of DmpG Variants D18N, H200A and H202A. Amino acid substitutions were made for the DmpG metal ligands, D18, H200 or H202, generating D18N, H200A and H202A. The effects of each substitution on the kinetics of the physically-associated DmpF were examined. The apparent k_{cat} and K_m values for NAD^+ or CoA of H200A and H202A were similar to those of WT (Table 4.1), while for D18N the K_m was 3-fold lower for NAD^+, 3-fold higher for CoA, and k_{cat} was 2-fold lower compared with WT (Table 4.1). The substitutions at the DmpG active site therefore affected the DmpF active site of the bifunctional enzyme minimally. The effects of the substitutions on DmpG activity were examined next.

Metal and Aldolase Activity Measurements of DmpG WT, D18N, H200A and H202A. Prior to this work the identity and function of metal ion associated with DmpFG had not been rigorously established. ICP-MS showed that WT DmpFG contained Fe, Mn, Zn and Cu metals in order of decreasing abundance, with a stoichiometry of one mol DmpG subunit to one mol of total metals, with Fe and Mn predominant (Table 4.2). Mutagenesis of the metal ligands identified by x-ray crystallography (Asp-18, His-200 or His-202) resulted in almost complete loss of Fe and Mn, but elevated Cu contents: total metal content was about half of that of WT (Table 4.2). Aldolase activity of these variants was decreased to 0.12–2.2% relative to that of WT enzyme, indicating that tightly bound metals were associated with the aldolase activity of WT DmpFG in the absence of added metal ions.

Table 4.1 DmpF enzyme kinetic parameters for WT and metal ligand variant DmpFG proteins

DmpFG protein	apparent K_m		apparent k_{cat} (sec^{-1})
	NAD^+ (μM)	CoA (μM)	
WT	156.1 ± 11.5[a]	8.7 ± 1.3[a]	32.2 ± 0.91[b]
D18N	51.2 ± 2.7	26.9 ± 2.1	15.4 ± 1.3
H200A	126.5 ± 8.4	11.2 ± 3.1	36.2 ± 2.8
H202A	145.9 ± 10.1	12.4 ± 2.9	41.3 ± 5.1

[a] adapted from reference (*119*).

[b] adapted from Chapter 3

Table 4.2 Metal content and activity of WT and the metal ligand variants of DmpFG

DmpFG	metal content [a] (mol./mol. DmpG subunit)								spec. act.[b] (nmol./min.mg)	% of spec. act.
	Fe	Mn	Zn	Cu	Ni	Co	Cd	total		
WT	0.58	0.21	0.13	0.06	nd	nd	nd	0.98	765.0	4.99
D18N	0.07	–	0.19	0.32	0.04	nd	nd	0.62	2.54	0.02
H200A	0.03	–	0.09	0.30	0.02	nd	nd	0.44	0.9	0.01
H202A	0.02	–	0.01	0.33	0.01	nd	nd	0.37	17.08	0.11
WT + Mn^{2+}	0.57	0.75	0.18	0.09	0.02	0.01	nd	1.62	15,340	100
WT + Co^{2+}	0.41	0.15	0.12	0.03	nd	1.20	nd	1.91	13,580	88.5

"–" denotes less than 0.01mol. metal /mol. DmpG subunit; "nd" indicates non-detectable.

[a] The metal contents were estimated using three different preparations of WT and two preparations for each of the metal ligant variants, and each determination was done in triplicate. Averages are given in the Table with errors of less than or equal to ± 15 %.

[b] Specific activities were measured in the absence of added metal ions, except WT + Mn^{2+} and WT + Co^{2+} assays which were carried out in the presence of Mn^{2+} (10 mM) or Co^{2+} (5 mM), respectively. The 50 mM HEPES assay buffer (pH 8, 25 °C) included 554 μM NAD^+, 106 μM CoA and 133 μM 4H2KV.

Metal and Aldolase Activity Measurements of Other DmpG Active Site Variants. Three active site residues potentially involved in catalysis were targeted for substitution: R17, H21 and Y291, as well as H203 which is adjacent to the metal ligand, H202. None of these residues was observed as a ligand to the metal ion in the crystal structure: however, with the exception of H203 they have been postulated previously to be otherwise involved in catalysis (*4*). The H21A, H21Q and H203A variants contained similar amounts of total metal and bound Fe as WT, but significantly less Mn, especially the H21Q variant (Table 4.3). Residues R17 and Y291 were previously observed in the crystal structure to interact with what appeared to be a substrate or product analogue at the active site (*4*). R17Q, Y291A and Y291F had Fe contents that were decreased somewhat relative to WT, and Mn levels that were either the same as WT (Y291 variants), or similar to the H21 and H203 variants (Table 4.3). The substitutions at R17 and H21 abolished residual aldolase activity, whereas the specific activities of H203 and Y291 were either similar to or half, respectively, that of WT (Table 4.3).

Effect of Metal Chelators on Aldolase Activity. DmpFG was incubated with either ethylenediaminetetraacetic acid (EDTA), o-phenanthroline or 8-hydroxyquinoline-5-sulfonate (5 mM) at room temperature (22 °C). At intervals over a 24 h period aliquots were removed for aldolase activity assay and examination of metal content after desalting on a NAP-5 column. A parallel control experiment without any added chelator was carried out simultaneously. Incubation of DmpFG with these chelators did not significantly alter the metal contents or the aldolase activity in the absence of added metal ions compared to the control experiment (data not shown). Therefore, the metal ions detected by ICP-MS are tightly bound to the enzyme.

Table 4.3 Metal content and activity of WT and variants DmpG without added Me^{2+}

DmpFG	metal content [a] (mol./mol. DmpG subunit)								spec. act.[b] (nmol./min.mg)
	Fe	Mn	Zn	Cu	Ni	Co	Cd	total	
WT	0.58	0.21	0.13	0.15	nd	nd	nd	0.98	765.0
R17Q	0.32	0.04	0.14	0.15	nd	nd	nd	0.65	nd
H21A	0.53	0.02	0.21	0.35	nd	nd	nd	1.11	nd
H21Q	0.51	–	0.18	0.07	nd	nd	nd	0.76	nd
H203A	0.54	0.08	0.21	0.11	–	nd	nd	0.94	820
Y291A	0.30	0.12	0.18	0.44	–	nd	nd	1.04	351
Y291F	0.22	0.11	0.17	0.12	nd	nd	nd	0.62	400

"–" denotes less than 0.01mol. metal /mol. DmpG subunit, "nd" indicates non-detectable.

[a] The metal contents were measured for two different preparations of each of the DmpG variants, and each determination was done in triplicate. Averages are given in the Table with errors of less than or equal to ± 16 %.

[b] Specific activity of each variant was measured in 50 mM HEPES buffer (pH 8, 25 °C) containing 554 μM NAD^+, 107 μM CoA and 133 μM 4H2KV in the absence of added metal ions.

Stimulation of Aldolase Activity by Divalent Cations. As shown in Table 4.4, Mn^{2+} or Co^{2+} in the assay buffer activated WT aldolase activity 26– and 20–fold over the activity without added Me^{2+}, respectively, with corresponding K_m values of 1.3 and 0.35 mM. Ni^{2+} enhanced WT DmpG activity 3-fold while Cd^{2+} only slightly increased the aldolase activity. The apparent *K*m for substrate, 4H2KV, varied up to 5-fold with the various metal ions, but was very similar for the two most active cations, Co^{2+} and Mn^{2+}. Surprisingly, Fe^{2+} did not enhance aldolase activity when added to the assay even though Fe was the most abundant metal detected in WT (data not shown). Together, these data suggest the possibility that a more weakly bound divalent metal ion, distinct from the metal ion bound by D18, H200 and H202 at the DmpG active site, significantly stimulates aldolase activity. Furthermore, it appears that tightly and weakly bound metal ions may be the same or different types of ions.

Effect of Metal Ions on Metal Ligand Variant Activities. As noted above, the metal ligand variants of DmpG were all essentially depleted of Mn and Fe (Table 4.2). Interestingly, the aldolase activity of H202A could be completely restored by addition of Mn^{2+} to the assay, and even gained higher activity upon incubation with Co^{2+} compared to the WT enzyme (Table 4.5). In contrast, activity could not be restored to the D18N variant with Mn^{2+}, and only minimal activity was observed with Co^{2+}. H200A was activated with Co^{2+}, but to a level well below WT: with Mn^{2+}, activity was low, and the K_m for metal ion apparently very high compared to WT (Table 4.5). The apparent K_m values of the substrate, 4H2KV, were similar for WT and the three variants D18A, H200A and H202A in the presence of Co^{2+}, but in the presence of Mn^{2+}, considerably higher for the H200A and H202A variants compared to WT. As with WT, for all three

Table 4.4 Steady-state kinetic parameters for DmpG

Me^{2+}	*apparent* k_{cat} (s^{-1})	*apparent* $K_{m,\ Me^{2+}}$ (mM)	*apparent* $K_{m,\ 4H2KV}$ (μM)
Mn^{2+}	24.7 ± 1.75	1.28 ± 0.14	26.4 ± 4.66
Co^{2+}	18.7 ± 1.75	0.35 ± 0.05	15.8 ± 1.53
Ni^{2+}	4.0 ± 0.18	0.11 ± 0.02	8.2 ± 1.33
Cd^{2+}	1.27 ± 0.03	0.02 ± 0.0002	5.4 ± 0.54
none	0.93 ± 0.03	—	6.2 ± 0.63

Table 4.5 Apparent steady-state kinetic parameters for D18N, H200A, H202A variants and WT of DmpG

protein	Mn^{2+}			Co^{2+}		
	k_{cat} (s^{-1})	$K_{m,\ Mn}^{2+}$ (mM)	$K_{m,\ 4H2KV}$ (μM)	k_{cat} (s^{-1})	$K_{m,\ Co}^{2+}$ (mM)	$K_{m,\ 4H2KV}$ (μM)
WT	24.7 ± 1.75	1.28 ± 0.14	26.4 ± 4.66	18.7 ± 1.75	0.35 ± 0.05	26.4 ± 4.66
D18N	–	–	–	0.5 ± 0.1	0.18 ± 0.05	42.5 ± 14.4
H200A	1.4 ± 0.4	66.4 ± 31.8	416.3 ± 132.1	7.1 ± 0.3	1.6 ± 0.1	18.3 ± 3.4
H202A	21.8 ± 1.9	0.40 ± 0.1	112.1 ± 15.8	36.2 ± 1.6	0.086 ± 0.02	27.0 ± 2.7

"–" denotes activity too low to estimate kinetic parameters accurately.

variants the apparent K_m values for Co^{2+} were lower than those for Mn^{2+}: for H200A the K_m values of the metal ions were considerably higher than those for WT, whereas for H202A they were significantly lower. The fact that there may be high and low affinity metal binding sites complicates the interpretation of the results as K_m values of the three DmpG variants may reflect complex affinity of the two types of metal ions.

Binding of Additional Metal Ion to WT DmpFG. The observation that approximately one mol of divalent metal ion is associated with purified DmpFG but that additional metal ion is required in the assay for optimal activity suggests that a second metal binding site may be involved in catalysis. Additional metal binding was examined by incubating the enzyme with Mn^{2+} or Co^{2+}, followed by removal of the excess on a desalting column and quantitation of protein-associated metal ions by ICP-MS. In the control experiments without enzyme, elution of the NAP-5 column with 500 μL of 50 mM metal-free HEPES buffer (pH 8) resulted in no Mn^{2+} or Co^{2+} being detected above that in control samples prepared without incubation with metal ion. However, when the NAP-5 column was eluted with 500 μL buffer applied to the protein samples in the column, 1.6 and 1.9 mol of total metal content to one mol of DmpG subunit were obtained for Mn^{2+} and Co^{2+} incubation, respectively, representing significant increases over the one mol of metal present originally (Table 4.2). Since there is only one metal ion accommodated by the HMGL-familty associated Asp-His-His metal binding motif observed by x-ray crystallography, this result may reflect the existence of a second divalent cation binding site.

Secondary, Tertiary and Quaternary Structure Probes of Metal Ligand Variants. Far–UV CD showed that all three metal ligand variant proteins, D18N, H200A, and H202A,

shared similar secondary structure contents with WT DmpFG, since the spectra were almost identical in the range of 210–260 nm (Figure 4.1).

The tertiary structures of the variants were probed using fluorescence spectroscopy. The emission spectra of WT, and the variants D18N and H202A, when excited at 280 nm or 295nm, showed similar peak shapes and emission λ_{max} of 310 nm and 333 nm, respectively, although there were minor differences in intensities (Figure 4.2). The variant H200A had a similar fluorescence emission spectrum to WT and the other variants when excited at 295 nm (Figure 4.2B), but upon excitation at 280 nm the emission λ_{max} of H200A was red-shifted by 10 nm to 320 nm, and the peak was broadened considerably (Figure 4.2A). The inability to fully activate this variant with metal ion (Table 4.5) may be associated with the perturbed structure reflected by the changed fluorescence properties.

Analytical ultracentrifugation (AUC) experiments were carried out to probe whether metal ligand substitution affected the quaternary structure of DmpFG. The three variant proteins all showed similar peaks at 6S, similar to WT, which corresponds to the 140K Da of biological tetramer of DmpFG (Figure 4.3A).

Structural Stability of Metal Ligand Variants. To further investigate the effects of metal ligand replacement on structural stability, DmpFG WT and variant proteins were subjected to thermal and chemical denaturation experiments. Preliminary results showed that either thermal or guanidine·HCl–mediated denaturation caused insoluble precipitates of WT to form (*173*). Thus, urea was used as the denaturant, and unfolding/denaturation was monitored using far–UV CD and AUC. WT and variants D18N, H200A or H202A, were equilibrated with 0–5 M urea, then the α-helical content of the samples was

examined at 222 nm using far-UV CD. The α-helical fractional content decreased as a function of urea concentration with $[urea]_{50\% \text{ unfolding}}$ of 3 M, 2.3 M, 2.1 M and 0.7 M for WT, D18N, H200A and H202A, respectively (Figure 4.4). Therefore, WT DmpFG was more resistant to urea-induced unfolding than the variant proteins indicating that DmpFG was destabilized upon mutagenesis of the metal ligands.

Next, the effects of added Mn^{2+} on unfolding by urea were examined. Similar denaturation profiles were observed for WT, and variants D18N and H200A in the presence or absence of 1 mM Mn^{2+} (Figure 4.4). However, the H202A variant was markedly stabilized to urea-induced unfolding in the presence of added Mn^{2+}, with a shift of $[urea]_{50\% \text{ unfolding}}$ from 0.7 M in the absence of Mn^{2+} to 2.8 M in its presence, bringing the stability very close to that of WT in the absence of added divalent metal ion (Figure 4.4).

The effects of urea on WT and the H202A variant were also examined by AUC. Only a single protein species sedimenting at 6S was observed for WT in the presence or absence of 0.5 M urea, as expected for the 140 KDa DmpFG tetramer (Figure 4.3). For the H202A variant, the tetramer was observed in the absence of urea (Figure 4.3A); in the presence of 0.5 M urea, besides the 6S peak, a species with sedimentation coefficient of 1.8S appeared, consistent with the dissociation of DmpFG to 30K–40K Da monomers (Figure 4.3B).

Effect of Monovalent Cations on DmpG Activity. The effect of monovalent cations on DmpG activity in the absence of and in the presence of divalent cations was investigated. In the presence of 50 or 100 mM Li^+, Na^+, K^+, Rb^+ or NH_4^+ in the assays, no significant effect was observed on DmpG activity either with or without added Mn^{2+} or Co^{2+}, and

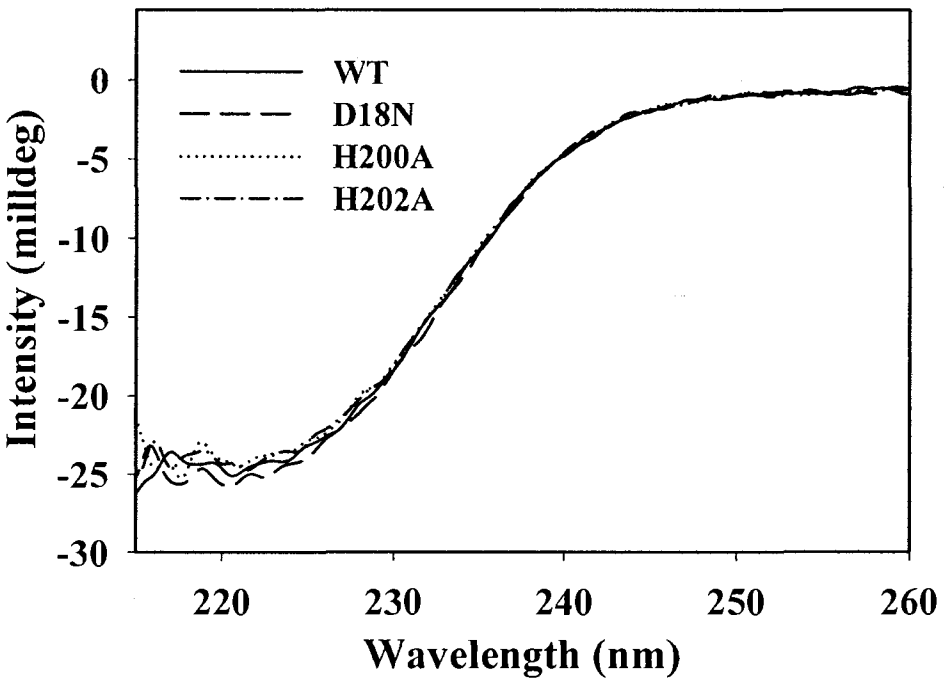

Figure 4.1 Far-UV CD spectra of DmpFG WT and the three metal ligand variant proteins.

The samples were prepared in 50 mM HEPES buffer (pH8) with final concentration of protein 0.5mg/mL.

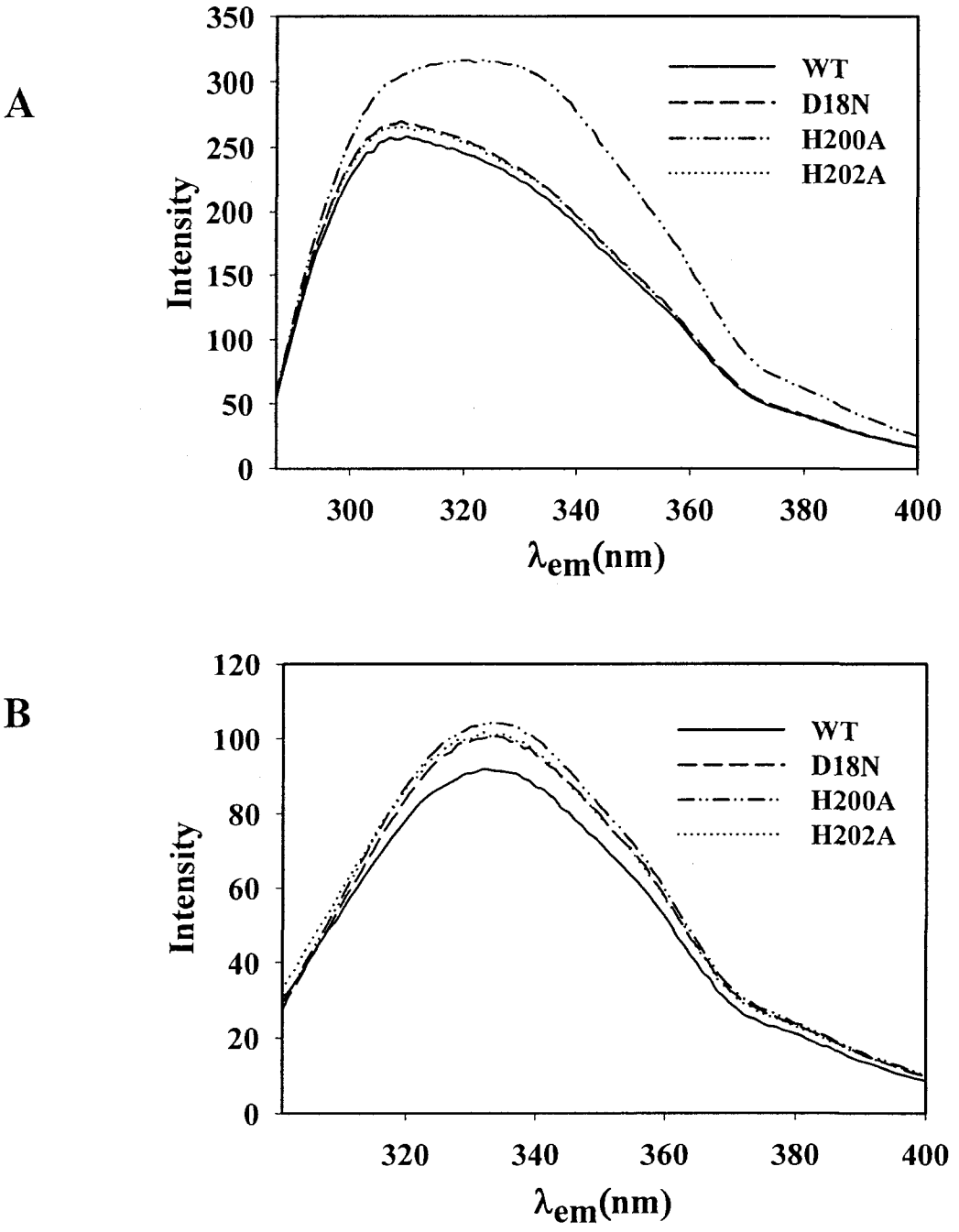

Figure 4.2 Fluorescence spectra of DmpFG WT and the three metal ligand variant proteins. (A) Spectra obtained by excitation at 280 nm; (B) spectra obtained by excitation at 295 nm. The samples were prepared in 50 mM HEPES buffer (pH 8) with final concentration of protein 0.2 mg/mL.

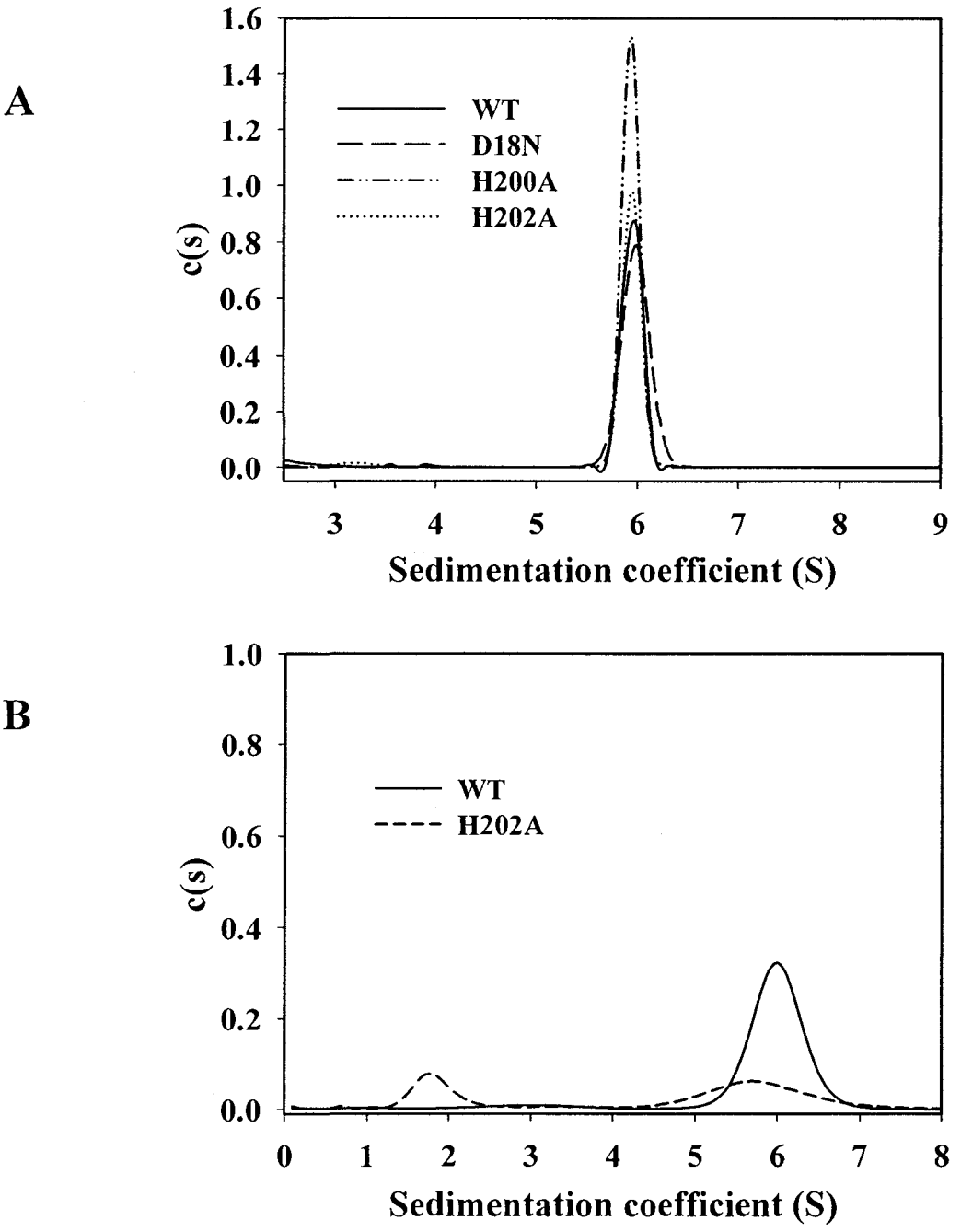

Figure 4.3 Analytical ultracentrifugation of DmpFG protein.

(A) Sedimentation velocity for WT and the three metal ligand variant proteins; (B) sedimentation velocity for WT and variant H202A proteins in the presence of 0.5 M urea. The buffer used was 50 mM metal-free HEPES, pH 8, with 0.5 M urea and samples contained 0.2 mg/mL of protein.

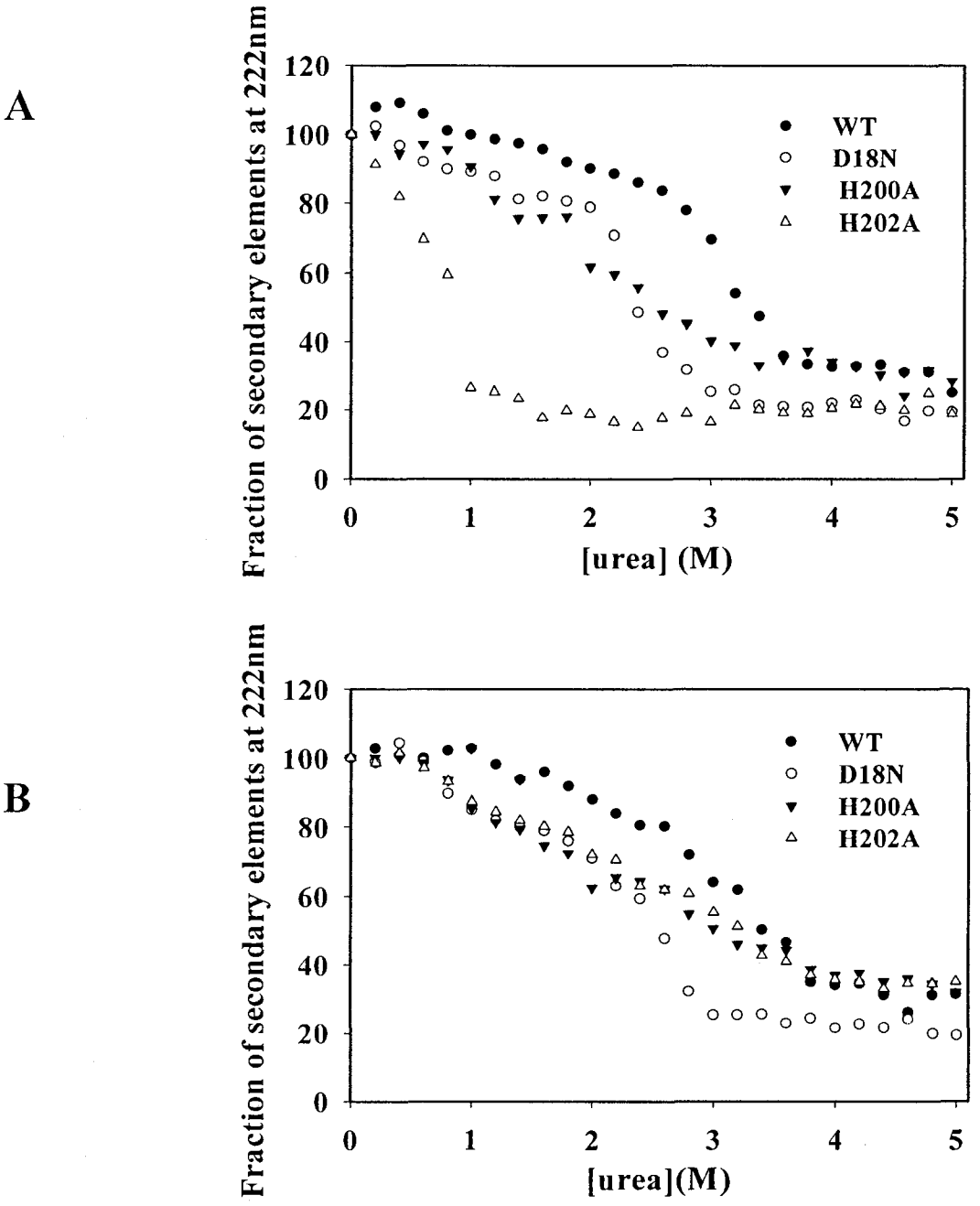

Figure 4.4 Urea-induced unfolding of DmpFG WT and the three metal ligand variant proteins monitored by far-UV CD.

(A) In the absence of added Mn^{2+} and (B) in the presence of added Mn^{2+}. The experiments were carried out in 50 mM metal-free HEPES buffer, pH 8, without added Mn^{2+} or with added 1 mM Mn^{2+}, and containing 0.2 mg/mL of protein.

regardless of whether the assays were carried out in HEPES or Tris-HCl buffers (data not shown).

Zn^{2+} Inhibition of Divalent Cation-Stimulated DmpG Activity. At a low Zn^{2+} concentration (0–125 μM), no effect on adolase activity was observed in the absence of added divalent cation in assays: higher concentrations of Zn^{2+} caused turbidity in the assay buffer and precluded enzyme activity detection. However, low concentrations of Zn^{2+} strongly inhibited Mn^{2+}– or Co^{2+}–stimulated DmpG activity: the higher the Mn^{2+} or Co^{2+} concentration, the stronger the Zn^{2+} ion inhibition. As well, Zn^{2+} decreased both the V_{max} and K_m values for the stimulating cation, which is characteristic of uncompetitive inhibition (data not shown). Inhibition by Zn^{2+} was quantitated by calculating K_i and IC_{50} values in the presence of added Mn^{2+} or Co^{2+} (Table 4.6).

Oxalate Inhibition of Aldolase Activity. Oxalate, an analogue of pyruvate which is a product of the DmpG reaction, was found to competitively inhibit aldolase activity of DmpFG with respect to the substrate, 4H2KV (data not shown). Oxalate inhibits DmpG activity with an IC_{50} of 6.1 μM and $K_i = 0.49$ μM (Table 4.6).

Mutagenesis of Potential Catalytic Residues at the Active Site of DmpG. Arg-17 is conserved in the HMGL-like family members, while His-21 and Tyr-291 are unique for DmpG; however they are all located at positions where they may be involved in DmpG catalysis, according to the crystal structure (*4*). Site-directed mutagenesis was performed to investigate these residues' potential involvement in aldolase activity. Activity was not detectable in variants R17Q or H21A/H21Q without added divalent cation, while Y291A/Y291F activity was similar to WT (Table 4.2 and 4.3). In the presence of added Mn^{2+} or Co^{2+}, variants R17Q, H21A and H21Q showed significant, but low, aldolase

activity relative to WT (Table 4.7 and 4.2). Variant Y291A and Y291F activities increased slightly in the presence of added Mn^{2+} or Co^{2+}, but were still only 9 and 16%, respectively, compared with WT (Tables 4.2 and 4.7).

Detection of Intermediate Carbanion in Aldolase Catalytic Reaction. Tetranitromethane (TNM) has been successfully used to trap the carbanionic enzyme-substrate intermediates of fructose 1,6-bisphosphate aldolases from either rabbit muscle (*170*) or yeast (*169*). TNM was reduced to nitroformate, which strongly absorbs at 350 nm, by the carbanionic intermediates generated during the reaction. In Co^{2+}-containing buffer, incubation of WT DmpFG with substrate, 4-hydroxy-2-ketovalerate, or the product, pyruvate, either of which might be expected to produce enolate carbanions, failed to show any evidence of nitroformate formation (data not shown).

Table 4.6 Effects of inhibitors Zn^{2+} and oxalate on DmpG activity

inhibitor	inhibition pattern	K_i (μM)	IC_{50} (μM)
Zn^{2+}	uncompetitive	8.8 ± 0.7 (Mn^{2+}) 9.0 ± 0.9 (Co^{2+})	11.2 ± 2.1 (Mn^{2+}) 16.3 ± 1.8 (Co^{2+})
oxalate	competitive	0.49 ± 0.08	6.1 ± 0.9

Table 4.7 Specific activity of DmpG WT and variants with added Me^{2+}

variant	specific activity [a] (nmol./min.mg)	
	with added Mn^{2+}	with added Co^{2+}
WT	15,340	13,580
R17Q	2.2	2.7
H21A	11.4	20.1
H21Q	8.0	17.5
Y291A	1,340	2,020
Y291F	1,370	2,512

[a] The specific activities were estimated in 50 mM HEPES assay buffer (pH 8, 25 °C) containing 554 μM NAD^+, 107 μM CoA and 133 μM 4H2KV with addition of 10 mM Mn^{2+} or 5 mM Co^{2+}. The values shown are the average of three determinations, with errors of less than or equal to ± 13 %.

4.5 Discussion

The active site of DmpG was investigated using site-directed mutagenesis. One group of targeted residues comprised the three metal ligands observed in the crystal structure (*4*), D18, H200 and H202, which are all strictly conserved in the HMGL-like family (*6*). Another group of residues identified as potentially important for catalytic mechanism, R17 (*6*), H21 and Y291 (*4*), were also targets for mutagenesis.

The metal ligand variants, D18N, H200A or H202A, all showed dehydrogenase activity and substrate binding affinities similar to WT, as might be expected since they are remote from the DmpF active site (Table 4.1). The small differences that were observed may reflect structural coupling between the DmpF and DmpG subunits that was evident in the crystal structure (*4*). The similarity in dehydrogenase activities allowed a coupled activity assay to be used to investigate and compare aldolase kinetics in the variants.

Determination of the DmpFG structure showed that the DmpG active site included a metal ion, even though the enzyme was crystallized in the absence of any added metal salts (*4*). The ICP-MS studies reported here showed that one DmpFG dimer contained one equivalent of a mixture of Fe, Mn, Zn and Cu, of which Fe and Mn were predominant (Table 4.2). These tightly-bound metals, which could not be removed by various chelators, only supported residual aldolase activity (~5% of optimal, Table 4.2). Site-directed mutagenesis of the active site metal ligands, Asp-18, His-200 and His-202, led to almost complete loss of Fe and Mn (Table 4.2): the increased Cu content of some of the variants suggests that Cu may also bind at the same site, but the lower specific

activity suggests decreased functionality of Cu^{2+}. The broad selectivity suggests a flexible metal binding site within the DmpG active site.

The effects of replacing each of the metal ligands varied. The most pronounced effect on activity was observed in the D18A variant. Tightly bound Fe and Mn were almost completely lost (Table 4.2): activity in the absence of added metal ions was also lost and could not be stimulated by Mn^{2+}, and only to a small extent by Co^{2+} (~3% of WT) (Table 4.4 and 4.5). Although biophysical probes of secondary, tertiary and quaternary structure showed that this variant was very similar to WT (Figures 4.1, 4.2 and 4.3A), the fact that binding to the NAD^+ affinity column became tighter suggested a conformational change in this variant, at least in the DmpF subunit. The stability to denaturation by urea was lower than WT, and was not affected by the addition of Mn^{2+} (Figure 4.4). Taken together, these results suggest that removal of D18 results in an enzyme that is unable to bind active site metal to regain activity. Removal of the aspartate ligand may have a larger effect than removal of either of the histidine ligands, as the carboxyl sidechain has higher affinity for Co^{2+} or Mn^{2+} than does the imidazole sidechain.

Substitution of His-200 with Ala produced a variant with a significantly different fluorescence emission spectrum compared to WT, when excited at 280 nm (Figure 4.2A). This result is consistent with a significantly perturbed structure for H200A indicating that loss of aldolase activity of this variant cannot be exclusively attributed to removal of tightly-bound metal ion. Indeed, addition of metal ion only partially restored the aldolase activity (Tables 4.4 and 4.5) and the K_m for metal ion was far higher than that of WT, indicating that the ability of this variant to bind metal was impaired.

Replacement of His-202 with alanine also resulted in complete loss of bound Fe and Mn, accompanied by almost total loss of aldolase activity (0.11% compared to WT) (Table 4.2). However, unlike H200A, the activity of H202A could be restored to levels similar to or higher than WT aldolase activity by the addition of Mn^{2+} or Co^{2+} (Tables 4.4 and 4.5). In addition, the K_m values for the metal ions appeared to be lower than WT, which may reflect the combination of affinity for both metal binding sites since most of the "tightly-bound" sites of variant H202A were initially unoccupied. This variant showed biophysical behavior similar to that of WT in fluorescence, far-UV CD and AUC experiments (Figures 4.1, 4.2 and 4.3A). However, it was extremely destabilized to denaturation by urea, which was reversed in the presence of Mn^{2+} (Figure 4.4). AUC experiments showed that, unlike WT, this variant dissociated in the presence of a low concentration of urea (Figure 4.3B), suggesting that in the absence of metal ion, the interaction between subunits in H202A was affected. In the presence of additional metal ion, this variant behaved most like WT. Taken together, the results are consistent with the notion that the tightly-bound divalent cation is essential for the residual aldolase activity of WT DmpFG, and also plays a structural role.

It has long been established that divalent metal ion is an integral part of the class II FBPA active site, and that a monovalent cation also participates in catalysis. In some cases, such as FBPA from *E. coli*, two divalent cation binding sites have been identified (*25, 168*). The "catalytic" Zn^{2+} site located at the active site in the C-terminal end of an $(\alpha/\beta)_8$ barrel is coordinated by three histidines, H110, H226 and H264: the proposed function of the catalytic Zn^{2+} is to precisely align the substrate in the active site as well as serve as a Lewis acid to polarize the carbonyl bond of the substrate for efficient catalysis

(*25, 177*). A second Zn^{2+} was proposed to organize and stabilize the catalytic site (*25, 168*), but as the secondary binding sites were observed upon soaking crystals with solutions containing excess divalent metal ion it is not clear whether these sites represent specific or non-specific binding. This uncertainty was further enhanced by the observation that only one Zn atom was detected in the purified holo–protein (*24, 178*). Interestingly, the Zn atom only supported residual activity of the enzyme (14% of the full activity) whereas full activity depended on the presence of K^+ in the assay (*24*).

Similar observations have been made regarding metal ion participation in the other three HMGL-like family members, HMG-CoA lyase, α-isopropylmalate synthase, and transcarboxylase. As with DmpG, all of these enzymes have been observed by x-ray crystallography to contain a metal ion coordinated to two His and one Asp residues (*6-9*). Unlike yeast (*24, 178*) or *E. coli* (*25*) FBPA, and α-isopropylmalate synthases (IPMS) from *Mycobacterium tuberculosis* (*21*), yeast (*179*) and *Neurospora* I. (*180*), where full activity depends on the presence of K^+, DmpG activity was not stimulated by monovalent cations. Similarly, the activities of the other two HMGL-like family members, HMG-CoA lyase and TC 5S unit, have not been reported to depend on the presence of monovalent cations.

The identity and stoichiometry of divalent metal ion binding varies between HMGL-family members. Metal analysis of yeast α-isopropylmalate synthases (IPMS) showed that one subunit of enzyme contained two Zn atoms (*181*): one tightly bound, which was essential for enzyme activity, and one less tightly bound which was catalytically inactive. In contrast, although *Mycobacterium tuberculosis* IPMS was crystallized with Zn^{2+} bound at the active site, Zn^{2+} is actually a competitive inhibitor of catalytic Mg^{2+} (*21*).

Nevertheless, on the basis of the crystal structure, the divalent metal ion was proposed to correctly align the substrate and polarize the C-C bond of the substrate for its efficient cleavage (*8*). Various studies of the 5S subunit of transcarboxylase (TC) from *Propionibacterium shermanti* indicated involvement of Co^{2+}, Zn^{2+} or Cu^{2+} ions with a stoichiometry of one 5S monomer to two metal ions, and while enzyme with Co^{2+} or Zn^{2+} was active, that with Cu^{2+} had low or no activity (*23, 59, 60*). The preparation used for crystal structure determination was purified from bacteria growing in Co^{2+}– and Zn^{2+}–containing medium: Co^{2+} was the metal ion identified by ICP-MS, and a single binding site was observed (25). The Co^{2+} in 5S unit of transcarboxylase was proposed to polarize the carboxyl bond of oxaloacetate and promote C-C bond cleavage.

Amongst the HMGL-family proteins, the best published evidence for a second divalent cation binding site is associated with HMG-CoA lyases. Tightly-bound metal ion associated with the HXH motif was identified by site-directed mutagenesis studies (*17, 19*) and crystallographic evidence (*6, 7*). For instance, purified HMG-CoA lyase from *Pseudomonas mevalonii* predominantly contained tightly bound Cu^{2+} which was proposed to be involved in a structural, not a stimulatory, role (*20, 182*). It is reasonable to suppose that the metal ion participates in catalysis by polarizing the carbonyl group of substrate, leading to efficient C-C bond cleavage. Despite the presence of tightly-bound metal, such as Cu^{2+}, activation by the addition of Mg^{2+} or Mn^{2+} to the enzyme assay was still observed, suggesting a requirement for a more loosely-associated divalent metal ion.

The observation that optimal DmpG aldolase activity required the presence of divalent metal ion in the assay indicates that the tightly-bound metal ion detected by ICP-MS in the purified protein is not sufficient. It was possible to augment the metal content

of the enzyme by 0.6 and 0.9 equivalent upon incubation with excess Mn^{2+} or Co^{2+}, respectively, followed by gel filtration (Table 4.2). The lower amount of Mn^{2+} detected is consistent with the 3-fold higher K_m for this metal ion. These represent lower limits for additional metal ion binding to the enzyme and suggest the presence of a second metal ion binding site.

Additional support for a second divalent metal ion binding site was provided by the results of experiments on the effects of Zn^{2+} on aldolase activity. While the activity of the enzyme in the absence of additional divalent metal ion in the assay was unaffected by Zn^{2+}, Zn^{2+} acted as an uncompetitive inhibitor of activity in the presence of Mn^{2+} or Co^{2+}. This result indicates that Zn^{2+} binds to a site distinct from Mn^{2+} or Co^{2+}, and the site is only available after Mn^{2+} (or Co^{2+}) binding, which may trigger protein conformational change to make a Zn^{2+} binding site functional. Conformational change incurred by the weakly-bound metal ion may stimulate aldolase activity by inducing optimal conformation of the active site and proper substrate orientation. Zn^{2+} inhibition was also observed in α-isopropylmalate synthase from *Mycobacterium tuberculosis,* but was competitive which might result from Zn^{2+} substitution for Mg^{2+} at the active site and from the distinct coordination geometry (*21*).

In summary, the class II aldolases discussed above commonly include a metal ion binding site at the active centers which involves binding to a divalent cation for catalysis. The binding of this metal ion may only support residual activity of the enzymes. The full aldolase activities require a second ion to bind, either monovalent cation or divalent cation: apparently, the class II FBPAs and α-IPMS need a monovalent cation (e.g. K^+) for stimulation, while a divalent cation (Mn^{2+} or Co^{2+}) has to be present for full aldolase

activity of DmpFG. While multiple ion involvement in HMG-CoA lyase or TC 5S subunit reactions has not been fully delineated, like DmpG there is evidence in the reported experimental data that both contain tight- and weak-binding sites for metal ions.

Oxalate strongly inhibited DmpG activity with a competitive pattern. Estimations of IC_{50} and K_i values were done without added cations in the assay, since oxalate is a well-known chelator for many divalent cations. The high affinity of oxalate (IC_{50} = 6.1 μM, K_i = 0.49 μM) is consistent with the observation of a ligand in the DmpFG crystal structure.

In human HMG-CoA lyase, removal of the histidine or aspartate metal ligands resulted in enzymes with lower activities, in the order WT>H235A>D42N>H233A; K_m values for Mg^{2+} ranged from unchanged for H233A to 18- and 80-fold higher for H235A and D42N variants in comparison with the value for WT enzyme, respectively (*17-19*) . Similar results were observed for the corresponding DmpG variants, although removal of the aspartate ligand, rather than one of the histidines, appeared to have the most deleterious effect. In the case of two of the HMG-CoA lyase variants, direct metal binding experiments established that the variants were unable to bind metal ion in the absence of substrate. Although metal binding abilities of the DmpG variants were not measured in this study, the fact that they lacked metal ions after isolation suggests a similar conclusion.

An arginine residue (Arg-17 of DmpG) is highly conserved in the active sites of HMGL-like family enzymes. Arg-41, the corresponding residue of human HMG-CoA lyase, has been studied in detail: the R41Q and R41M variants exhibited five and six orders of magnitude lower activity, respectively, relative to WT (*10*). This residue was proposed to stabilize the negatively-charged enolate intermediate during catalysis (*6*).

The DmpG R17Q variant retained structural integrity based on fluorescence emission and far-UV CD spectra, and similar behavior as WT during purification. However, R17Q exhibited no detectable aldolase activity without added metal ion (Table 4.3) and three and half orders of magnitude lower activity with added either Mn^{2+} or Co^{2+} compared with WT (Tables 4.2 and 4.7). Thus, Arg-17 of DmpG, while not essential for catalysis, does contribute significantly to the rate enhancement by the enzyme as does Arg-47 in human HMG-CoA lyase.

Based on the crystal structure, His-21 and Tyr-291 in DmpG have been proposed to be involved as general acid/bases in deprotonation of 4H2KV substrate, and protonation of the enolate form of the product pyruvate, respectively (*4*). DmpG variants H21A and H21Q showed no detectable aldolase activity without added metal ion (Table 4.3). With added Mn^{2+}, aldolase activity of H21A or H21Q was three orders of magnitude lower than WT, while with Co^{2+}, activity was 600-800 fold lower (Table 4.7). While it can be concluded that this residue is indeed important for catalysis, additional experiments are required to determine its role. In the case of Tyr-291, both variants, Y291A and Y291F, showed aldolase activity comparable to WT (Tables 4.2, 4.3 and 4.7), indicating that Tyr-291 is not required for aldolase catalysis.

In the crystal structure, Arg-17 and Tyr-291 of DmpG are involved in direct interaction with what appeared to be a product analogue, oxalate, that supplies two ligands for the active site metal ion. It is interesting to note that variants R17Q, Y291A and Y291F contain significantly less Fe and Mn than WT, while for His-21 and His-203 which do not contact the active site metal ion or oxalate molecule, variants H21A, H21Q and H203A retain similar amounts of Fe as WT (Table 4.3).

A number of enzyme intermediate carbanions, including those associated with aldolases, have been reported to be reactive with external oxidants including oxygen (*183, 184*). The carbanions' accessibility to oxidants is a prerequisite for these reactions. Catalysis in HMGL-like family members has been proposed to involve formation of carbanionic intermediates (*6*) although no direct evidence has been reported previously and none was detected here using the external oxidant, tetranitromethane. This does not exclude the formation of carbanionic intermediate during the DmpG-catalyzed aldolase reaction, as the aldolase active site may be solvent-inaccessible during catalysis.

4.6 Acknowledgements

This work was supported by a Discovery grant to Justin Powlowski from the Natural Sciences and Engineering Research Council of Canada.

Chapter 5 Summary

DmpFG is bifunctional enzyme that is representative of numerous related enzymes involved in bacterial aromatic degradation pathways. Although the structure of the enzyme was determined previously, few functional studies have been done on it, or its close relatives. Studies of more distantly-related enzymes are useful, but of limited value in understanding how the two enzyme activities work together.

Published work on DmpFG and related enzymes is summarized in Chapter 1.

In Chapter 2, the coenzyme A (CoA) binding site of DmpF was delineated using H–D exchange, and supported by modelling studies, inhibition studies, and cofactor protection experiments. Although NAD^+-and CoA-binding Rossmann folds have been described previously, this is the first time that a Rossmann fold designed to alternately bind NAD^+ and CoA has been reported. The mode of CoA inhibition of DmpF, observed previously for other aldehyde dehydrogenases but not ascribed a cause, was shown to be consistent with disulfide bond formation between the thiol groups of Cys-132 and CoA. This conclusion was supported by results of DTT reactivation experiments, NAD^+ protection assays, and modelling studies (Chapter 2), as well as site-directed mutagenesis evidence (Chapter 3).

Chapter 3 extended the characterization of the DmpF active site to examine the role of a conserved putative active site cysteine residue, Cys-132. Cys-132 was previously proposed to be the essential cysteine of DmpF, and this was supported by the site-directed mutagenesis studies reported here. Mass spectrometry-based investigations detected formation of an acetyl-S-Cys132 enzyme intermediate during turnover in either direction. Results were consistent with the separate observation of a ping-pong kinetic mechanism. In contrast to reported results of acetaldehyde-mediated inactivation of other

proteins, inactivation of DmpF by acetaldehyde was found to be correlated with apparent oxidation of Cys-132 to cysteine sulfinic acid by oxygen. In common with other aldehyde dehydrogenases, kinetic evidence was obtained indicating that the unhydrated form of acetaldehyde is a preferred DmpF substrate. Channelling of acetaldehyde from the active site of DmpG, where it is generated, to that of DmpF where it is oxidized to the final product acetyl-CoA, as suggested by observation of a hydrophobic tunnel between the active sites, may protect acetaldehyde from hydration prior to entry to the DmpF active site.

In Chapter 4, metal ion requirements, together with the involvement of proposed active site residues, were probed for the class II aldolase, DmpG: this enzyme is a recent member of the relatively poorly-studied HMGL-like family of enzymes. Although the tightly-bound metal ion in the DmpG active site appeared to be important for the overall stability of DmpFG, it only supported residual aldolase activity. Full activity required the presence of a weakly-bound stimulatory divalent cation. The notion that DmpG needs an extra metal ion for full activity was further supported by the observation that Zn^{2+} is an uncompetitive inhibitor of the stimulatory divalent cation. A combination of ICP-MS and metal ligand mutagenesis demonstrated that metals in the DmpG active site comprise a mixture, with Fe and Mn predominating. According to previous data reported from our laboratory, the optimal stimulatory ions were Mn^{2+} and Co^{2+}. The relative importance of residues Asp-18, His-200 and His-202 in metal ion binding were assessed using site-directed mutagenesis, and site-directed mutagenesis also showed that Arg-17 and His-21 are important for catalysis, but that Tyr-291 is not.

Future experiments are required to better delineate the roles of active site residues in the DmpG catalytic mechanism, and to provide experimental support for proposed channelling of acetaldehyde from the active site of DmpG to that of DmpF. This would involve more detailed kinetics of the DmpG active site variants, as well as site-directed mutagenesis of residues lining the tunnel, followed by kinetic investigation of the corresponding variants.

References

1. Shingler, V., Powlowski, J., and Marklund, U. (1992) Nucleotide sequence and functional analysis of the complete phenol/3,4-dimethylphenol catabolic pathway of *Pseudomonas* sp. strain CF600. *J. Bacteriol. 174*, 711-724.
2. Powlowski, J., Sahlman, L., and Shingler, V. (1993) Purification and properties of the physically associated meta-cleavage pathway enzymes 4-hydroxy-2-ketovalerate aldolase and aldehyde dehydrogenase (acylating) from *Pseudomonas* sp. strain CF600. *J. Bacteriol. 175*, 377-385.
3. Monastiriakos, S. (1998) Characterization of the meta-cleavage pathway enzymes, 4-Hydroxy-2-ketovalerate aldolase and aldehyde dehydrogenase (acylating), from *Pseudomonas* sp. strain CF600 *M.Sc. thesis (Concordia University, Canada)*.
4. Manjasetty, B. A., Powlowski, J., and Vrielink, A. (2003) Crystal structure of a bifunctional aldolase-dehydrogenase: Sequestering a reactive and volatile intermediate. *Proc. Natl. Acad. Sci. U. S. A. 100*, 6992-6997.
5. Bateman, A., Coin, L., Durbin, R., Finn, R. D., Hollich, V., Griffiths-Jones, S., Khanna, A., Marshall, M., Moxon, S., Sonnhammer, E. L., Studholme, D. J., Yeats, C., and Eddy, S. R. (2004) The Pfam protein families database. *Nucleic. Acids Res. 32*, D138-141.
6. Forouhar, F., Hussain, M., Farid, R., Benach, J., Abashidze, M., Edstrom, W. C., Vorobiev, S. M., Xiao, R., Acton, T. B., Fu, Z., Kim, J. J., Miziorko, H. M., Montelione, G. T., and Hunt, J. F. (2006) Crystal structures of two bacterial 3-hydroxy-3-methylglutaryl-CoA lyases suggest a common catalytic mechanism

among a family of TIM barrel metalloenzymes cleaving carbon-carbon bonds. *J. Biol. Chem. 281*, 7533-7545.

7. Fu, Z., Runquist, J. A., Forouhar, F., Hussain, M., Hunt, J. F., Miziorko, H. M., and Kim, J. J. (2006) Crystal structure of human 3-hydroxy-3-methylglutaryl-CoA Lyase: Insights into catalysis and the molecular basis for hydroxymethylglutaric aciduria. *J. Biol. Chem. 281*, 7526-7532.

8. Koon, N., Squire, C. J., and Baker, E. N. (2004) Crystal structure of LeuA from *Mycobacterium tuberculosis*, a key enzyme in leucine biosynthesis. *Proc. Natl. Acad. Sci. U. S. A. 101*, 8295-8300.

9. Hall, P. R., Zheng, R., Antony, L., Pusztai-Carey, M., Carey, P. R., and Yee, V. C. (2004) Transcarboxylase 5S structures: Assembly and catalytic mechanism of a multienzyme complex subunit. *Embo. J. 23*, 3621-3631.

10. Tuinstra, R. L., Wang, C. Z., Mitchell, G. A., and Miziorko, H. M. (2004) Evaluation of 3-hydroxy-3-methylglutaryl-coenzyme A lyase arginine-41 as a catalytic residue: Use of acetyldithio-coenzyme A to monitor product enolization. *Biochemistry 43*, 5287-5295.

11. Stegink, L. D., and Coon, M. J. (1968) Stereospecificity and other properties of highly purified β-hydroxy-β-methylglutaryl coenzyme A cleavage enzyme from bovine liver. *J. Biol. Chem. 243*, 5272-5279.

12. Pie, J., Lopez-Vinas, E., Puisac, B., Menao, S., Pie, A., Casale, C., Ramos, F. J., Hegardt, F. G., Gomez-Puertas, P., and Casals, N. (2007) Molecular genetics of HMG-CoA lyase deficiency. *Mol. Genet. Metab. 92*, 198-209.

13. Robinson, A. M., and Williamson, D. H. (1980) Physiological roles of ketone bodies as substrates and signals in mammalian tissues. *Physiol. Rev. 60*, 143-187.

14. Krissinel, E., and Henrick, K. (2004) Secondary-structure matching (SSM), a new tool for fast protein structure alignment in three dimensions. *Acta. Crystallogr. D Biol. Crystallogr. 60*, 2256-2268.

15. Roberts, J. R., Narasimhan, C., and Miziorko, H. M. (1995) Evaluation of cysteine 266 of human 3-hydroxy-3-methylglutaryl-CoA lyase as a catalytic residue. *J. Biol. Chem. 270*, 17311-17316.

16. Hruz, P. W., Anderson, V. E., and Miziorko, H. M. (1993) 3-Hydroxy-3-methylglutaryldithio-CoA: Utility of an alternative substrate in elucidation of a role for HMG-CoA lyase's cation activator. *Biochim. Biophys. Acta. 1162*, 149-154.

17. Roberts, J. R., and Miziorko, H. M. (1997) Evidence supporting a role for histidine-235 in cation binding to human 3-hydroxy-3-methyglutaryl-CoA lyase. *Biochemistry 36*, 7594-7600.

18. Roberts, J. R., Mitchell, G. A., and Miziorko, H. M. (1996) Modeling of a mutation responsible for human 3-hydroxy-3-methylglutaryl-CoA lyase deficiency implicates histidine 233 as an active site residue. *J. Biol. Chem. 271*, 24604-24609.

19. Tuinstra, R. L., and Miziorko, H. M. (2003) Investigation of conserved acidic residues in 3-hydroxy-3-methylglutaryl-CoA lyase: Implications for human disease and for functional roles in a family of related proteins. *J. Biol. Chem. 278*, 37092-37098.

20. Narasimhan, C., and Miziorko, H. M. (1992) *Pseudomonas mevalonii* 3-hydroxy-3-methylglutaryl-CoA lyase: Characterization of the isolated recombinant protein and investigation of the enzyme's cation requirements. *Biochemistry 31*, 11224-11230.

21. de Carvalho, L. P., and Blanchard, J. S. (2006) Kinetic analysis of the effects of monovalent cations and divalent metals on the activity of *Mycobacterium tuberculosis* a-isopropylmalate synthase. *Arch. Biochem. Biophys. 451*, 141-148.

22. Singh, K., and Bhakuni, V. (2007) Cation induced differential effect on structural and functional properties of *Mycobacterium tuberculosis* α-isopropylmalate synthase. *BMC Struct. Biol. 7*, 39.

23. Fung, C. H., Mildvan, A. S., and Leigh, J. S., Jr. (1974) Electron and nuclear magnetic resonance studies of the interaction of pyruvate with transcarboxylase. *Biochemistry 13*, 1160-1169.

24. Kobes, R. D., Simpson, R. T., Vallee, R. L., and Rutter, W. J. (1969) A functional role of metal ions in a class II aldolase. *Biochemistry 8*, 585-588.

25. Hall, D. R., Leonard, G. A., Reed, C. D., Watt, C. I., Berry, A., and Hunter, W. N. (1999) The crystal structure of *Escherichia coli* class II fructose-1, 6-bisphosphate aldolase in complex with phosphoglycolohydroxamate reveals details of mechanism and specificity. *J. Mol. Biol. 287*, 383-394.

26. Cooper, S. J., Leonard, G. A., McSweeney, S. M., Thompson, A. W., Naismith, J. H., Qamar, S., Plater, A., Berry, A., and Hunter, W. N. (1996) The crystal structure of a class II fructose-1,6-bisphosphate aldolase shows a novel binuclear metal-binding active site embedded in a familiar fold. *Structure 4*, 1303-1315.

27. Blom, N. S., Tetreault, S., Coulombe, R., and Sygusch, J. (1996) Novel active site in *Escherichia coli* fructose 1,6-bisphosphate aldolase. *Nat. Struct. Biol. 3*, 856-862.

28. Galkin, A., Kulakova, L., Melamud, E., Li, L., Wu, C., Mariano, P., Dunaway-Mariano, D., Nash, T. E., and Herzberg, O. (2007) Characterization, kinetics, and crystal structures of fructose-1,6-bisphosphate aldolase from the human parasite, *Giardia lamblia. J. Biol. Chem. 282*, 4859-4867.

29. Izard, T., and Sygusch, J. (2004) Induced fit movements and metal cofactor selectivity of class II aldolases: Structure of *Thermus aquaticus* fructose-1,6-bisphosphate aldolase. *J. Biol. Chem. 279*, 11825-11833.

30. Conduah Birt, J. E., Shuker, D. E., and Farmer, P. B. (1998) Stable acetaldehyde--protein adducts as biomarkers of alcohol exposure. *Chem. Res. Toxicol. 11*, 136-142.

31. Braun, K. P., Cody, R. B., Jr., Jones, D. R., and Peterson, C. M. (1995) A structural assignment for a stable acetaldehyde-lysine adduct. *J. Biol. Chem. 270*, 11263-11266.

32. Koterba, A. P., Smolen, S., Joseph, A., Basista, M. H., and Brecher, A. S. (1995) Coagulation protein function. II. Influence of thiols upon acetaldehyde effects. *Alcohol 12*, 49-57.

33. Cobessi, D., Tete-Favier, F., Marchal, S., Branlant, G., and Aubry, A. (2000) Structural and biochemical investigations of the catalytic mechanism of an NADP-dependent aldehyde dehydrogenase from *Streptococcus mutans. J. Mol. Biol. 300*, 141-152.

34. Marchal, S., Rahuel-Clermont, S., and Branlant, G. (2000) Role of glutamate-268 in the catalytic mechanism of nonphosphorylating glyceraldehyde-3-phosphate dehydrogenase from Streptococcus mutans. *Biochemistry 39*, 3327-3335.

35. Blanco, J., Moore, R. A., and Viola, R. E. (2003) Capture of an intermediate in the catalytic cycle of L-aspartate-β-semialdehyde dehydrogenase. *Proc. Natl. Acad. Sci. U. S. A. 100*, 12613-12617.

36. D'Ambrosio, K., Pailot, A., Talfournier, F., Didierjean, C., Benedetti, E., Aubry, A., Branlant, G., and Corbier, C. (2006) The first crystal structure of a thioacylenzyme intermediate in the ALDH family: New coenzyme conformation and relevance to catalysis. *Biochemistry 45*, 2978-2986.

37. Fermani, S., Ripamonti, A., Sabatino, P., Zanotti, G., Scagliarini, S., Sparla, F., Trost, P., and Pupillo, P. (2001) Crystal structure of the non-regulatory A_4 isoform of spinach chloroplast glyceraldehyde-3-phosphate dehydrogenase complexed with NADP. *J. Mol. Biol. 314*, 527-542.

38. Moras, D., Olsen, K. W., Sabesan, M. N., Buehner, M., Ford, G. C., and Rossmann, M. G. (1975) Studies of asymmetry in the three-dimensional structure of lobster D-glyceraldehyde-3-phosphate dehydrogenase. *J. Biol. Chem. 250*, 9137-9162.

39. Steinmetz, C. G., Xie, P., Weiner, H., and Hurley, T. D. (1997) Structure of mitochondrial aldehyde dehydrogenase: The genetic component of ethanol aversion. *Structure 5*, 701-711.

40. Hempel, J., Perozich, J., Chapman, T., Rose, J., Boesch, J. S., Liu, Z. J., Lindahl, R., and Wang, B. C. (1999) Aldehyde dehydrogenase catalytic mechanism. A proposal. *Adv. Exp. Med. Biol. 463*, 53-59.

41. Marchal, S., and Branlant, G. (1999) Evidence for the chemical activation of essential Cys-302 upon cofactor binding to nonphosphorylating glyceraldehyde 3-phosphate dehydrogenase from *Streptococcus mutans*. *Biochemistry 38*, 12950-12958.

42. Racker, E., and Krimsky, I. (1952) The mechanism of oxidation of aldehydes by glyceralde-hyde-3-phosphate dehydrogenase. *J. Biol. Chem. 198*, 731-743.

43. Segal, H. L., and Boyer, P. D. (1953) The role of sulfhydryl groups in the activity of D-glyceraldehyde 3-phosphate dehydrogenase. *J. Biol. Chem. 204*, 265-281.

44. Hadfield, A., Kryger, G., Ouyang, J., Petsko, G. A., Ringe, D., and Viola, R. (1999) Structure of aspartate-b-semialdehyde dehydrogenase from *Escherichia coli*, a key enzyme in the aspartate family of amino acid biosynthesis. *J. Mol. Biol. 289*, 991-1002.

45. Feldman, R. I., and Weiner, H. (1972) Horse liver aldehyde dehydrogenase. II. Kinetics and mechanistic implications of the dehydrogenase and esterase activity. *J. Biol. Chem. 247*, 267-272.

46. Sheikh, S., Ni, L., Hurley, T. D., and Weiner, H. (1997) The potential roles of the conserved amino acids in human liver mitochondrial aldehyde dehydrogenase. *J. Biol. Chem. 272*, 18817-18822.

47. Faehnle, C. R., Le Coq, J., Liu, X., and Viola, R. E. (2006) Examination of key intermediates in the catalytic cycle of aspartate-β-semialdehyde dehydrogenase from a gram-positive infectious bacteria. *J. Biol. Chem. 281*, 31031-31040.

48. Rudolph, F. B., Purich, D. L., and Fromm, H. J. (1968) Coenzyme A-linked aldehyde dehydrogenase from *Escherichia coli*. I. Partial purification, properties, and kinetic studies of the enzyme. *J. Biol. Chem. 243*, 5539-5545.

49. Shone, C. C., and Fromm, H. J. (1981) Steady-state and pre-steady-state kinetics of coenzyme A linked aldehyde dehydrogenase from *Escherichia coli*. *Biochemistry 20*, 7494-7501.

50. Yan, R. T., and Chen, J. S. (1990) Coenzyme A-acylating aldehyde dehydrogenase from *Clostridium beijerinckii* NRRL B592. *Appl. Environ. Microbiol. 56*, 2591-2599.

51. Sohling, B., and Gottschalk, G. (1993) Purification and characterization of a coenzyme-A-dependent succinate-semialdehyde dehydrogenase from *Clostridium kluyveri*. *Eur. J. Biochem. 212*, 121-127.

52. Smith, L. T., and Kaplan, N. O. (1980) Purification, properties, and kinetic mechanism of coenzyme A-linked aldehyde dehydrogenase from *Clostridium kluyveri*. *Arch. Biochem. Biophys. 203*, 663-675.

53. Palosaari, N. R., and Rogers, P. (1988) Purification and properties of the inducible coenzyme A-linked butyraldehyde dehydrogenase from *Clostridium acetobutylicum*. *J. Bacteriol. 170*, 2971-2976.

54. Buschhorn, H., Dürre, P., and Gottschalk, G. (1992) Purification and properties of the coenzyme A-linked acetaldehyde dehydrogenase of *Acetobacterium woodii* *Arch. Microbiol.* ***158***, 132-138.

55. Spivey, H. O., and Ovadi, J. (1999) Substrate channeling. *Methods 19*, 306-321.

56. Huang, X., Holden, H. M., and Raushel, F. M. (2001) Channeling of substrates and intermediates in enzyme-catalyzed reactions. *Annu. Rev. Biochem. 70*, 149-180.

57. Williams, P. A., and Sayers, J. R. (1994) The evolution of pathways for aromatic hydrocarbon oxidation in *Pseudomonas*. *Biodegradation 5*, 195-217.

58. Forouhar, F., Hussain, M., Farid, R., Benach, J., Abashidze, M., Edstrom, W. C., Vorobiev, S. M., Xiao, R., Acton, T. B., Fu, Z., Kim, J. J., Miziorko, H. M., Montelione, G. T., and Hunt, J. F. (2006) Crystal structures of two bacterial 3-hydroxy-3-methylglutaryl-CoA lyases suggest a common catalytic mechanism among a family of TIM barrel metalloenzymes cleaving carbon-carbon bonds. *J Biol Chem 281*, 7533-7545.

59. Northrop, D. B., and Wood, H. G. (1969) Transcarboxylase. V. The presence of bound zinc and cobalt. *J. Biol. Chem. 244*, 5801-5807.

60. Ahmad, F., Lygre, D. G., Jacobson, B. E., and Wood, H. G. (1972) Transcarboxylase. XII. Identification of the metal-containing subunits of transcarboxylase and stability of the binding. *J. Biol. Chem. 247*, 6299-6305.

61. Plater, A. R., Zgiby, S. M., Thomson, G. J., Qamar, S., Wharton, C. W., and Berry, A. (1999) Conserved residues in the mechanism of the *E. coli* class II FBP-aldolase. *J. Mol. Biol. 285*, 843-855.

62. Rose, I. A., O'Connell, E. L., and Mehler, A. H. (1965) Mechanism of the aldolase reaction. *J. Biol. Chem. 240*, 1758-1765.

63. Ismail, S. A., and Park, H. W. (2005) Structural analysis of human liver glyceraldehyde-3-phosphate dehydrogenase. *Acta. Crystallogr. D Biol. Crystallogr. 61*, 1508-1513.

64. Didierjean, C., Corbier, C., Fatih, M., Favier, F., Boschi-Muller, S., Branlant, G., and Aubry, A. (2003) Crystal structure of two ternary complexes of phosphorylating glyceraldehyde-3-phosphate dehydrogenase from *Bacillus stearothermophilus* with NAD and D-glyceraldehyde 3-phosphate. *J. Biol. Chem. 278*, 12968-12976.

65. Paquin, J., Baugh, C. M., and MacKenzie, R. E. (1985) Channeling between the active sites of formiminotransferase-cyclodeaminase. Binding and kinetic studies. *J. Biol. Chem. 260*, 14925-14931.

66. Schlichting, I., Yang, X. J., Miles, E. W., Kim, A. Y., and Anderson, K. S. (1994) Structural and kinetic analysis of a channel-impaired mutant of tryptophan synthase. *J. Biol. Chem. 269*, 26591-26593.

67. Thoden, J. B., Holden, H. M., Wesenberg, G., Raushel, F. M., and Rayment, I. (1997) Structure of carbamoyl phosphate synthetase: A journey of 96 A from substrate to product. *Biochemistry 36*, 6305-6316.

68. Kim, J. H., Krahn, J. M., Tomchick, D. R., Smith, J. L., and Zalkin, H. (1996) Structure and function of the glutamine phosphoribosylpyrophosphate amidotransferase glutamine site and communication with the phosphoribosylpyrophosphate site. *J. Biol. Chem. 271*, 15549-15557.

69. Stroud, R. M. (1994) An electrostatic highway. *Nat. Struct. Biol. 1*, 131-134.

70. Poels, P. A., Groen, B. W., and Duine, J. A. (1987) $NAD(P)^+$-independent aldehyde dehydrogenase from *Pseudomonas testosteroni*. A novel type of molybdenum-containing hydroxylase. *Eur. J. Biochem. 166*, 575-579.

71. Mukund, S., and Adams, M. W. (1993) Characterization of a novel tungsten-containing formaldehyde ferredoxin oxidoreductase from the hyperthermophilic archaeon, *Thermococcus litoralis*. A role for tungsten in peptide catabolism. *J. Biol. Chem. 268*, 13592-13600.

72. Perozich, J., Nicholas, H., Wang, B. C., Lindahl, R., and Hempel, J. (1999) Relationships within the aldehyde dehydrogenase extended family. *Protein Sci 8*, 137-146.

73. Hempel, J., Nicholas, H., and Lindahl, R. (1993) Aldehyde dehydrogenases: Widespread structural and functional diversity within a shared framework. *Protein Sci. 2*, 1890-1900.

74. Sophos, N. A., and Vasiliou, V. (2003) Aldehyde dehydrogenase gene superfamily: The 2002 update. *Chem. Biol. Interact. 143-144*, 5-22.

75. Toth, J., Ismaiel, A. A., and Chen, J. S. (1999) The ald gene, encoding a coenzyme A-acylating aldehyde dehydrogenase, distinguishes *Clostridium beijerinckii* and two other solvent-producing clostridia from *Clostridium acetobutylicum*. *Appl. Environ. Microbiol. 65*, 4973-4980.

76. Sanchez, L. B. (1998) Aldehyde dehydrogenase (CoA-acetylating) and the mechanism of ethanol formation in the amitochondriate protist, *Giardia lamblia*. *Arch. Biochem. Biophys. 354*, 57-64.

77. Stines-Chaumeil, C., Talfournier, F., and Branlant, G. (2006) Mechanistic characterization of the MSDH (methylmalonate semialdehyde dehydrogenase) from *Bacillus subtilis*. *Biochem. J. 395*, 107-115.

78. Finn, R. D., Mistry, J., Schuster-Bockler, B., Griffiths-Jones, S., Hollich, V., Lassmann, T., Moxon, S., Marshall, M., Khanna, A., Durbin, R., Eddy, S. R., Sonnhammer, E. L., and Bateman, A. (2006) Pfam: Clans, web tools and services. *Nucleic. Acids Res. 34*, D247-251.

79. Hadfield, A., Shammas, C., Kryger, G., Ringe, D., Petsko, G. A., Ouyang, J., and Viola, R. E. (2001) Active site analysis of the potential antimicrobial target aspartate semialdehyde dehydrogenase. *Biochemistry 40*, 14475-14483.

80. Dubourg, H., Stines-Chaumeil, C., Didierjean, C., Talfournier, F., Rahuel-Clermont, S., Branlant, G., and Aubry, A. (2004) Expression, purification, crystallization and preliminary X-ray diffraction data of methylmalonate-semialdehyde dehydrogenase from *Bacillus subtilis*. *Acta. Crystallogr. D Biol. Crystallogr. 60*, 1435-1437.

81. Liu, Z. J., Sun, Y. J., Rose, J., Chung, Y. J., Hsiao, C. D., Chang, W. R., Kuo, I., Perozich, J., Lindahl, R., Hempel, J., and Wang, B. C. (1997) The first structure of an aldehyde dehydrogenase reveals novel interactions between NAD and the Rossmann fold. *Nat. Struct. Biol. 4*, 317-326.

82. Weiner, H., and Hurley, T. D. (2005) in *ENCYCLOPEDIA OF LIFE SCIENCES. John Wiley & Sons, Ltd: Chichester* http://www.els.net/ *[doi: 10.1038/npg.els.0003049].*

83. Skarzynski, T., Moody, P. C., and Wonacott, A. J. (1987) Structure of holo-glyceraldehyde-3-phosphate dehydrogenase from *Bacillus stearothermophilus* at 1.8 Å resolution. *J. Mol. Biol. 193*, 171-187.

84. Al-Karadaghi, S., Cedergren-Zeppezauer, E. S., and Hovmoller, S. (1994) Refined crystal structure of liver alcohol dehydrogenase-NADH complex at 1.8 Å resolution. *Acta. Crystallogr. D Biol. Crystallogr. 50*, 793-807.

85. Miroux, B., and Walker, J. E. (1996) Over-production of proteins in *Escherichia coli*: Mutant hosts that allow synthesis of some membrane proteins and globular proteins at high levels. *J. Mol. Biol. 260*, 289-298.

86. Sambrook, J., Fritsch, E. F., and Maniatis, T. (1989) *Molecular Cloning: a Laboratory Manual*, 2nd ed., Cold Spring Harbor Laboratory Press, Cold Spring Harbor.

87. Tabor, S., and Richardson, C. C. (1985) A bacteriophage T7 RNA polymerase/promoter system for controlled exclusive expression of specific genes. *Proc. Natl. Acad. Sci. U. S. A. 82*, 1074-1078.

88. Tynan, J., Forde, J., McMahon, M., and Mulcahy, P. (2000) Synthesis of a highly substituted N^6-linked immobilized NAD^+ derivative using a rapid solid-phase modular approach: Suitability for use with the kinetic locking-on tactic for bioaffinity purification of NAD^+-dependent dehydrogenases. *Protein Expr. Purif. 20*, 421-434.

89. Mandell, J. G., Falick, A. M., and Komives, E. A. (1998) Measurement of amide hydrogen exchange by MALDI-TOF mass spectrometry. *Anal. Chem. 70*, 3987-3995.

90. Mandell, J. G., Baerga-Ortiz, A., Akashi, S., Takio, K., and Komives, E. A. (2001) Solvent accessibility of the thrombin-thrombomodulin interface. *J. Mol. Biol. 306*, 575-589.

91. Andersen, M. D., Shaffer, J., Jennings, P. A., and Adams, J. A. (2001) Structural characterization of protein kinase A as a function of nucleotide binding. Hydrogen-deuterium exchange studies using matrix-assisted laser desorption ionization-time of flight mass spectrometry detection. *J. Biol. Chem. 276*, 14204-14211.

92. Pentz, L., Thornton, E. R. (1967) Isotope effects on the basicity of 2-nitrophenoxide, 2,4-dinitrophenoxide, hydroxide, and imidazole in protium oxide-deuterium oxide mixtures. *J. Am. Chem. Soc. 89*, 6931-6938.

93. Resing, K. A., and Ahn, N. G. (1998) Deuterium exchange mass spectrometry as a probe of protein kinase activation. Analysis of wild-type and constitutively active mutants of MAP kinase kinase-1. *Biochemistry 37*, 463-475.

94. Gattiker, A., Bienvenut, W. V., Bairoch, A., and Gasteiger, E. (2002) FindPept, a tool to identify unmatched masses in peptide mass fingerprinting protein identification. *Proteomics 2*, 1435-1444.

95. Mann, M., and Wilm, M. (1994) Error-tolerant identification of peptides in sequence databases by peptide sequence tags. *Anal. Chem. 66*, 4390-4399.

96. Kleywegt, G. J., and Jones, T.A. (1994) A super position. *CCP4/ESF-EACBM Newsletter on Protein Crystallography 31*, 9-14.

97. Jones, T. A., Zou, J. Y., Cowan, S. W., and Kjeldgaard, M. (1991) Improved methods for building protein models in electron density maps and the location of errors in these models. *Acta. Crystallogr. A 47 (Pt 2)*, 110-119.

98. Morris, G. M., Goodsell, D. S., Halliday, R.S., Huey, R., Hart, W. E., Belew, R. K., and Olson, A. J. (1998) Automated docking using a Lamarckian genetic algorithm and an empirical binding free energy function. *Journal of Computational Chemistry 19*, 1639-1662.

99. DeLano, W. L. (2002) *The PyMOL Molecular Graphics System* DeLano Scientific, San Carlos, CA.

100. Bashton, M., and Chothia, C. (2002) The geometry of domain combination in proteins. *J. Mol. Biol. 315*, 927-939.

101. Wolodko, W. T., Fraser, M. E., James, M. N., and Bridger, W. A. (1994) The crystal structure of succinyl-CoA synthetase from *Escherichia coli* at 2.5 Å resolution. *J. Biol. Chem. 269*, 10883-10890.

102. Engel, C., and Wierenga, R. (1996) The diverse world of coenzyme A binding proteins. *Curr. Opin. Struct. Biol. 6*, 790-797.

103. Fraser, M. E., James, M. N., Bridger, W. A., and Wolodko, W. T. (1999) A detailed structural description of *Escherichia coli* succinyl-CoA synthetase. *J. Mol. Biol. 285*, 1633-1653.

104. Ricagno, S., Jonsson, S., Richards, N., and Lindqvist, Y. (2003) Formyl-CoA transferase encloses the CoA binding site at the interface of an interlocked dimer. *Embo. J. 22*, 3210-3219.

105. Pejchal, R., Sargeant, R., and Ludwig, M. L. (2005) Structures of NADH and CH_3-H_4folate complexes of *Escherichia coli* methylenetetrahydrofolate reductase reveal a spartan strategy for a ping-pong reaction. *Biochemistry 44*, 11447-11457.

106. Trimmer, E. E., Ballou, D. P., and Matthews, R. G. (2001) Methylenetetrahydrofolate reductase from *Escherichia coli*: Elucidation of the kinetic mechanism by steady-state and rapid-reaction studies. *Biochemistry 40*, 6205-6215.

107. van den Heuvel, R. H., Westphal, A. H., Heck, A. J., Walsh, M. A., Rovida, S., van Berkel, W. J., and Mattevi, A. (2004) Structural studies on flavin reductase PheA2 reveal binding of NAD in an unusual folded conformation and support novel mechanism of action. *J. Biol. Chem. 279*, 12860-12867.

108. Kirchner, U., Westphal, A. H., Muller, R., and van Berkel, W. J. (2003) Phenol hydroxylase from *Bacillus thermoglucosidasius* A7, a two-protein component monooxygenase with a dual role for FAD. *J. Biol. Chem. 278*, 47545-47553.

109. Faig, M., Bianchet, M. A., Talalay, P., Chen, S., Winski, S., Ross, D., and Amzel, L. M. (2000) Structures of recombinant human and mouse NAD(P)H:quinone oxidoreductases: Species comparison and structural changes with substrate binding and release. *Proc. Natl. Acad. Sci. U. S. A. 97*, 3177-3182.

110. Li, R., Bianchet, M. A., Talalay, P., and Amzel, L. M. (1995) The three-dimensional structure of NAD(P)H:quinone reductase, a flavoprotein involved in cancer chemoprotection and chemotherapy: Mechanism of the two-electron reduction. *Proc. Natl. Acad. Sci. U. S. A. 92*, 8846-8850.

111. Ferrer, J. L., Jez, J. M., Bowman, M. E., Dixon, R. A., and Noel, J. P. (1999) Structure of chalcone synthase and the molecular basis of plant polyketide biosynthesis. *Nat. Struct. Biol. 6*, 775-784.

112. Modis, Y., and Wierenga, R. K. (2000) Crystallographic analysis of the reaction pathway of *Zoogloea ramigera* biosynthetic thiolase. *J. Mol. Biol. 297*, 1171-1182.

113. Hsu, W. C., Hung, H. C., Tong, L., and Chang, G. G. (2004) Dual functional roles of ATP in the human mitochondrial malic enzyme. *Biochemistry 43*, 7382-7390.

114. Yang, Z., Lanks, C. W., and Tong, L. (2002) Molecular mechanism for the regulation of human mitochondrial $NAD(P)^+$-dependent malic enzyme by ATP and fumarate. *Structure 10*, 951-960.

115. Yang, Z., Floyd, D. L., Loeber, G., and Tong, L. (2000) Structure of a closed form of human malic enzyme and implications for catalytic mechanism. *Nat. Struct. Biol. 7*, 251-257.

116. Nagy, E., Henics, T., Eckert, M., Miseta, A., Lightowlers, R. N., and Kellermayer, M. (2000) Identification of the NAD^+-binding fold of glyceraldehyde-3-phosphate dehydrogenase as a novel RNA-binding domain. *Biochem. Biophys. Res. Commun. 275*, 253-260.

117. Soukri, A., Mougin, A., Corbier, C., Wonacott, A., Branlant, C., and Branlant, G. (1989) Role of the histidine 176 residue in glyceraldehyde-3-phosphate dehydrogenase as probed by site-directed mutagenesis. *Biochemistry 28*, 2586-2592.

118. Wilmouth, R. C., Edman, K., Neutze, R., Wright, P. A., Clifton, I. J., Schneider, T. R., Schofield, C. J., and Hajdu, J. (2001) X-ray snapshots of serine protease catalysis reveal a tetrahedral intermediate. *Nat. Struct. Biol. 8*, 689-694.

119. Lei, Y., Pawelek, P. D., and Powlowski, J. (2008) A shared binding site for NAD^+ and coenzyme A in an acetaldehyde dehydrogenase involved in bacterial degradation of aromatic compounds. *Biochemistry 47*, 6870-6882.

120. Dagley, S., and Gibson, D. T. (1965) The Bacterial Degradation of Catechol. *Biochem. J. 95*, 466-474.

121. Sambrook, J., Fritsch, E. F., and Maniatis, T. (1989) *Molecular Cloning: a Laboratory Manual*, 2nd ed., Cold Spring Harbor Laboratory Press, Cold Spring Harbor.

122. Coligan, J. E., Dunn, B. M., Ploegh, H. L., Speicher, D. W., and Wingfield, P. T. (1995) *Current protocols in protein science*, Vol. 2, John Wiley & Sons, Inc.

123. Brown, R. E., Jarvis, K. L., and Hyland, K. J. (1989) Protein measurement using bicinchoninic acid: Elimination of interfering substances. *Anal. Biochem. 180*, 136-139.

124. Mach, H., Middaugh, C. R., and Lewis, R. V. (1992) Statistical determination of the average values of the extinction coefficients of tryptophan and tyrosine in native proteins. *Anal. Biochem. 200*, 74-80.

125. Leatherbarrow, R. J. (2001) *GraFit Version 5*, Erithacus Software Ltd. , Horley, U.K.

126. Dawson, R. M. C., Elliott, D. C., Elliott, W. H., and Jones, K. M. (1986) *Data for Biochemical Research* 3ed., Clarendon Press, Oxford

127. Bernt, E., and Bergmeyer, H. U. (1974) Acetaldehyde determination with alcohol dehydrogenase from yeast, in *Methods of Enzymatic Analysis* pp 1506–1509, Academic, London.

128. Bell, R. P. (1966) The reversible hydration of carbonyl compounds. *Adv. Phys. Org. Chem. 4*, 1-12.

129. Sobolev, V., Sorokine, A., Prilusky, J., Abola, E. E., and Edelman, M. (1999) Automated analysis of interatomic contacts in proteins. *Bioinformatics 15*, 327-332.

130. Thompson, S., Mayerl, F., Peoples, O. P., Masamune, S., Sinskey, A. J., and Walsh, C. T. (1989) Mechanistic studies on β-ketoacyl thiolase from *Zoogloea ramigera*: Identification of the active-site nucleophile as Cys89, its mutation to Ser89, and kinetic and thermodynamic characterization of wild-type and mutant enzymes. *Biochemistry 28*, 5735-5742.

131. Fridovich, I. (1966) The mechanism of the enzymatic oxidation of aldehydes. *J. Biol. Chem. 241*, 3126-3128.

132. Naylor, J. F., 3rd, and Fridovich, I. (1968) The form of the aldehyde susceptible to enzymic oxidation. *J. Biol. Chem. 243*, 341-345.

133. Deetz, J. S., Luehr, C. A., and Vallee, B. L. (1984) Human liver alcohol dehydrogenase isozymes: Reduction of aldehydes and ketones. *Biochemistry 23*, 6822-6828.

134. Pocker, Y., and Meany, J. E. (1965) The catalytic versatility of carbonic anhydrase. *J. Am. Chem. Soc. 87*, 1809.

135. San George, R. C., and Hoberman, H. D. (1986) Reaction of acetaldehyde with hemoglobin. *J. Biol. Chem. 261*, 6811-6821.

136. Anni, H., Pristatsky, P., and Israel, Y. (2003) Binding of acetaldehyde to a glutathione metabolite: Mass spectrometric characterization of an acetaldehyde-cysteinylglycine conjugate. *Alcohol Clin. Exp. Res. 27*, 1613-1621.

137. Miranda, J. J. (2003) Position-dependent interactions between cysteine residues and the helix dipole. *Protein Sci. 12*, 73-81.

138. Kurz, J. L. (1967) The Hydration of Acetaldehyde. I. Equilibrium Thermodynamic Parameters. *J. Am. Chem. Soc. 89*, 3524-3528.

139. Abdallah, M. A., Biellmann, J. F., and Lagrange, P. (1979) Stopped-flow determination of the active form of acetaldehyde in the liver alcohol dehydrogenase catalyzed reaction. *Biochemistry 18*, 836-838.

140. Kazahaya, T., Kawai, K., Yashima, S., and Sasaki, Y. (1972) Aerobic dissimilation of glucose by heterolactic bacteria. III. Aldehyde dehydrogenase and alcohol dehydrogenase of *Leuconostoc mesenteroides*. *J. Gen. Appl. Microbiol. 18*, 43-55.

141. Hillmer, P., and Gottschalk, G. (1974) Solubilization and partial characterization of particulate dehydrogenases from *Clostridium kluyveri*. *Biochim Biophys Acta. 334*, 12-23.

142. Bruchhaus, I., and Tannich, E. (1994) Purification and molecular characterization of the NAD^+-dependent acetaldehyde/alcohol dehydrogenase from *Entamoeba histolytica*. *Biochem. J. 303 (Pt 3)*, 743-748.

143. Lurz, R., Mayer, F. and Gottschalk, G. (1979) Electron microscopic study on the quaternary structure of the isolated particulate alcohol-acetaldehyde dehydrogenase complex and on its identity with the polygonal bodies of *Clostridium kluyveri* *Arch. Microbiol. 120*, 255-262.

144. Nair, R. V., Bennett, G. N., and Papoutsakis, E. T. (1994) Molecular characterization of an aldehyde/alcohol dehydrogenase gene from *Clostridium acetobutylicum* ATCC 824. *J. Bacteriol. 176*, 871-885.

145. Souza, J. M., and Radi, R. (1998) Glyceraldehyde-3-phosphate dehydrogenase inactivation by peroxynitrite. *Arch. Biochem. Biophys. 360*, 187-194.

146. Olson, E. J., and Park, J. H. (1964) Studies on the mechanism and active site for the esterolytic activity of 3-phosphoglyceraldehyde dehydrogenase. *J. Biol. Chem. 239*, 2316-2327.

147. Little, C., and O'Brien, P. J. (1969) Mechanism of peroxide-inactivation of the sulphydryl enzyme glyceraldehyde-3-phosphate dehydrogenase. *Eur. J. Biochem. 10*, 533-538.

148. Mallis, R. J., Hamann, M. J., Zhao, W., Zhang, T., Hendrich, S., and Thomas, J. A. (2002) Irreversible thiol oxidation in carbonic anhydrase III: Protection by S-glutathiolation and detection in aging rats. *Biol. Chem. 383*, 649-662.

149. Fu, X., Kassim, S. Y., Parks, W. C., and Heinecke, J. W. (2001) Hypochlorous acid oxygenates the cysteine switch domain of pro-matrilysin (MMP-7). A mechanism for matrix metalloproteinase activation and atherosclerotic plaque rupture by myeloperoxidase. *J. Biol. Chem. 276*, 41279-41287.

150. Wang, Q., Dube, D., Friesen, R. W., LeRiche, T. G., Bateman, K. P., Trimble, L., Sanghara, J., Pollex, R., Ramachandran, C., Gresser, M. J., and Huang, Z. (2004) Catalytic inactivation of protein tyrosine phosphatase CD45 and protein tyrosine phosphatase 1B by polyaromatic quinones. *Biochemistry 43*, 4294-4303.

151. Canet-Aviles, R. M., Wilson, M. A., Miller, D. W., Ahmad, R., McLendon, C., Bandyopadhyay, S., Baptista, M. J., Ringe, D., Petsko, G. A., and Cookson, M. R. (2004) The Parkinson's disease protein DJ-1 is neuroprotective due to cysteine-sulfinic acid-driven mitochondrial localization. *Proc. Natl. Acad. Sci. U. S. A. 101*, 9103-9108.

152. Yang, K. S., Kang, S. W., Woo, H. A., Hwang, S. C., Chae, H. Z., Kim, K., and Rhee, S. G. (2002) Inactivation of human peroxiredoxin I during catalysis as the result of the oxidation of the catalytic site cysteine to cysteine-sulfinic acid. *J. Biol. Chem. 277*, 38029-38036.

153. Bozonet, S. M., Findlay, V. J., Day, A. M., Cameron, J., Veal, E. A., and Morgan, B. A. (2005) Oxidation of a eukaryotic 2-Cys peroxiredoxin is a molecular switch controlling the transcriptional response to increasing levels of hydrogen peroxide. *J. Biol. Chem. 280*, 23319-23327.

154. Woo, H. A., Jeong, W., Chang, T. S., Park, K. J., Park, S. J., Yang, J. S., and Rhee, S. G. (2005) Reduction of cysteine sulfinic acid by sulfiredoxin is specific to 2-Cys peroxiredoxins. *J. Biol. Chem. 280*, 3125-3128.

155. Jeong, W., Park, S. J., Chang, T. S., Lee, D. Y., and Rhee, S. G. (2006) Molecular mechanism of the reduction of cysteine sulfinic acid of peroxiredoxin to cysteine by mammalian sulfiredoxin. *J. Biol. Chem. 281*, 14400-14407.

156. Polgar, L. (1975) Ion-pair formation as a source of enhanced reactivity of the essential thiol group of D-glyceraldehyde-3-phosphate dehydrogenase. *Eur. J. Biochem. 51*, 63-71.

157. Choi, H. J., Kang, S. W., Yang, C. H., Rhee, S. G., and Ryu, S. E. (1998) Crystal structure of a novel human peroxidase enzyme at 2.0 Å resolution. *Nat. Struct. Biol. 5*, 400-406.

158. Lindley, H. (1960) A study of the kinetics of the reaction between thiol compounds and choloracetamide. *Biochem. J. 74*, 577-584.

159. Trentham, D. R. (1968) Aspects of the chemistry of D-glyceraldehyde 3-phosphate dehydrogenase. *Biochem. J. 109*, 603-612.

160. Powlowski, J., and Shingler, V. (1994) Genetics and biochemistry of phenol degradation by *Pseudomonas* sp. CF600. *Biodegradation 5*, 219-236.

161. Fessner, W. D. (1998) Enzyme mediated C-C bond formation. *Curr. Opin. Chem. Biol. 2*, 85-97.

162. Rutter, W. J., Hunsley, J. R., Groves, W. E., Calder, J., Rajkumar, T. V. and Woodfin, B. M. . (1966) Fructose diphosphate aldolase. *Methods in Enzymology 9*, 479-498.

163. Gamblin, S. J., Cooper, B., Millar, J. R., Davies, G. J., Littlechild, J. A., and Watson, H. C. (1990) The crystal structure of human muscle aldolase at 3.0 Å resolution. *FEBS Lett. 262*, 282-286.

164. Choi, K. H., Mazurkie, A. S., Morris, A. J., Utheza, D., Tolan, D. R., and Allen, K. N. (1999) Structure of a fructose-1,6-bis(phosphate) aldolase liganded to its

natural substrate in a cleavage-defective mutant at 2.3 Å. *Biochemistry 38*, 12655-12664.

165. Morris, A. J., and Tolan, D. R. (1993) Site-directed mutagenesis identifies aspartate 33 as a previously unidentified critical residue in the catalytic mechanism of rabbit aldolase A. *J. Biol. Chem. 268*, 1095-1100.

166. Dalby, A., Dauter, Z., and Littlechild, J. A. (1999) Crystal structure of human muscle aldolase complexed with fructose 1,6-bisphosphate: Mechanistic implications. *Protein Sci. 8*, 291-297.

167. Zgiby, S. M., Thomson, G. J., Qamar, S., and Berry, A. (2000) Exploring substrate binding and discrimination in fructose1, 6-bisphosphate and tagatose 1,6-bisphosphate aldolases. *Eur. J. Biochem. 267*, 1858-1868.

168. Hall, D. R., Kemp, L. E., Leonard, G. A., Marshall, K., Berry, A., and Hunter, W. N. (2003) The organization of divalent cations in the active site of cadmium *Escherichia coli* fructose-1,6-bisphosphate aldolase. *Acta. Crystallogr. D Biol. Crystallogr. 59*, 611-614.

169. Riordan, J. F., and Christen, P. (1969) Carbanion intermediates in the reaction of yeast and muscle aldolase. *Biochemistry 8*, 2381-2386.

170. Christen, P., and Riordan, J. F. (1968) Reaction of an aldolase-substrate intermediate with tetranitromethane. *Biochemistry 7*, 1531-1538.

171. Shindyalov, I. N., and Bourne, P. E. (1998) Protein structure alignment by incremental combinatorial extension (CE) of the optimal path. *Protein Eng. 11*, 739-747.

172. Holm, L., and Sander, C. (1997) An evolutionary treasure: Unification of a broad set of amidohydrolases related to urease. *Proteins 28*, 72-82.

173. Tait, A. (2004) Site-directed mutagenesis studies of conserved metal-binding residues in DmpFG, a bifunctional aldolase/dehydrogenase from *Pseudomonas* sp. strain CF600 *M.Sc. thesis (Concordia University, Canada)*.

174. Cleland, W. W. (1979) Statistical analysis of enzyme kinetic data. *Methods Enzymol. 63*, 103-138.

175. Philo, J. S. (2000) A method for directly fitting the time derivative of sedimentation velocity data and an alternative algorithm for calculating sedimentation coefficient distribution functions. *Anal. Biochem. 279*, 151-163.

176. Hayes, D. B., Laue, T., and Philo, J. (2003) Sedimentation interpretation program, version 1.08. *Durham, NH, University of New Hampshire*.

177. Kadonaga, J. T., and Knowles, J. R. (1983) Role of mono- and divalent metal cations in the catalysis by yeast aldolase. *Biochemistry 22*, 130-136.

178. Harris, C. E., Kobes, R. D., Teller, D. C., and Rutter, W. J. (1969) The molecular characteristics of yeast aldolase. *Biochemistry 8*, 2442-2454.

179. Ulm, E. H., Bohme, R., and Kohlhaw, G. (1972) α-isopropylmalate synthase from *yeast*: Purification, kinetic studies, and effect of ligands on stability. *J. Bacteriol. 110*, 1118-1126.

180. Webster, R. E. a. G., S.R. . (1965) The α-isopropylmalate synthetase of *Neurospora*. I. The kinetics and end product control of α-isopropylmalate synthetase function. *Biochemistry 4*, 2309-2327.

181. Roeder, P. R., and Kohlhaw, G. B. (1980) α-Isopropylmalate synthase from yeast. A zinc metalloenzyme. *Biochim. Biophys. Acta. 613*, 482-487.

182. Narasimhan, C., Antholine, W. E., and Miziorko, H. M. (1994) *P. mevalonii* 3-hydroxy-3-methylglutaryl-CoA lyase: Electron paramagnetic resonance investigation of the copper binding site. *Arch. Biochem. Biophys. 312*, 467-473.

183. Healy, M. J., and Christen, P. (1973) Mechanistic probes for enzymatic reactions. Oxidation-reduction indicators as oxidants of intermediary carbanions (studies with aldolase, aspartate aminotransferase, pyruvate decarboxylase, and 6-phosphogluconate dehydrogenase). *Biochemistry 12*, 35-41.

184. Abell, L. M., and Schloss, J. V. (1991) Oxygenase side reactions of acetolactate synthase and other carbanion-forming enzymes. *Biochemistry 30*, 7883-7887.